Dissipation and Intermittency in Gyrokinetic Turbulence and Beyond

Jason TenBarge

Collaborators
Greg Howes (U. Iowa), Kris Klein (U. Michigan), Bill Dorland (UMD), Daniel Told (UCLA), Frank Jenko (UCLA), Jimmy Juno (UMD), Ammar Hakim (PPPL), Greg Hammett (PPPL), Amitava Bhattacharjee (PPPL), Gkeyll Team

August 25, 2016

UNIVERSITY OF MARYLAND

Outline

- Introduce basic turbulence concepts and solar wind observations
- Motivate and introduce gyrokinetics
- Discuss results pointing toward Landau damping and entropy cascade
- Intermittency in KAW turbulence using the GENE code
- Field-particle correlations to diagnose dissipation
- Eulerian Vlasov-Maxwell code, Gkeyll

Solar Wind Turbulence

What is turbulence?

"The most important unsolved problem of classical physics." - Feynman

Cartoon Model of Turbulence

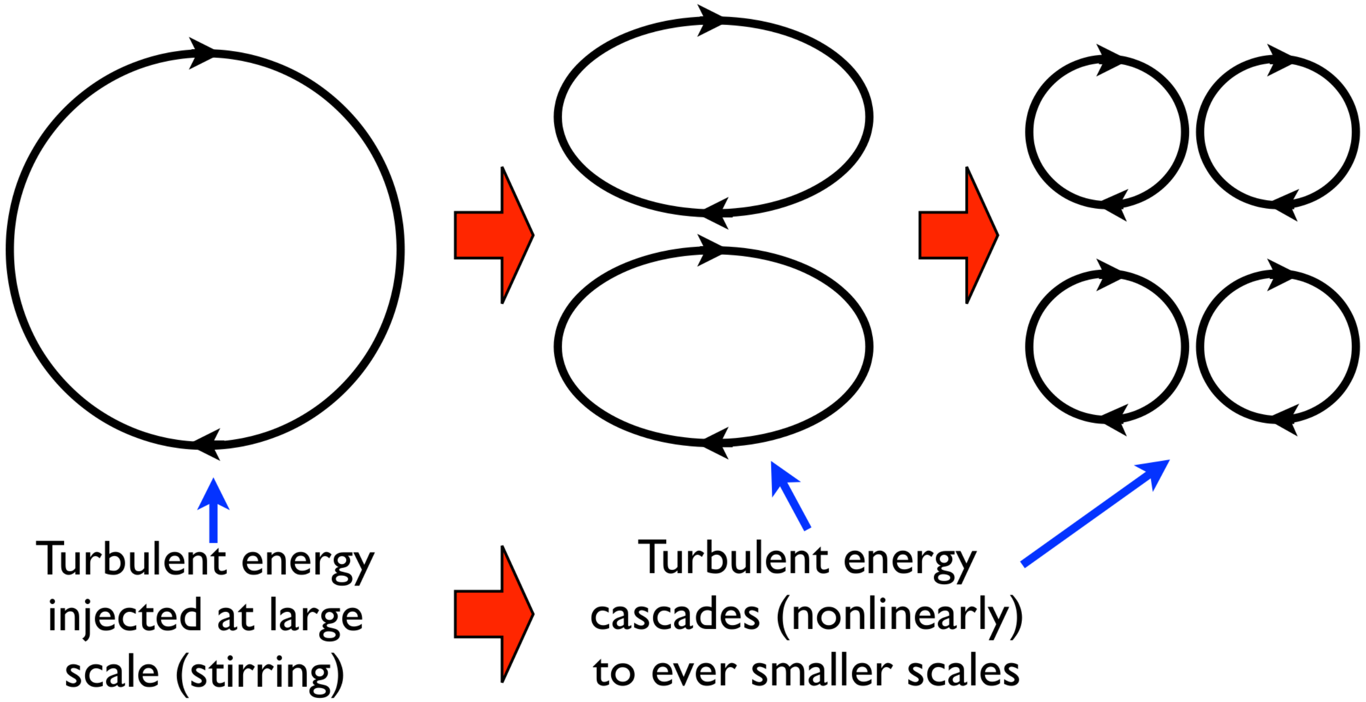

Turbulent energy injected at large scale (stirring)

Turbulent energy cascades (nonlinearly) to ever smaller scales

Why is turbulence important?

Turbulence in important because it governs the transport of

- Energy (energy flow, heating)
- Mass (mixing, accretion)
- Momentum (jet interactions, shocks)

Turbulence plays an important role in a large variety of space and astrophysical phenomena, e.g.,

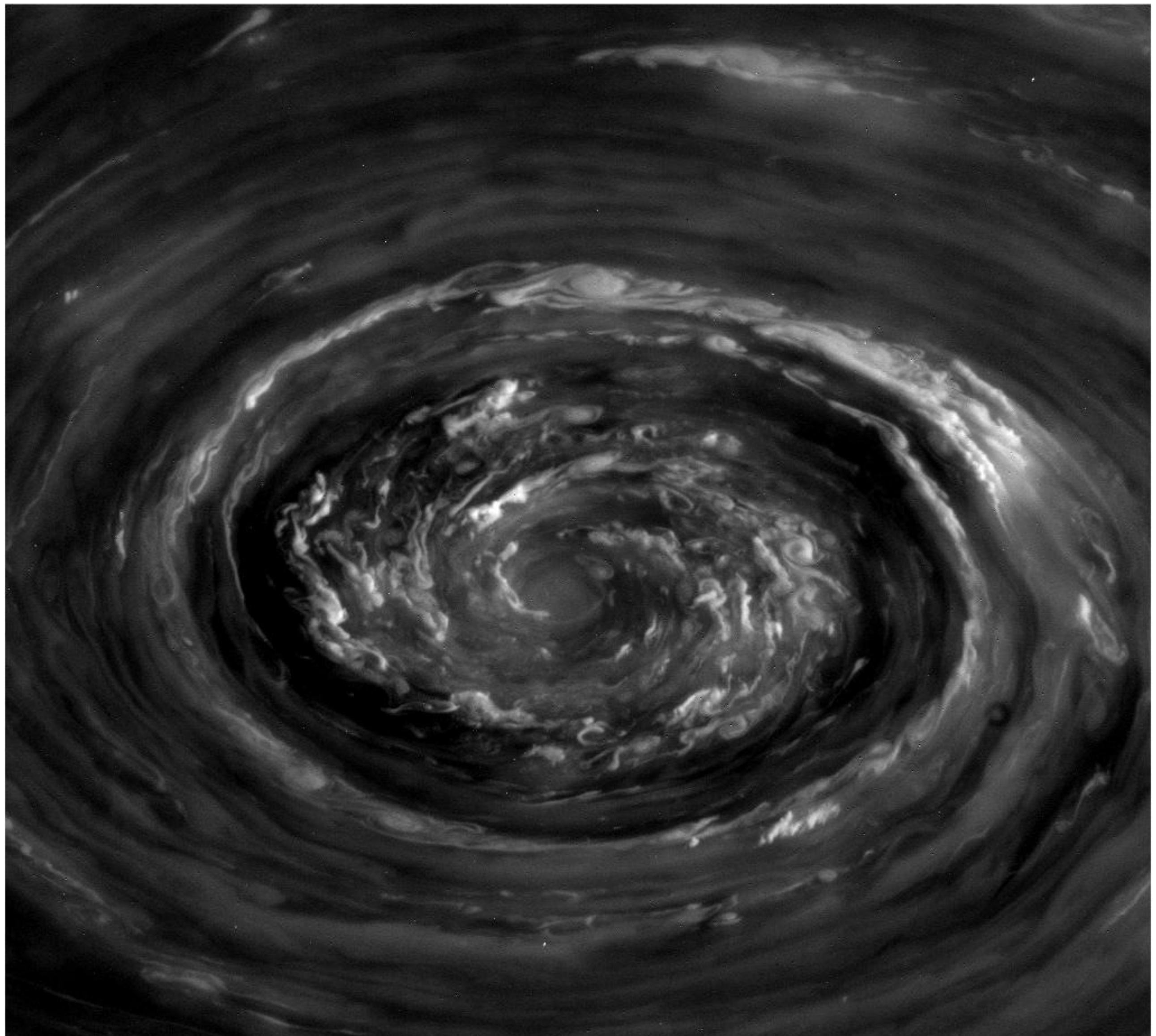

- Accretion discs
- Interstellar medium
- Star-forming nebulae
- Solar corona and solar wind

Energy spectrum

$$E(k) \sim v^2/k \propto k^{-5/3}$$

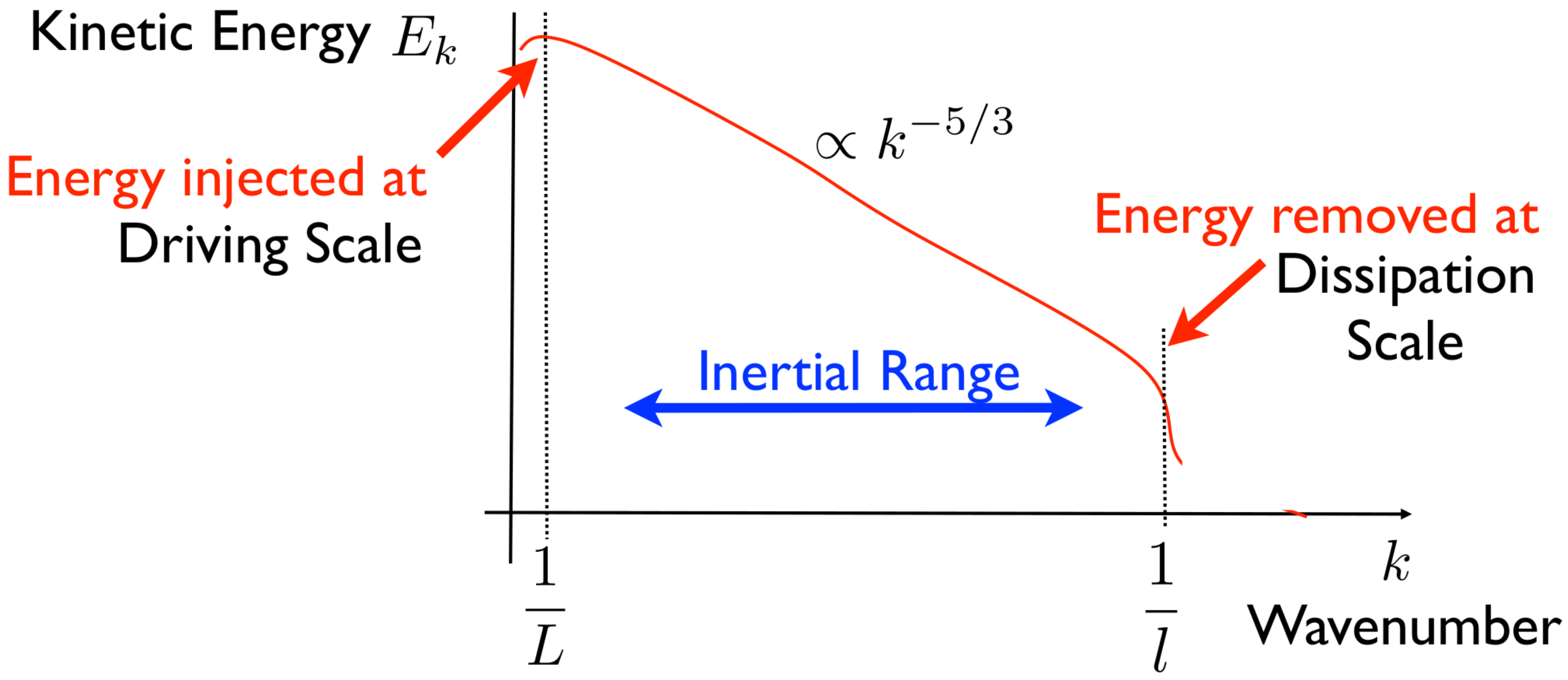

MHD turbulence

- Turbulence is no longer mediated by vortices but interacting Alfvén waves

- In a magnetized plasma, the large-scale magnetic field adds a preferential direction to the system

- Turbulence becomes anisotropic

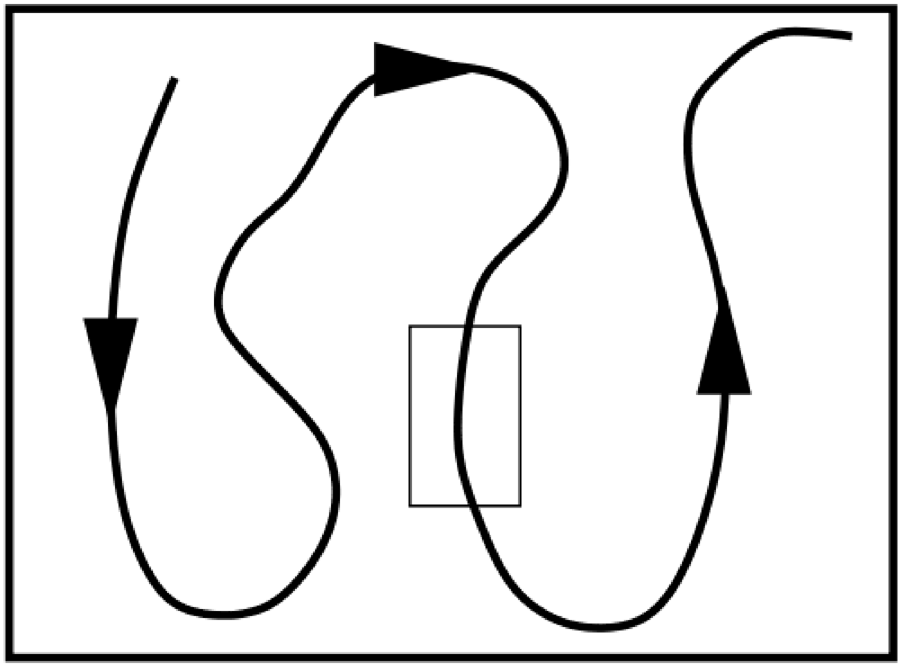

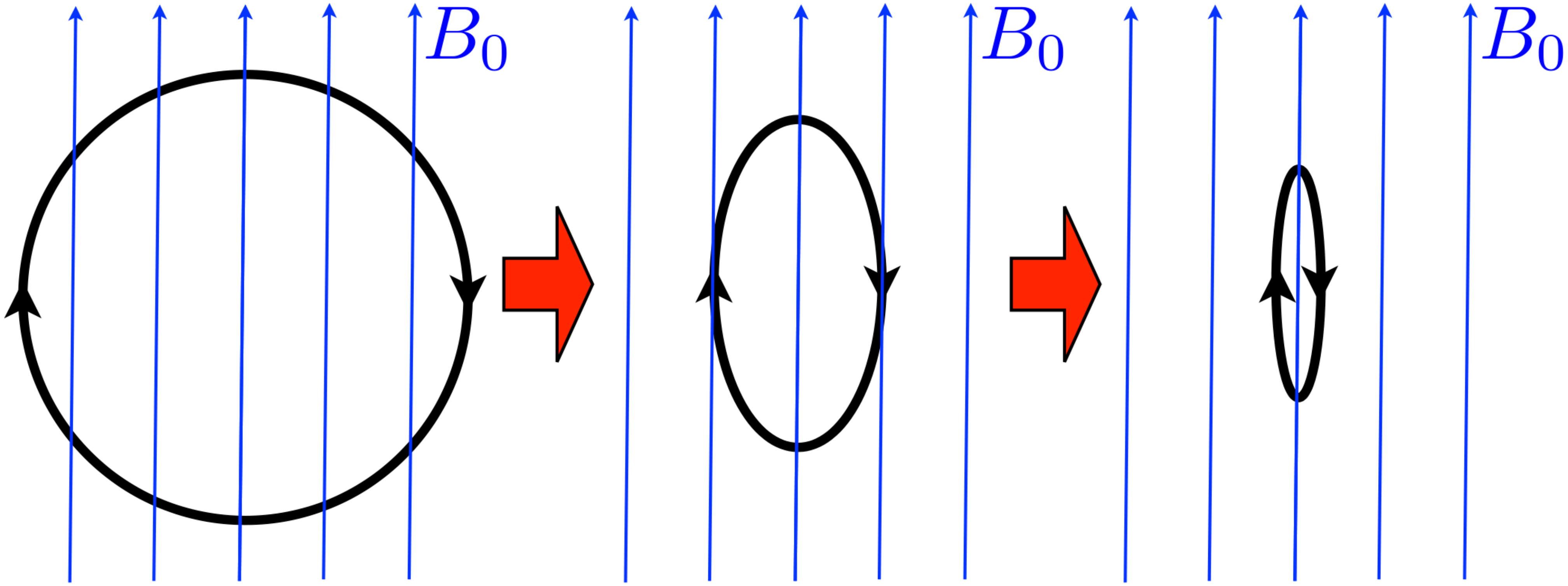

Solar wind energy spectrum

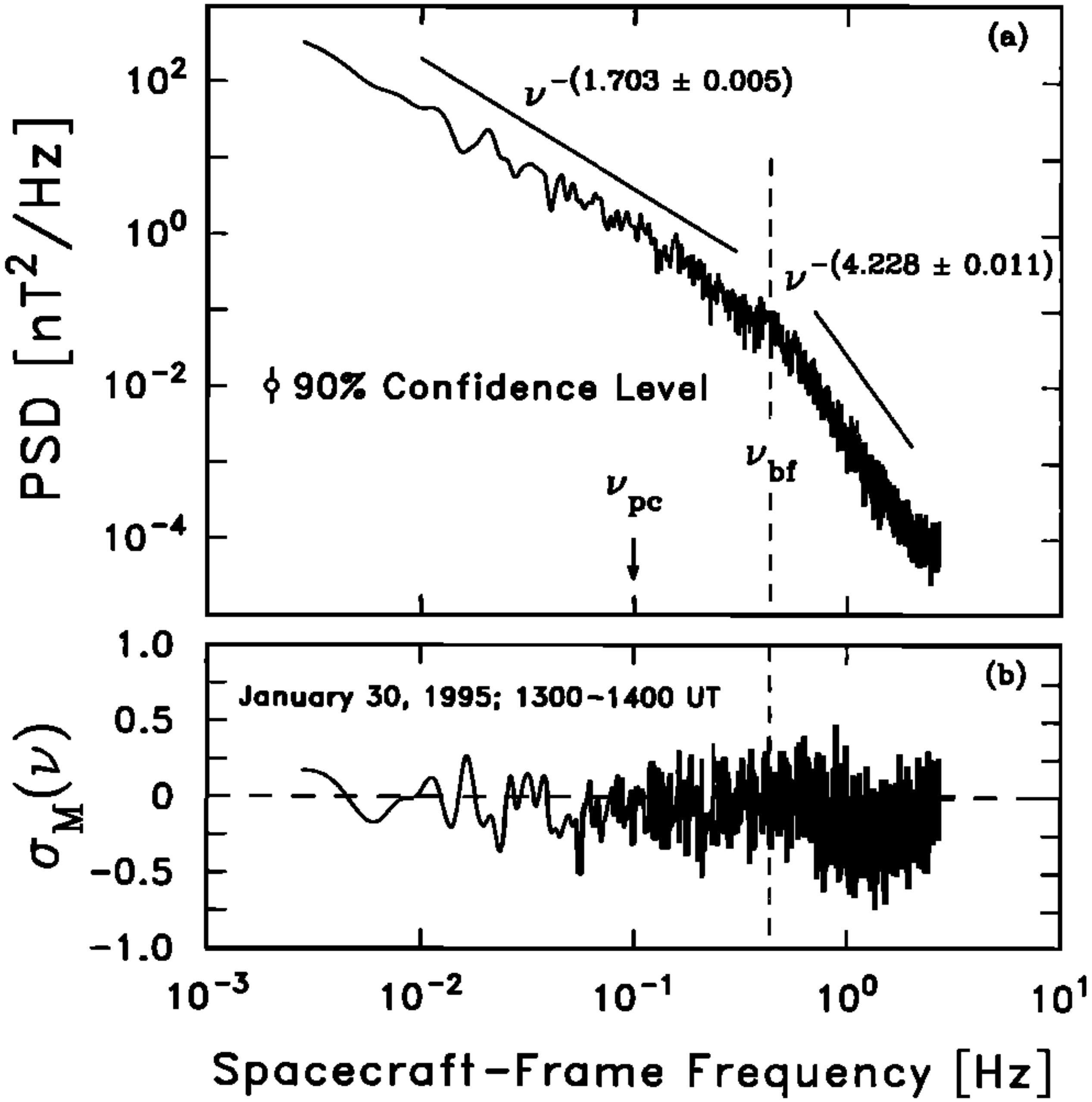

Magnetic energy (a) and helicity (b) from Leamon et al (1998).

- Alfvénic inertial range transitions into something else at the spectral break
- Proposed to be kinetic Alfvén waves, magnetosonic whistler waves, ion cyclotron waves, or current sheets

Wave modes

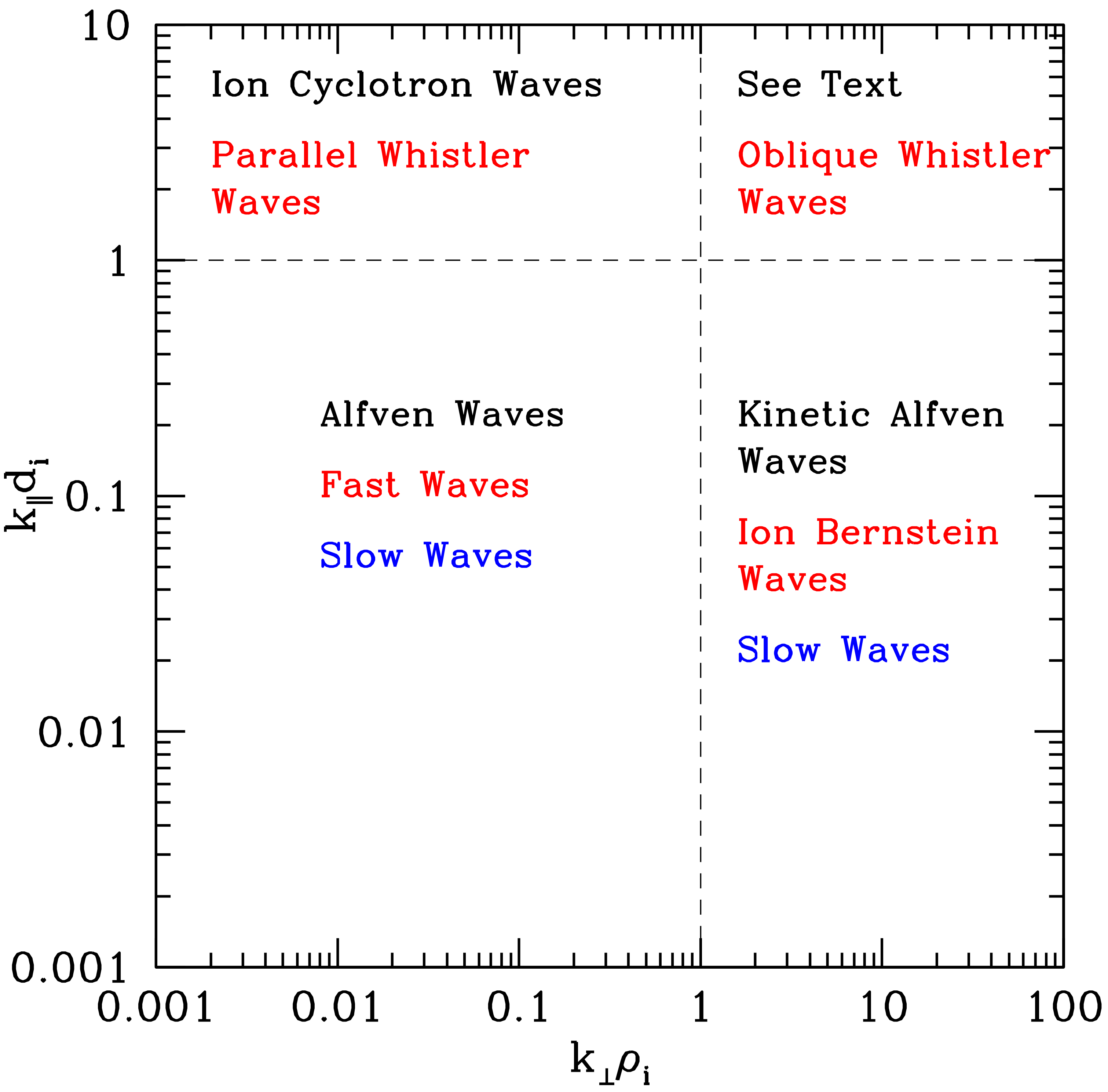

From TenBarge et al (2012)

Contemporary solar wind energy spectra

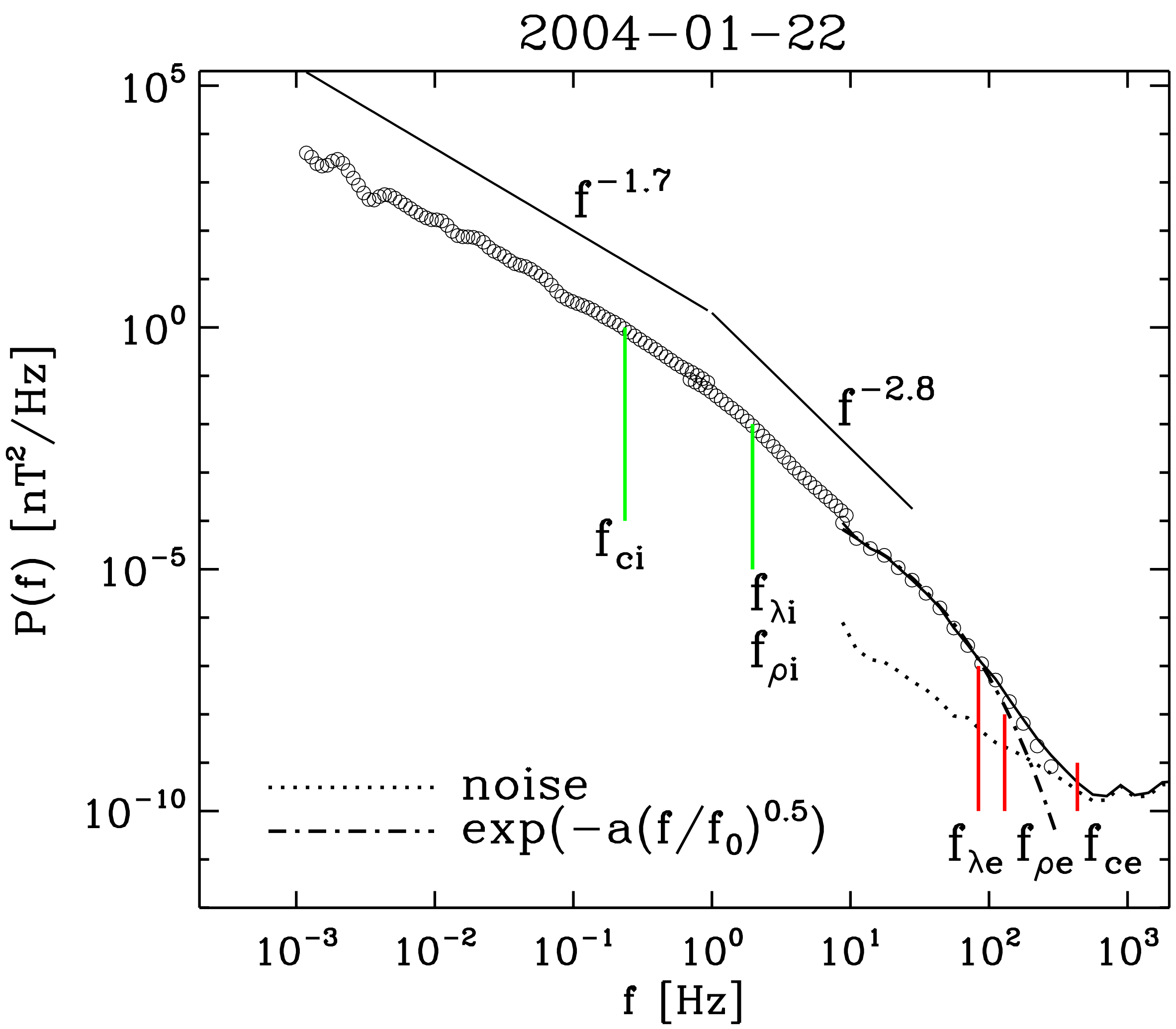

In situ magnetic energy spectrum measured by Cluster [Alexandrova et al (2009)]

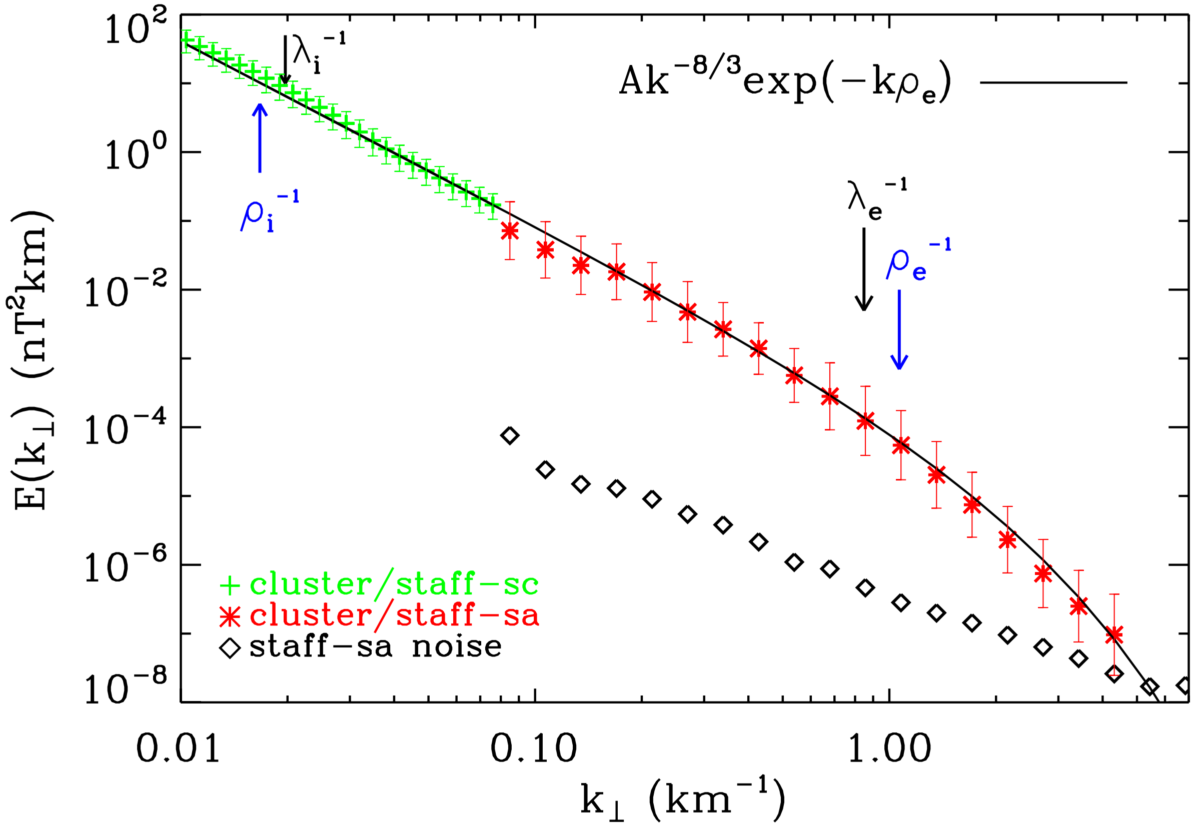

Average of 100 magnetic energy spectra from Alexandrova et al (2012).

Evidence of low frequency, oblique fluctuations

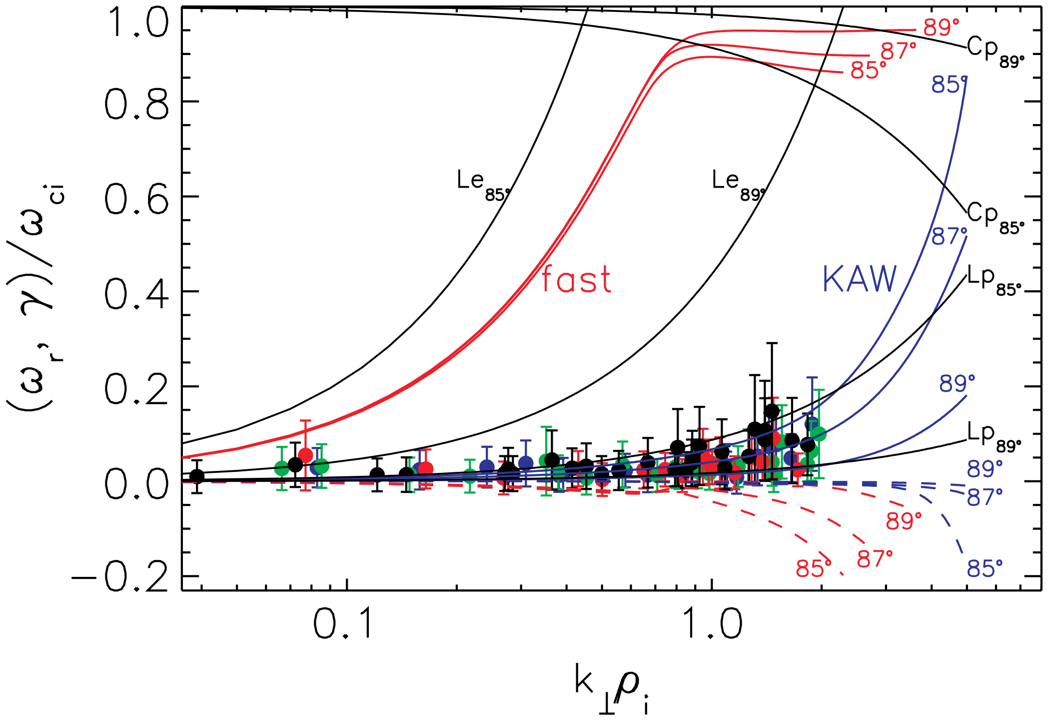

In situ solar wind dispersion relation. From Sahraoui et al (2010).

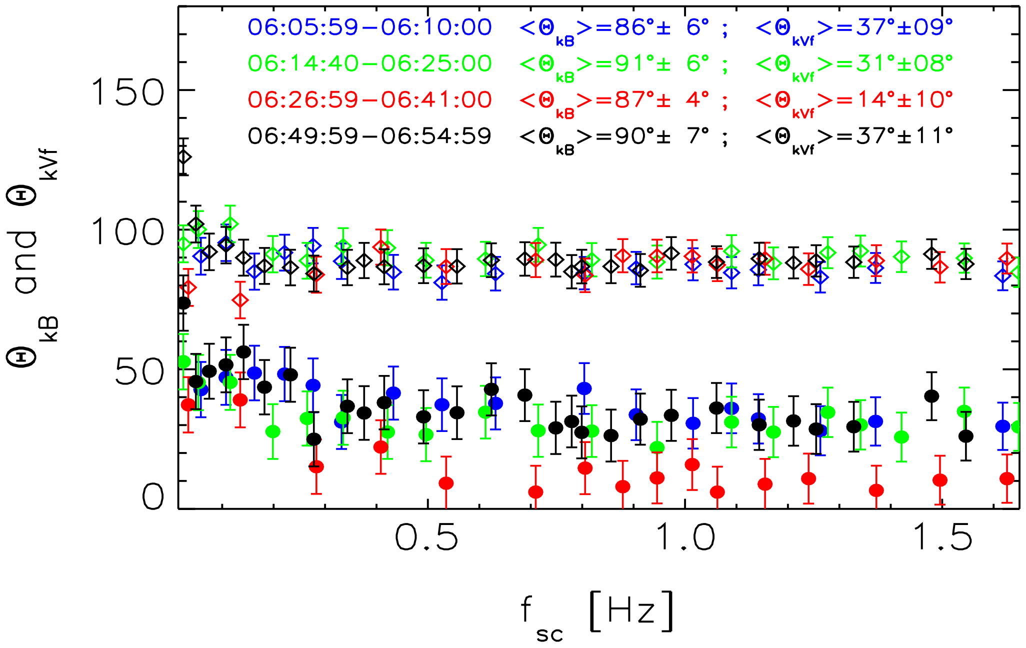

Angle between k and B and k and V_{SW}. From Sahraoui et al (2010).

In situ magnetic helicity suggests KAWs

- Magnetic helicity is a measure of the twist of the magnetic field.
- Fluctuating magnetic helicity is defined as

$$H'_m = \int d\mathbf{r} \delta \mathbf{A} \cdot \delta \mathbf{B}$$

- Normalizing and converting to Fourier space yields the normalized fluctuating magnetic helicity

$$\sigma_m(\mathbf{k}) = \frac{k H'_m(\mathbf{k})}{|\mathbf{B}(\mathbf{k})|^2}$$

- Measurements consistent with 95% power in KAW fluctuations [Klein et al (2014)].

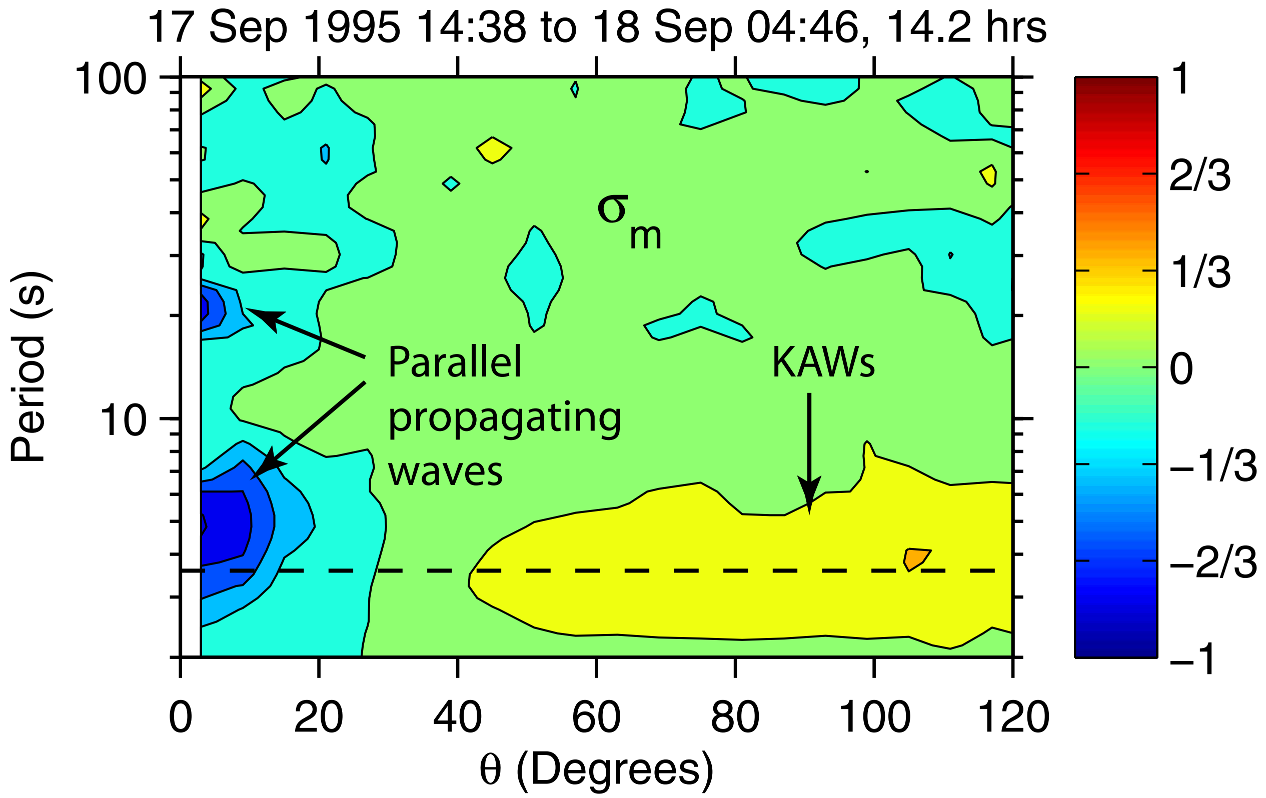

Normalized fluctuating magnetic helicity from Podesta & Gary (2011).

Intermittency in the solar wind

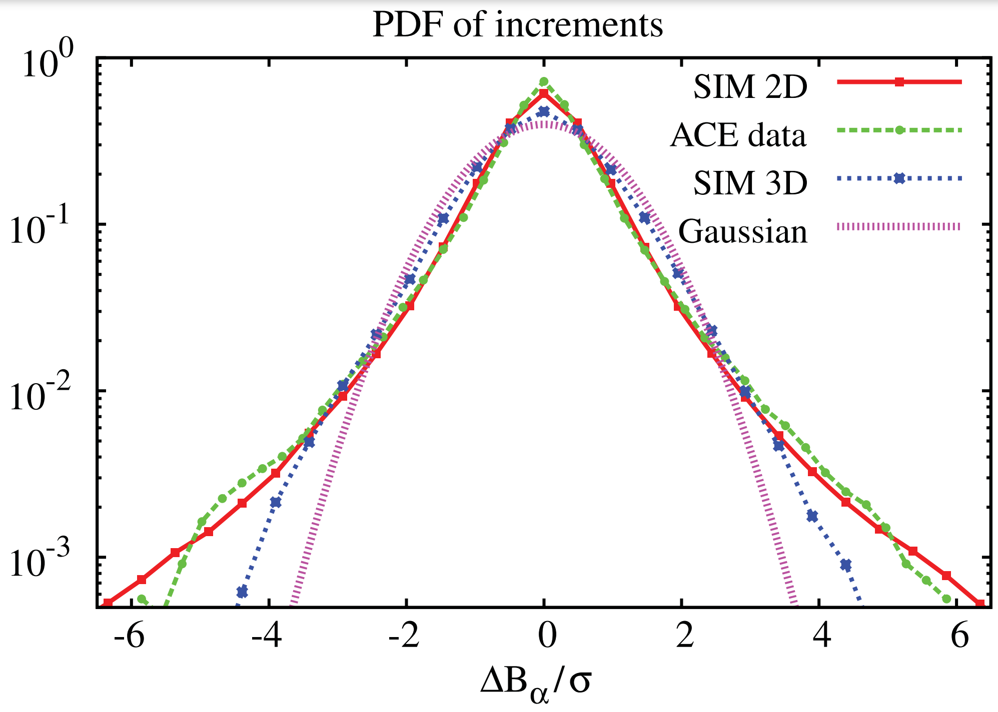

PDFs of 4 minute lag of radial solar magnetic field (green), 2D MHD, and 3D HMHD simulations. From Greco et al (2009)

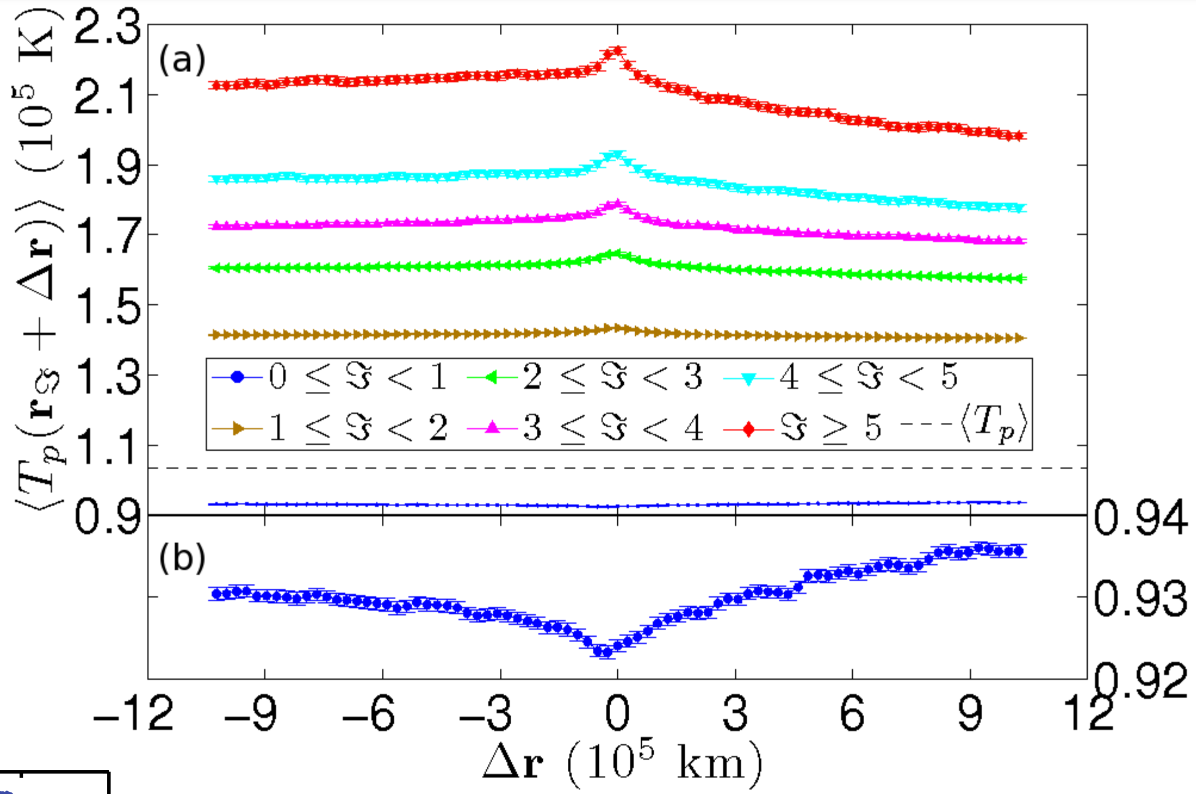

Evidence of local heating in the solar wind conditioned on PVI. From Osman et al (2012)

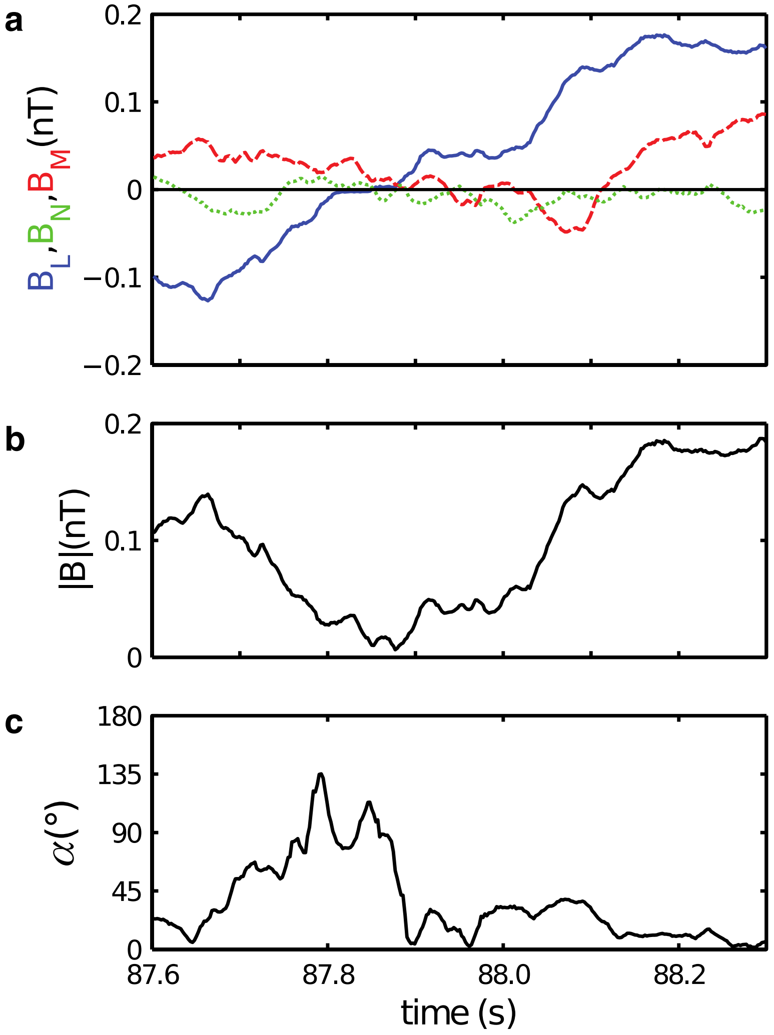

A current sheet observed in the solar wind at kinetic scales. From Perri et al (2012)

Turbulence at kinetic scales

- Anisotropic cascade of MHD Alfvén waves transitions to a cascade of kinetic Alfvén waves at the ion Larmor radius.
- Dissipation begins at ion kinetic scales in the form wave-particle interactions (Landau, transit-time, cyclotron, …).
- Current sheets also form at ion scales and may be responsible for dissipation.
- Which mechanism is dominant in weakly collisional kinetic plasmas?

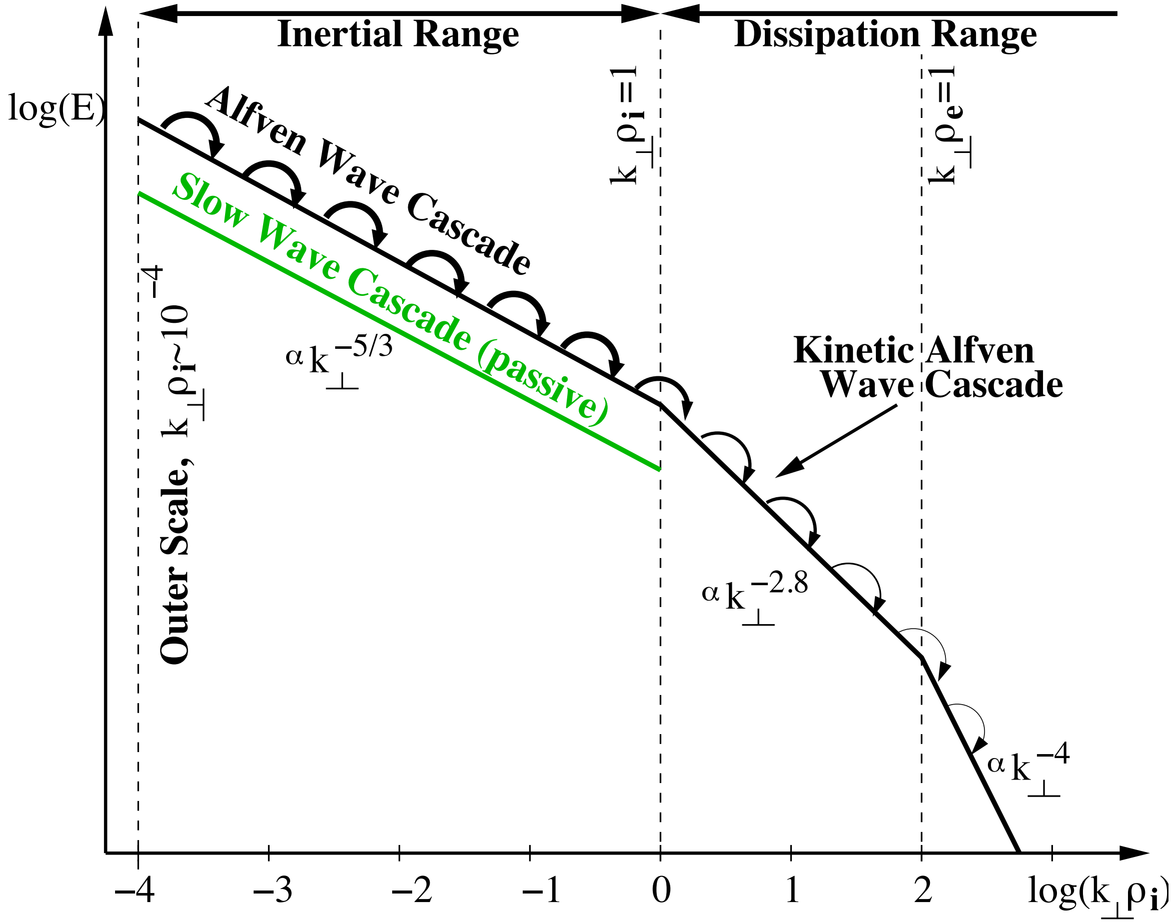

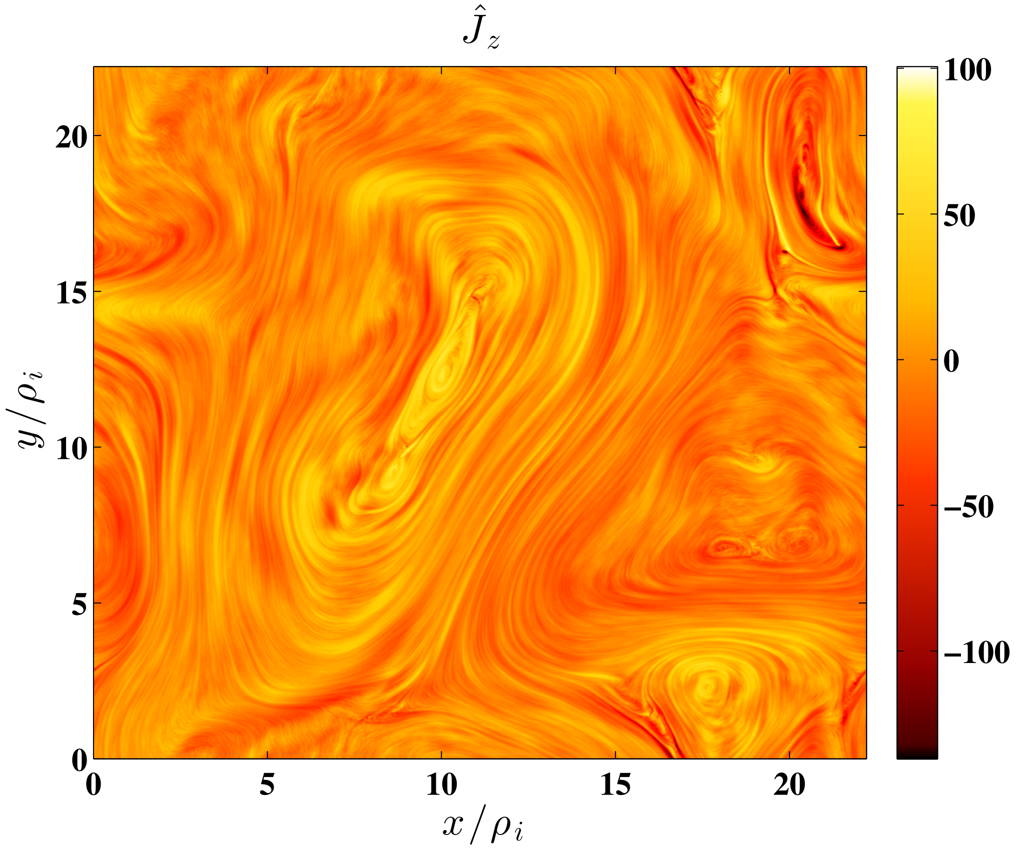

Turbulence at kinetic scales

- Anisotropic cascade of MHD Alfvén waves transitions to a cascade of kinetic Alfvén waves at the ion Larmor radius.

- Dissipation begins at ion kinetic scales in the form wave-particle interactions (Landau, transit-time, cyclotron, …).

- Current sheets also form at ion scales and may be responsible for dissipation.

- Which mechanism is dominant in weakly collisional kinetic plasmas?

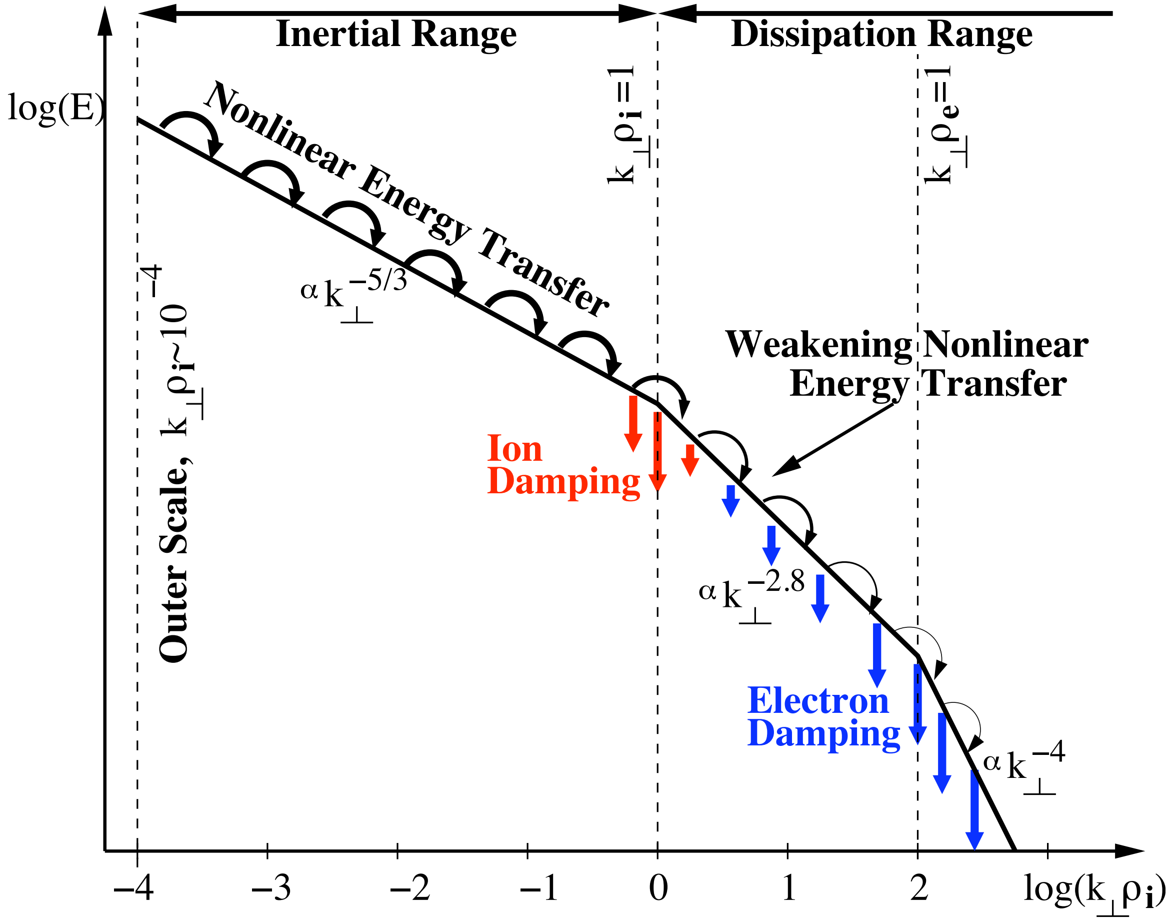

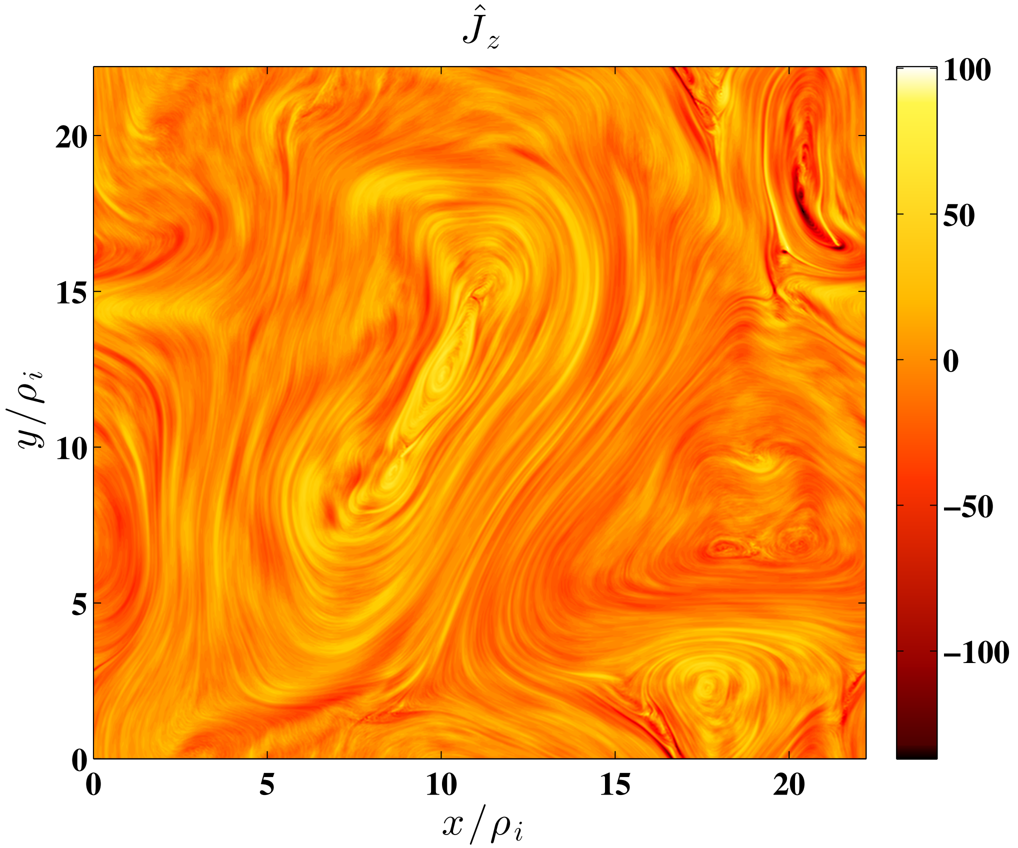

Gyrokinetic Turbulence

Gyrokinetics

What is gyrokinetics?

- Average quantities over the gyro-motion of particles and describe the evolution of rings rather than particles
- Gyro-averaged and ordered version of full Vlasov-Maxwell kinetic theory
- Basic ordering parameters:

$$\epsilon = \rho_i/L \sim \omega/\Omega_i \sim k_\parallel/k_\perp \ll 1$$

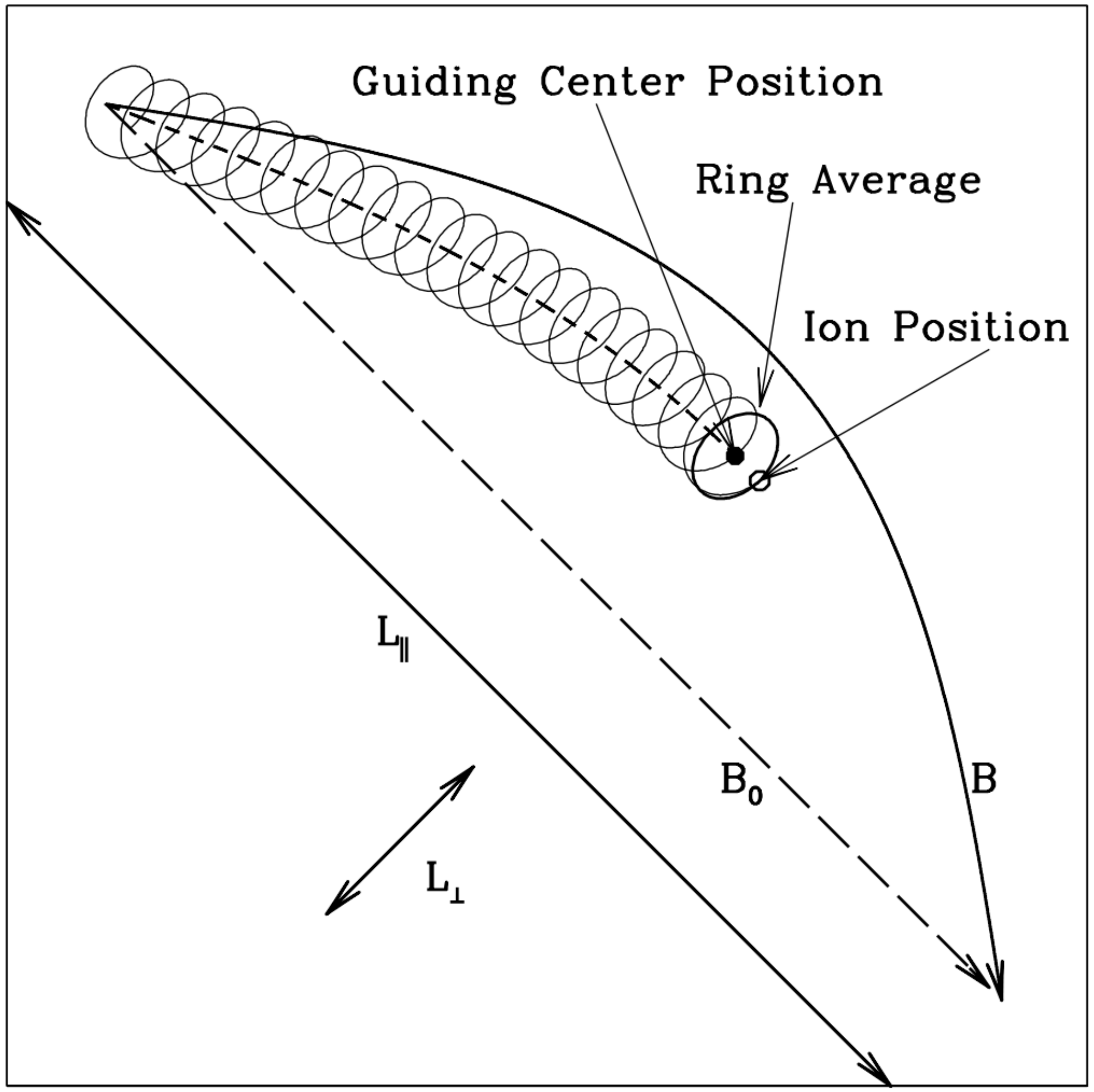

Why is it useful?

- Removes high frequency (> Ω_i) fluctuations and reduces the problem from 6 to 5 dimensions
- Retains non-linear physics and kinetic effects (FLR, Landau damping, collisions)

Gyrokinetic equations

$$f = F_0 + \delta f = F_0 \exp\left[-\frac{q\phi\left(\mathbf{r},t\right)}{T_0}\right] + h\left(\mathbf{R}, v_\parallel, v_\perp, t\right),$$

where $\mathbf{R} = \mathbf{r} + \frac{\mathbf{v}\times\hat{\mathbf{z}}}{\Omega_s}$ is the guiding center position.

$$\frac{\partial h_s}{\partial t} + v_\parallel \hat{\mathbf{z}} \cdot \frac{\partial h_s}{\partial \mathbf{R}} + \frac{c}{B_0}\left[\langle\chi\rangle_{\mathbf{R}}, h_s\right] - \left(\frac{\partial h_s}{\partial t}\right)_c = \frac{q_s}{T_0}\frac{\partial\langle\chi\rangle_R}{\partial t}F_0,$$

where $\chi = \phi - \mathbf{v}\cdot\mathbf{A}/c$ is the gyrokinetic potential and $\langle\cdot\rangle_x$ indicates gyro-averaging at constant x.

$$\sum_s\left(-\frac{q_s n_{0s}}{T_{0s}}\phi + q_s\int d^3\mathbf{v}\langle h_s\rangle_{\mathbf{r}}\right) = 0$$

$$-\nabla_\perp^2 A_\parallel = \frac{4\pi}{c}\left(\sum_s q_s \int d^3\mathbf{v} v_\parallel \langle h_s\rangle_{\mathbf{r}} + j_{\parallel ext}\right)$$

$$\nabla_\perp \delta B_\parallel = \frac{4\pi}{c}\left(\sum_s q_s \int d^3\mathbf{v}\langle\hat{\mathbf{z}}\times\mathbf{v}_\perp h_s\rangle_{\mathbf{r}} + \hat{\mathbf{z}}\times\mathbf{j}_{ext}\right)$$

AstroGK and GENE

- Based on mature fusion gyrokinetics codes
- Eulerian initial-value codes with periodic boundary conditions in slab geometry
- Evolves 5D phase space for each species
- Fully non-linear, with number, momentum, and energy conserving collision operators
- Driven at outer-scale with Langevin antenna current coupled to parallel vector potential—injects Alfvén like waves at outer-scale
- Real mass ratio, $\beta_p = 1$, $T_p = T_e$, weakly collisional ($\nu_s << \omega_{min}$)
- Have been rigorously compared to experimental results and un-ordered kinetic codes (PIC)

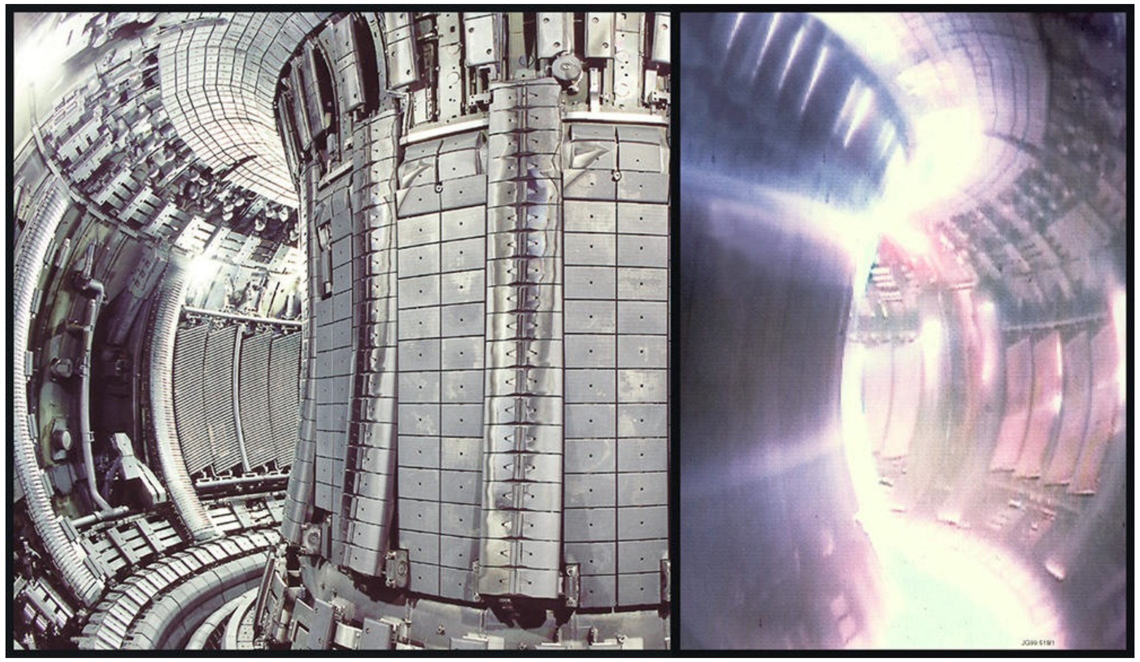

Internal view of the JET tokamak in the UK.

Ion scale spectrum

$(n_x, n_y, n_z, n_E, n_\lambda) = (128, 128, 128, 16, 32)$

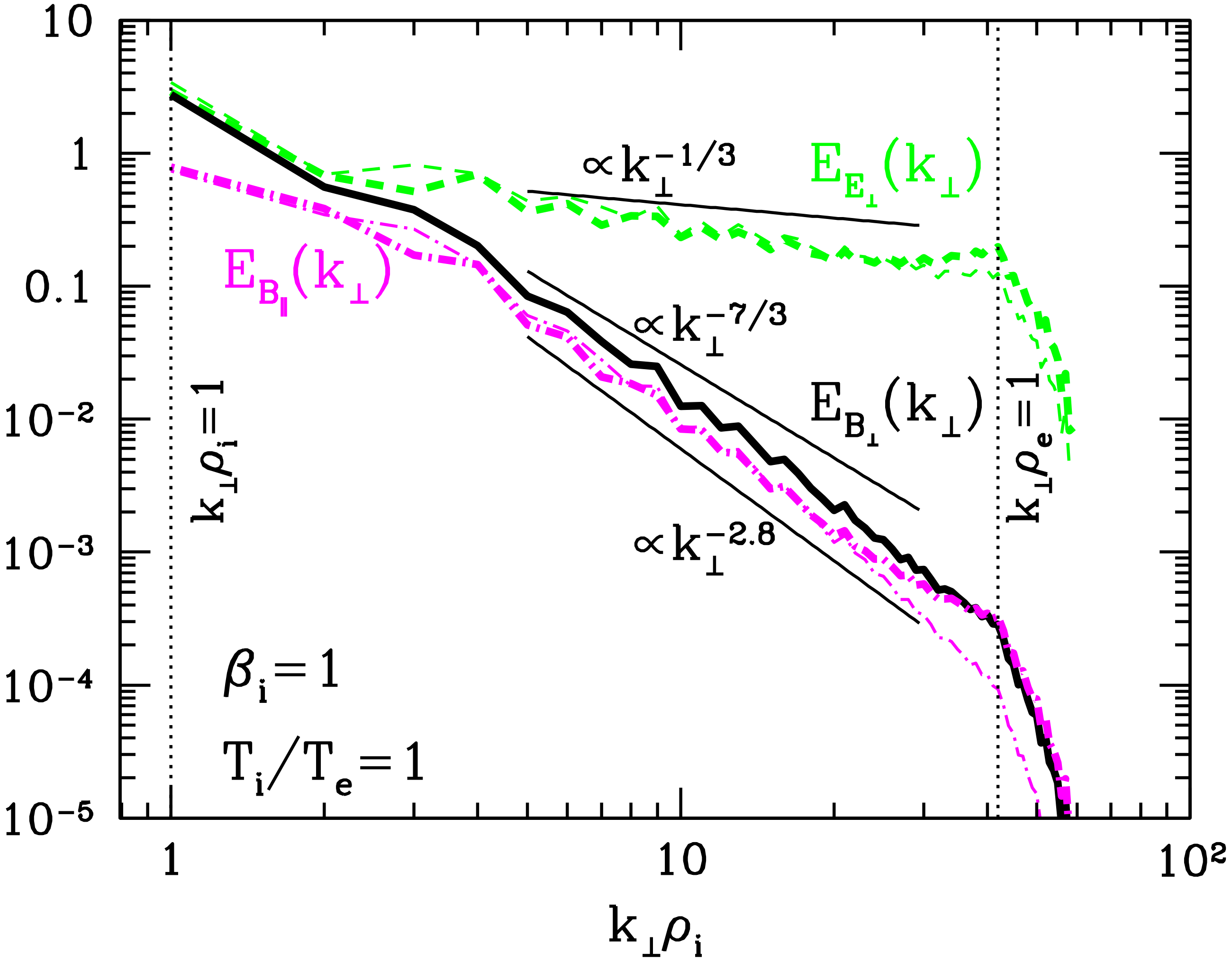

Energy spectra from AstroGK simulation from Howes et al (2011).

- Ion scale simulation, $k_\perp \rho_i \in [1, 42]$
- Spectrum agrees will with solar wind observations
- Field relationships are consistent with KAWs
- Heating broadly consistent with Landau damping and an ion entropy cascade
- Insufficient resolution to determine behavior at electron scales

Electron scale spectrum

$(n_x, n_y, n_z, n_E, n_\lambda) = (64, 64, 32, 16, 32)$

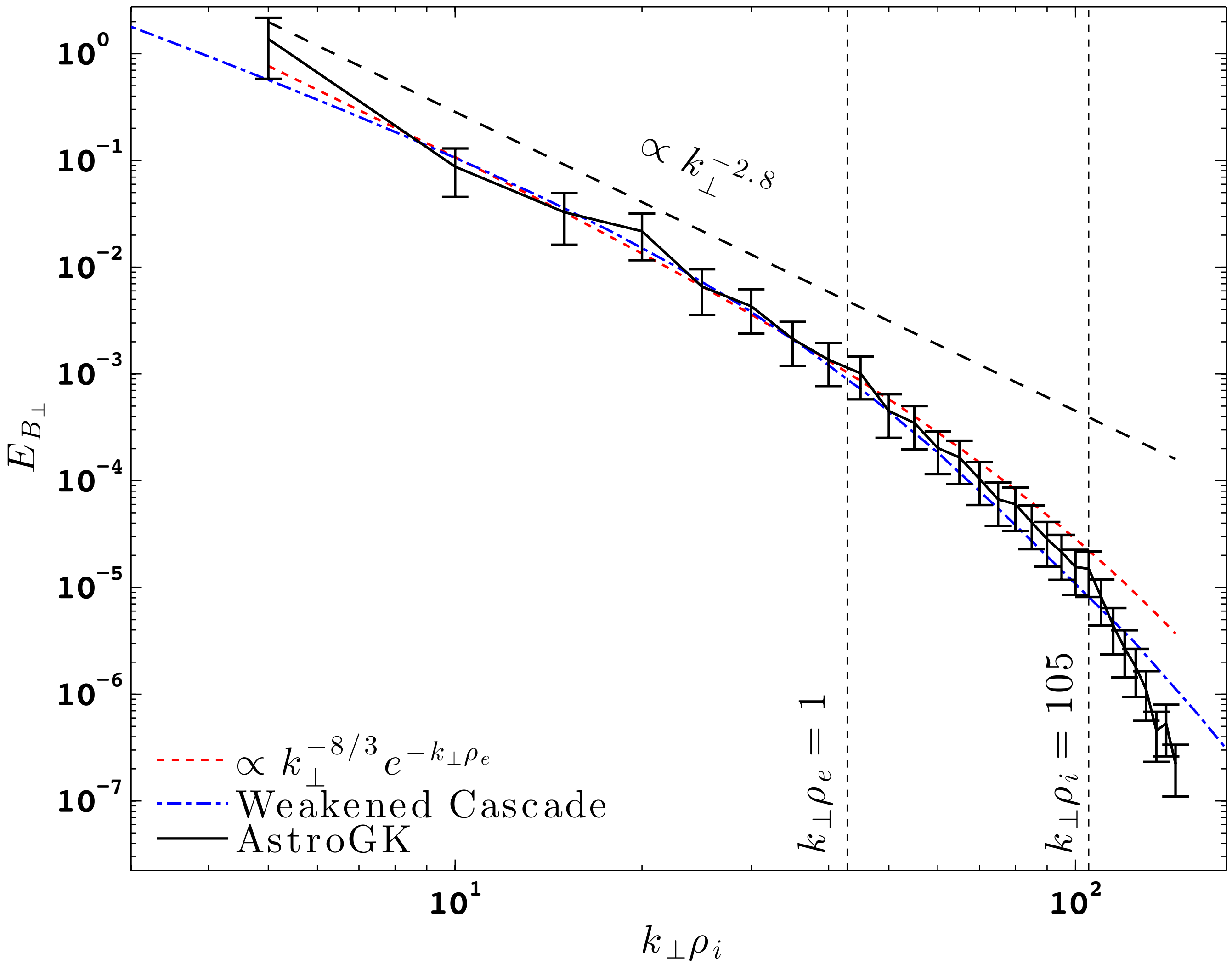

One dimensional magnetic energy spectra from AstroGK averaged over three turn-around times (black), weakened cascade model (blue dash-dotted), and the empirical form from Alexandrova et al (2012). From TenBarge et al (2013).

- Electron scale simulation, $k_\perp \rho_i \in [5, 105]$
- Averaged spectrum agrees well with in situ solar wind observations
- Also reproduced by the weakened cascade model
- Electron scale current sheets form naturally
- Measured heating rate consistent with enhanced Landau damping in current sheets

Electron collisional heating [TenBarge et al (2013)]

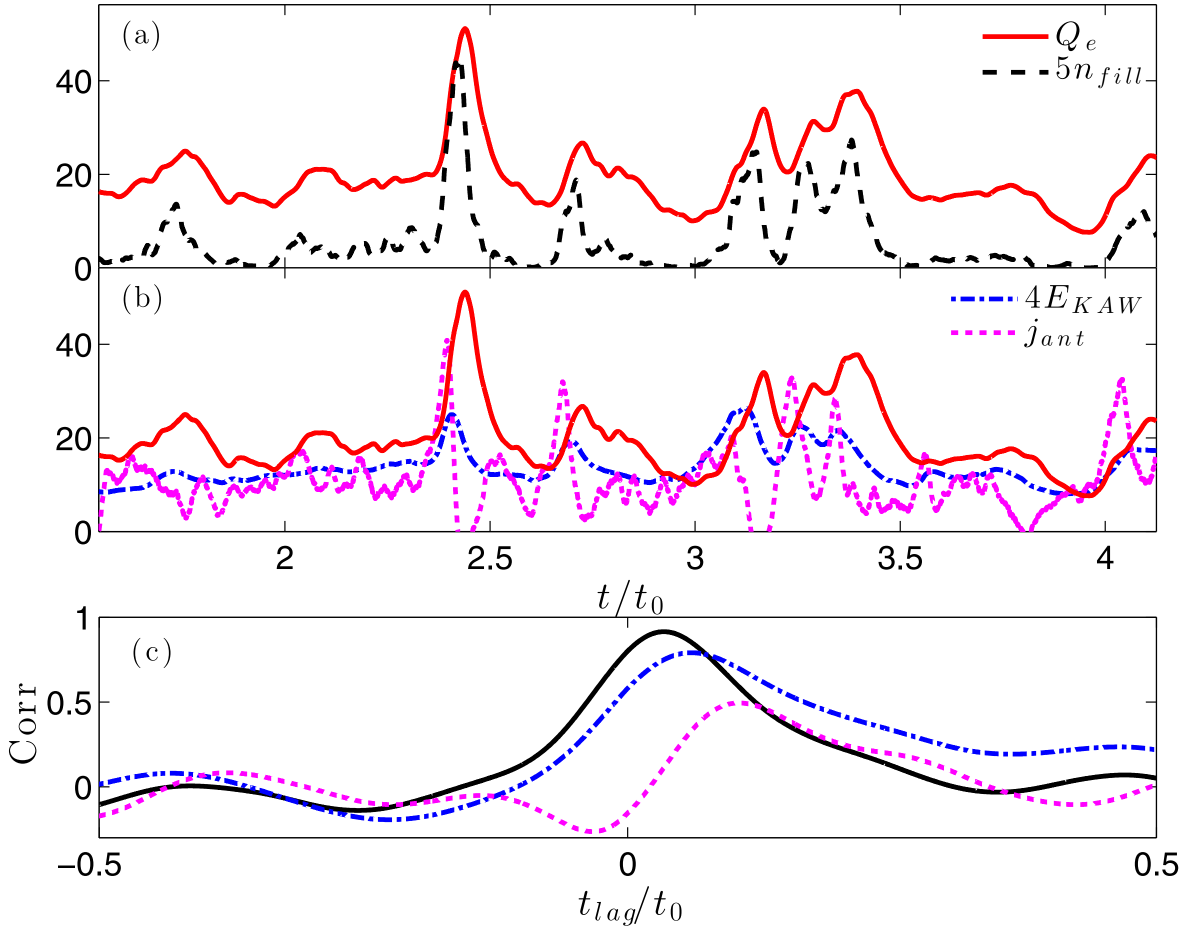

a) and b) time evolution of the collisional heating rate (red) compared to other energy diagnostics. c) Cross correlation between heating rate and other diagnostics.

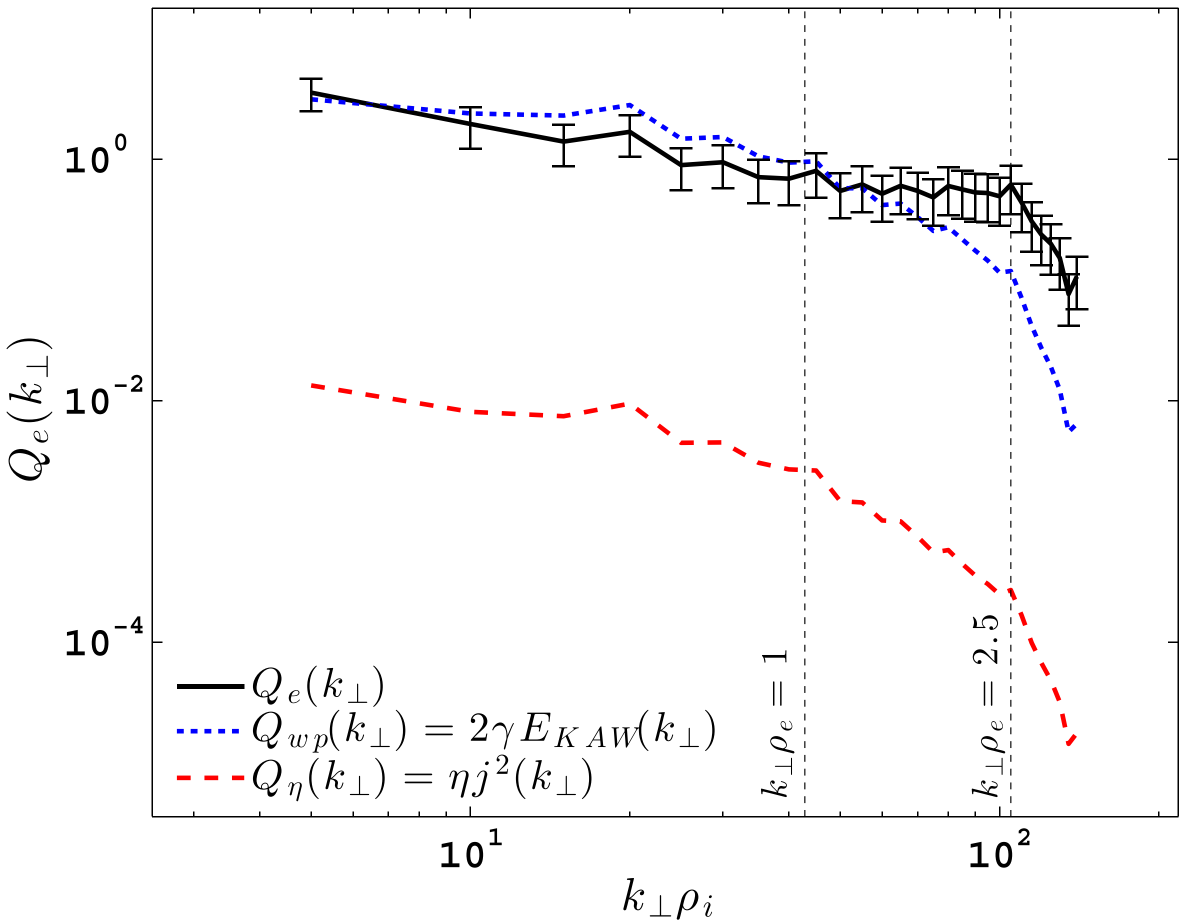

Total heating of the electrons from the simulation (solid black), an estimate of the electron heating based on linear wave-particle damping (dotted blue), and the Ohmic heating rate (dashed red).

GENE simulation energy spectra [Told et al (2015)]

GENE simulation with $(n_x, n_y, n_z, n_{v_\parallel}, n_\mu) = (768, 768, 96, 48, 15)$
Spanning $k_\perp \rho_i \in [0.28, 72]$, $L_x = L_y = 20\rho_i$, $L_z \sim 1/\epsilon$
$\beta_i = 1$, $T_{0i} = T_{0e}$, $m_i/m_e = 1836$

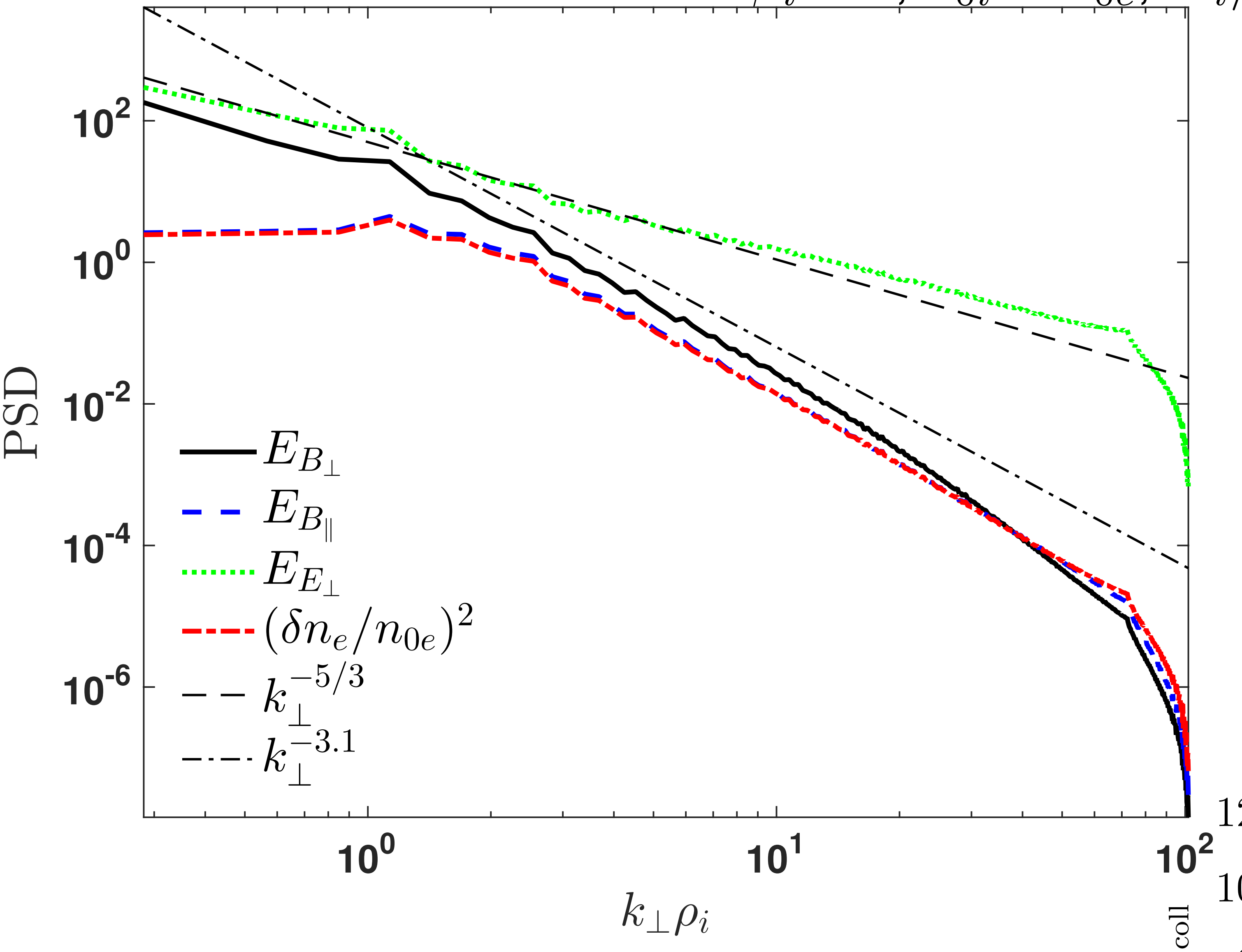

Collisional heating rates

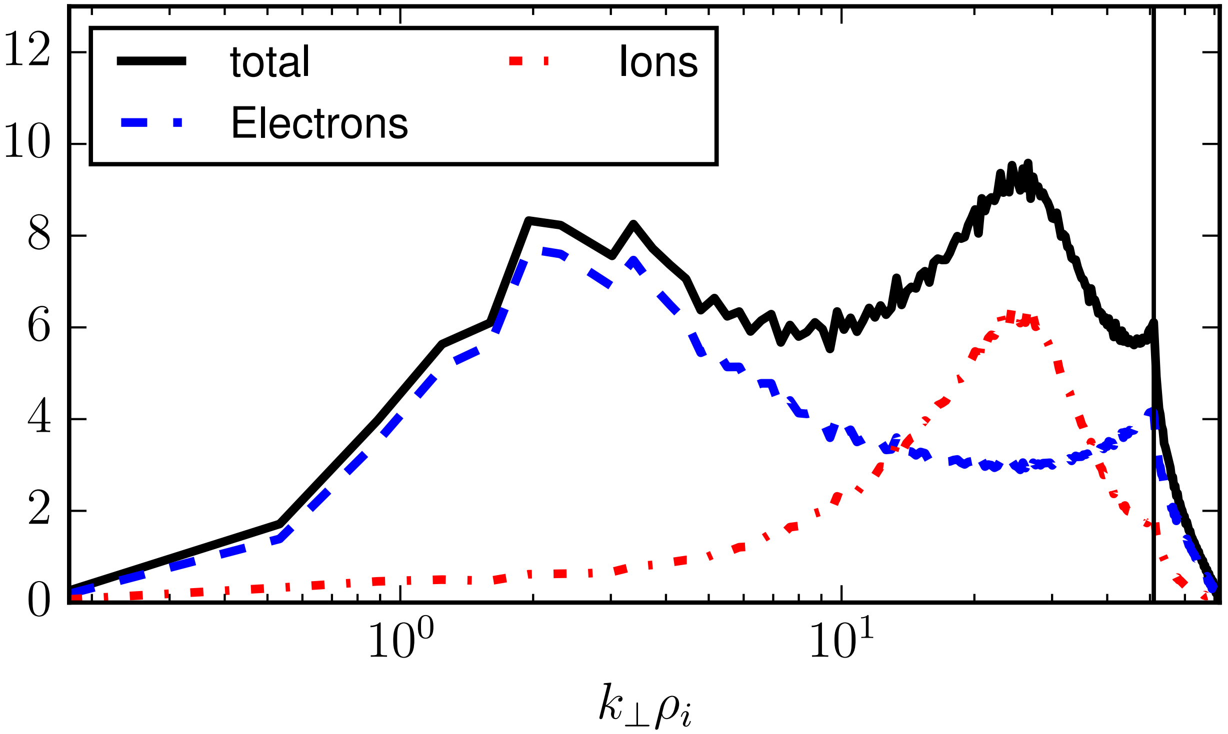

Intermittency and Coherent Structures

Measuring intermittency in the simulation

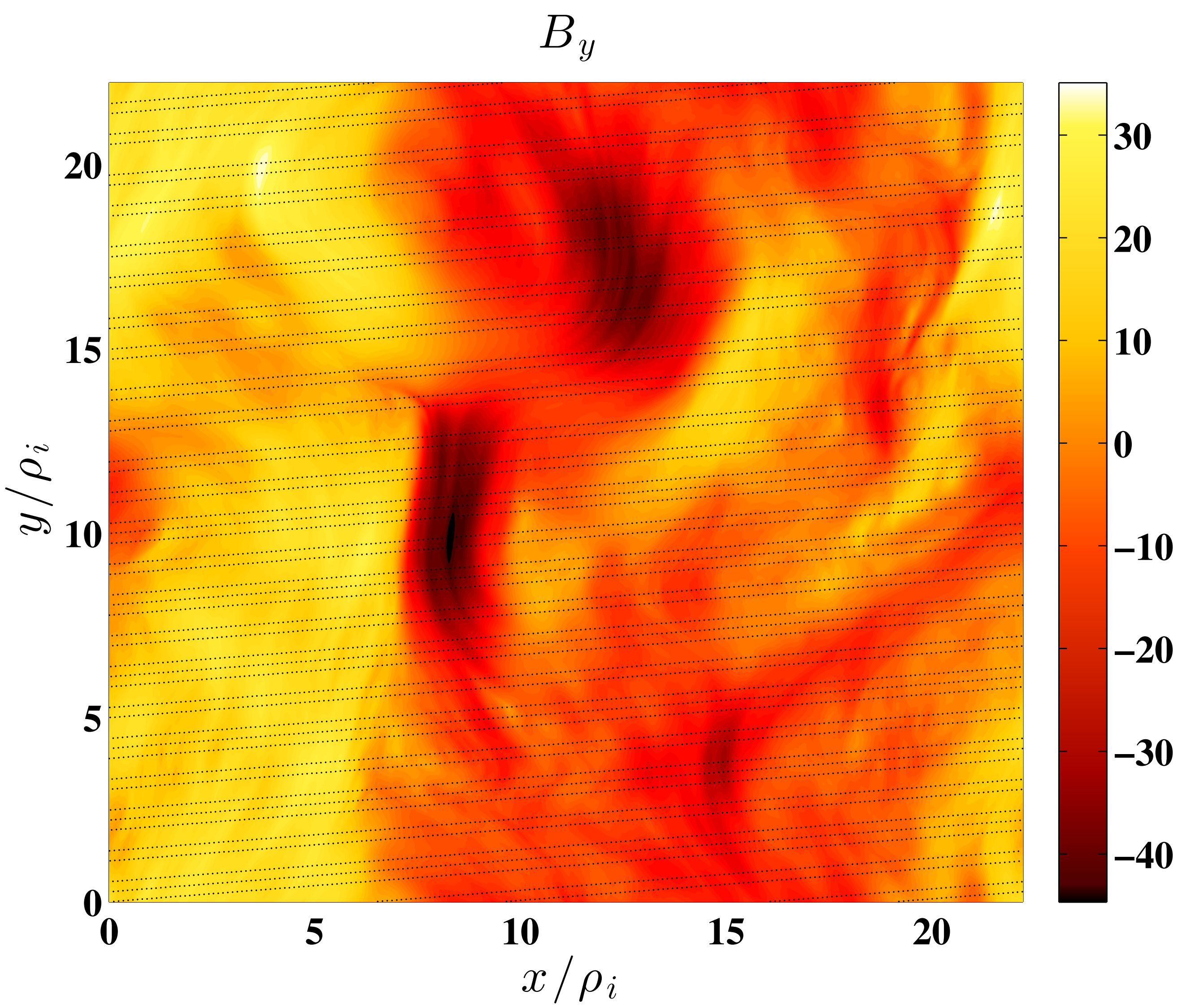

Contours of B_y with the sampling path overlaid.

Identifying intermittency

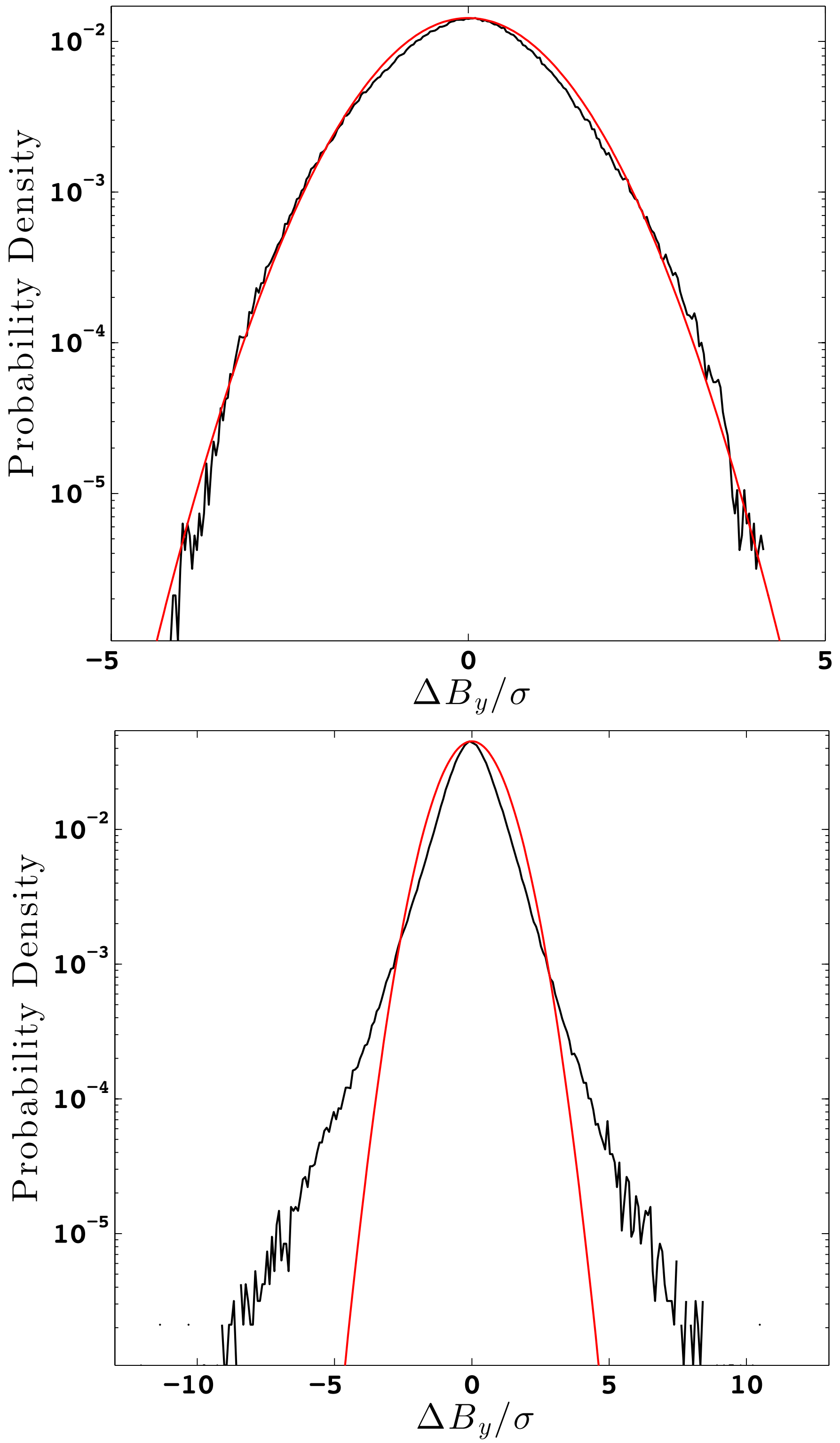

PDF of the increments with a spatial lag Δr ~ 4 ρ_i (black, upper) and Δr ~ 0.1 ρ_i (black, lower) and normal distributions (red).

Kurtosis provides a measure of the peakedness of a distribution

$$\kappa = \frac{\langle(\Delta B_y - \langle B_y\rangle)^4\rangle}{\langle(\Delta B_y - \langle B_y\rangle)^2\rangle^2}$$

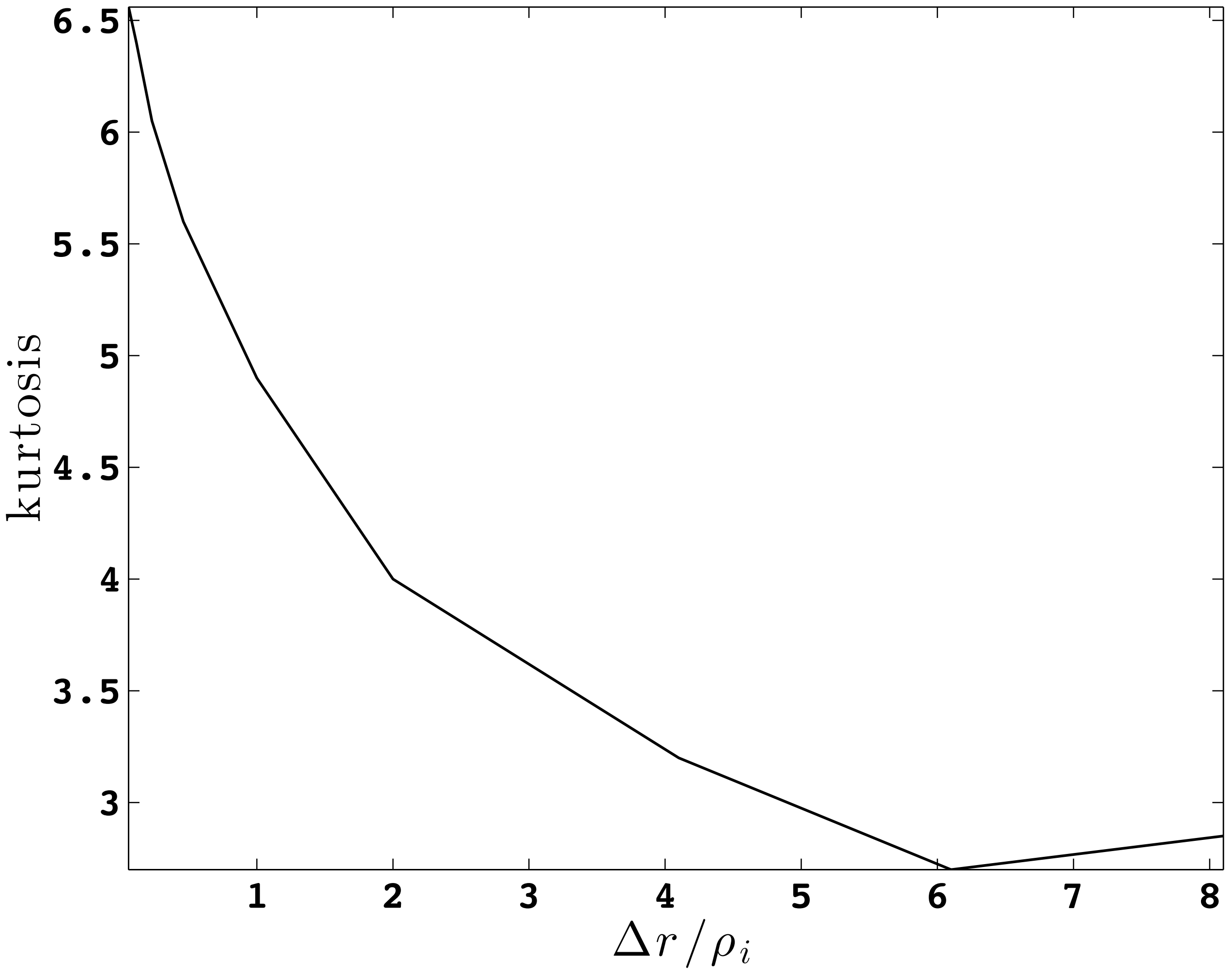

Scale dependent kurtosis indicating intermittency.

Intermittent structure identification

$$PVI = \frac{|\Delta B_y|}{\sigma}$$ Greco et al (2008)

$$\theta = \cos^{-1}\left[\frac{\mathbf{B}(\mathbf{x})\cdot\mathbf{B}(\mathbf{x}+\Delta\mathbf{r})}{|\mathbf{B}(\mathbf{x})||\mathbf{B}(\mathbf{x}+\Delta\mathbf{r})|}\right]$$

$$B_L = \max(|B_y(\mathbf{x})|, |B_y(\mathbf{x}+\Delta\mathbf{r})|)$$

Tsurutani & Smith (1979)

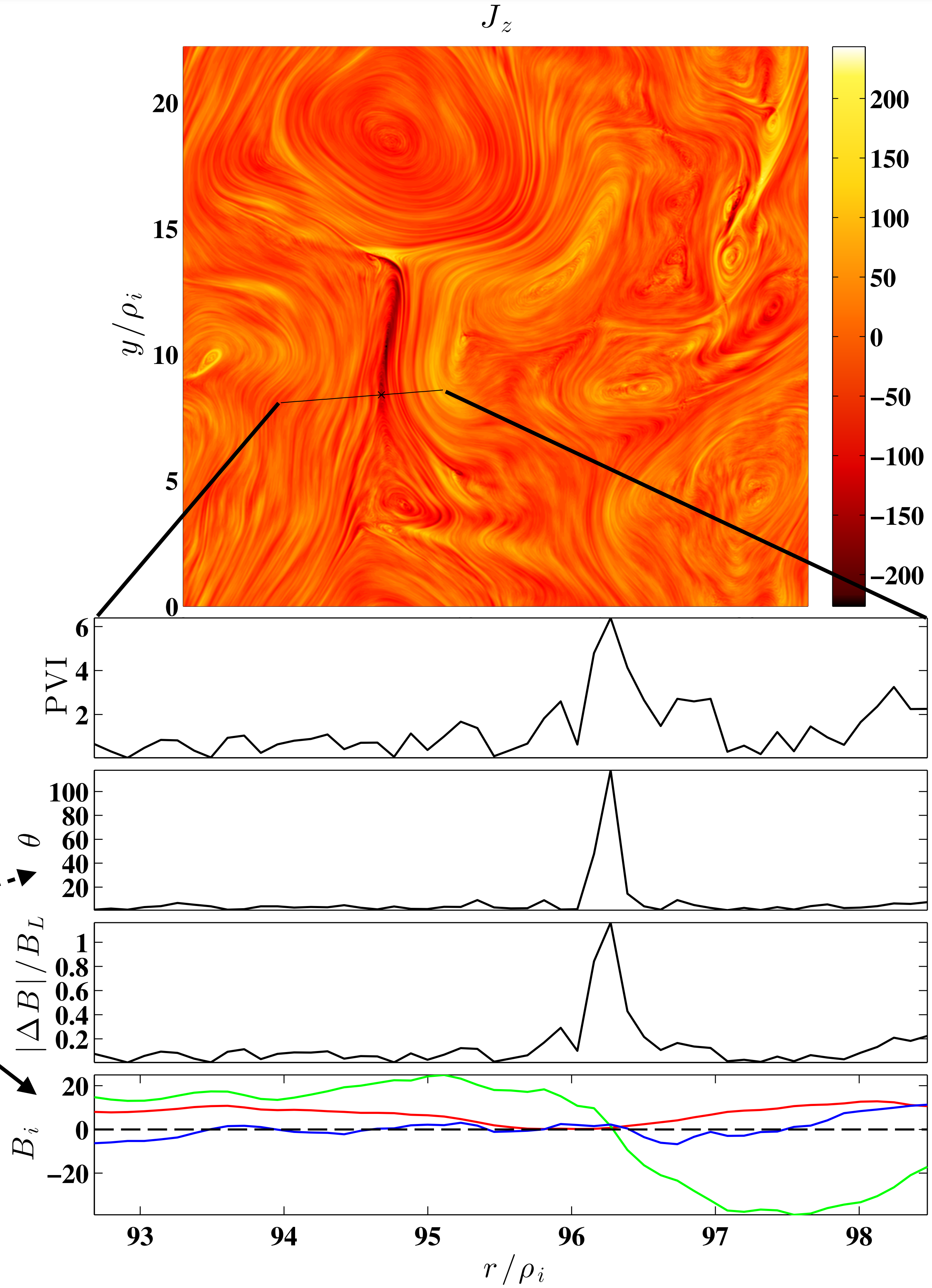

A comparison of methods to ID discontinuous structures

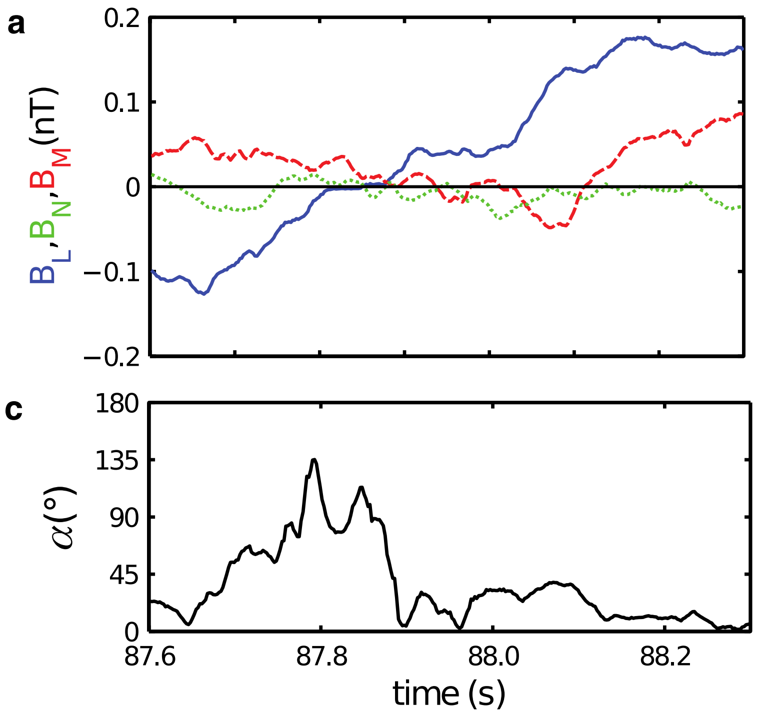

High pass filtered solar wind data from Perri et al, PRL (2012)

Fractal scaling

To quantify the intermittency and get a handle on the spatial structure, we employ a common high-order multi-scale analysis to determine the fractal nature of the turbulence:

$$S_i^m(\Delta r) = \frac{1}{N}\sum_{j=1}^{N} |\Delta B_i(\mathbf{r}_j, \Delta \mathbf{r})|^m \propto \Delta r^{\zeta(m)},$$

where

$$\Delta B_i(\mathbf{r}, \Delta r) = B_i(\mathbf{r} + \Delta \mathbf{r}) - B_i(\mathbf{r}).$$

If the scaling exponent, ζ, satisfies $\zeta(m) = Hm$, then the turbulence is monofractal, i.e., the turbulence is globally scale invariant.

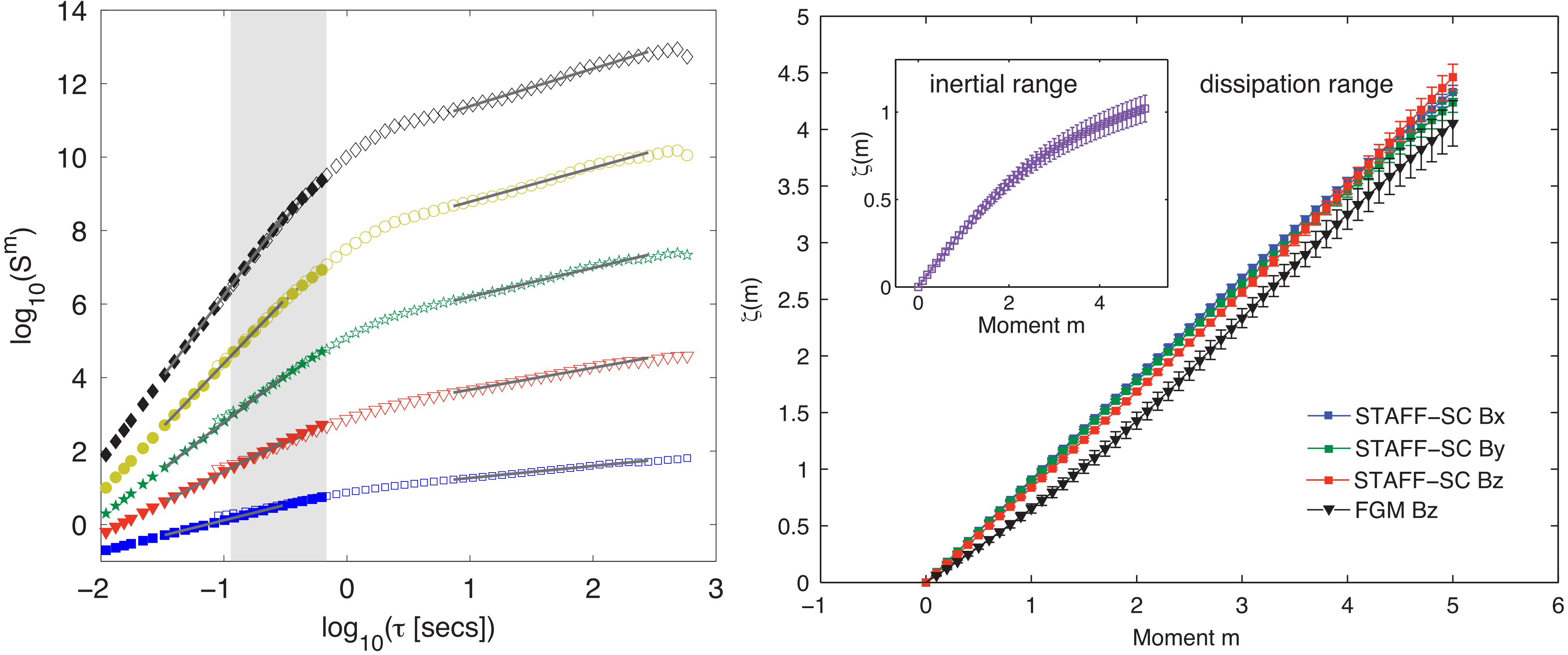

Cluster solar wind data from Kiyani et al, PRL (2009) depicting a multi-fractal inertial range and mono-fractal dissipation range. H ~ 0.85 in the dissipation range.

Fractal scaling in the simulation

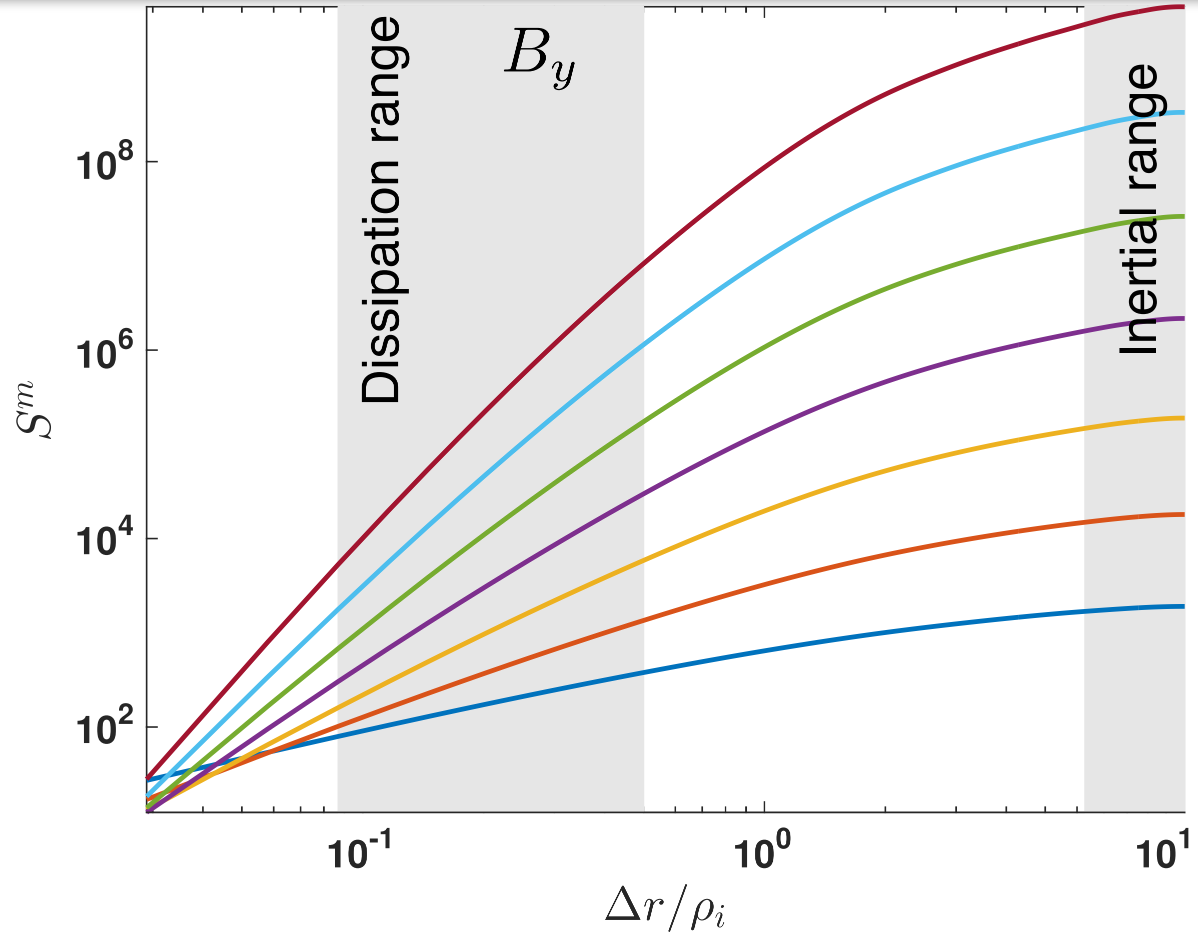

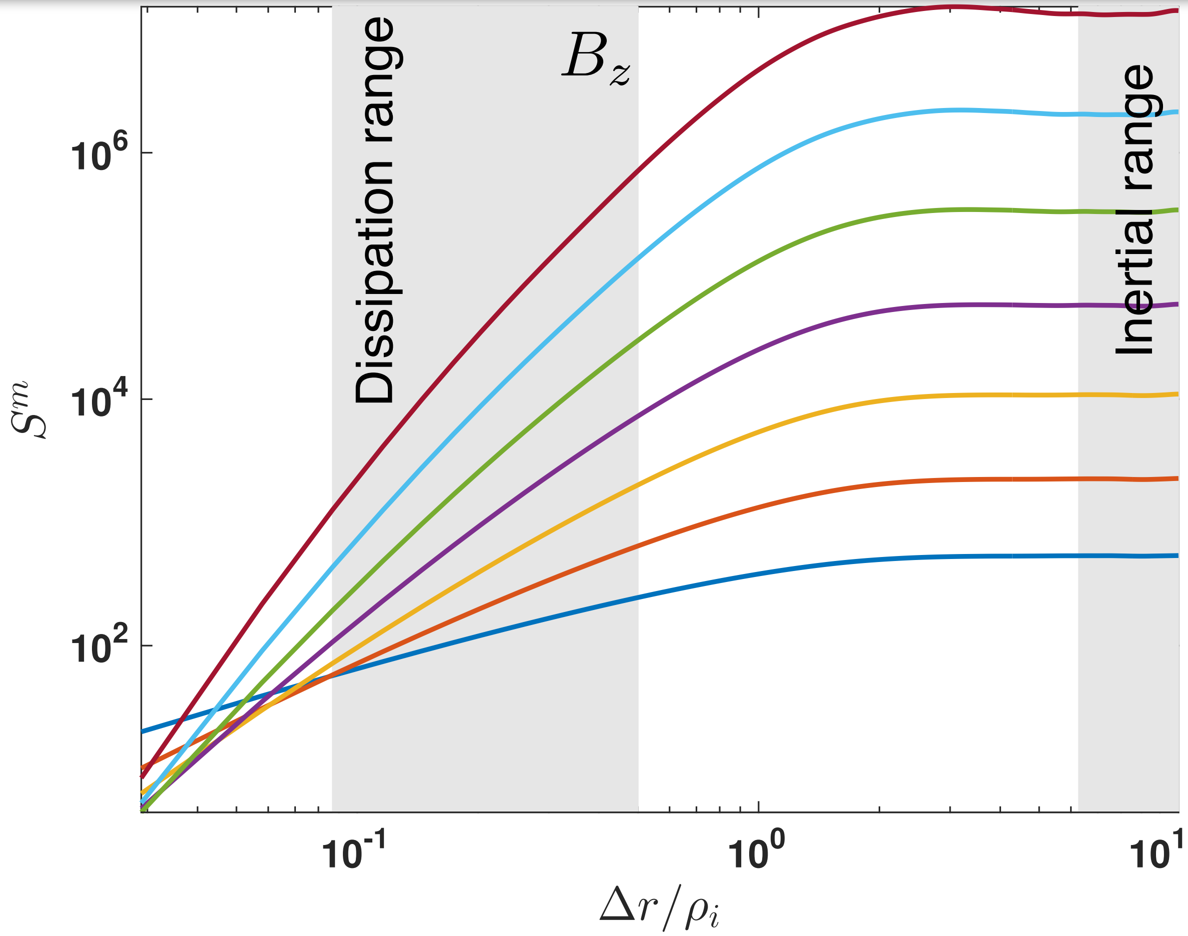

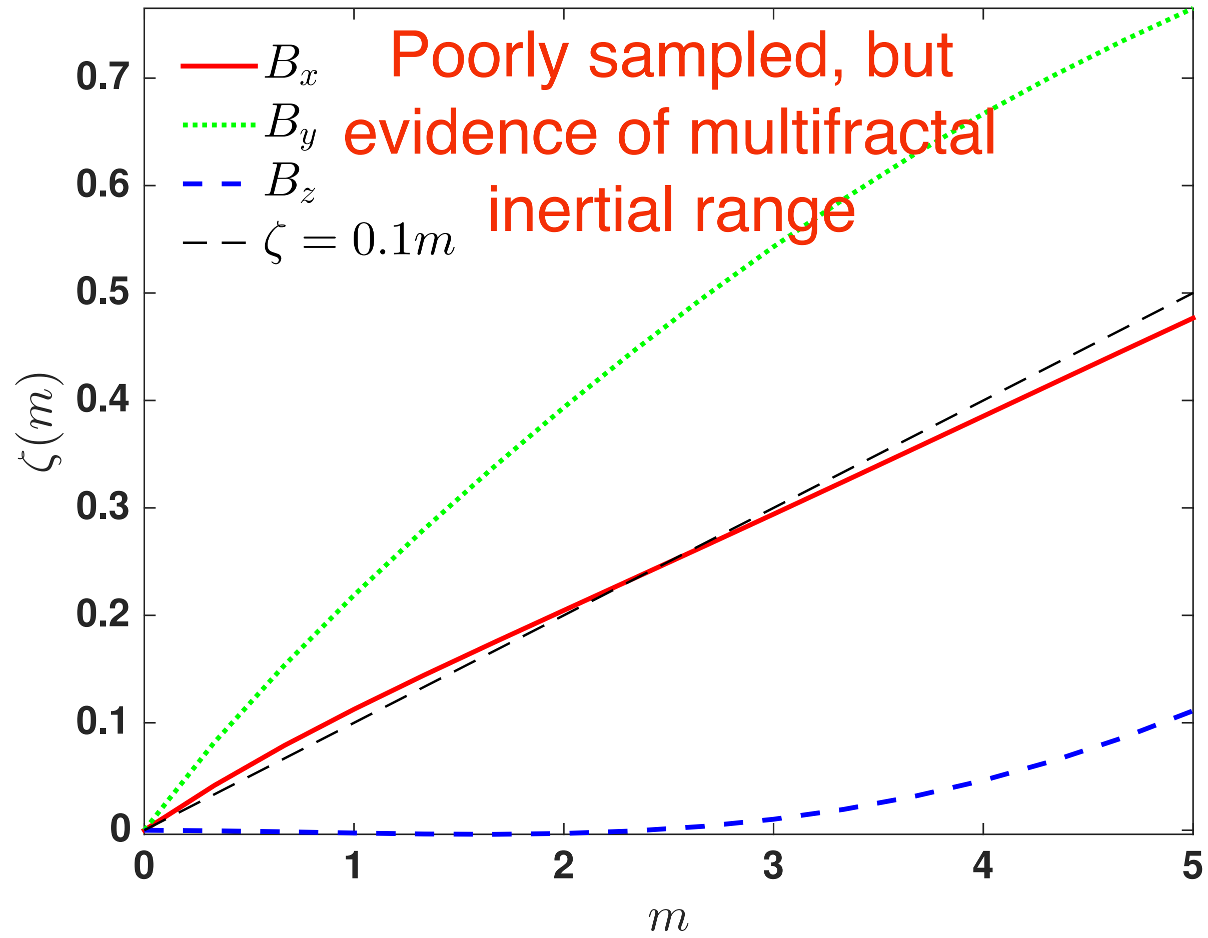

Poorly sampled, but evidence of multifractal inertial range

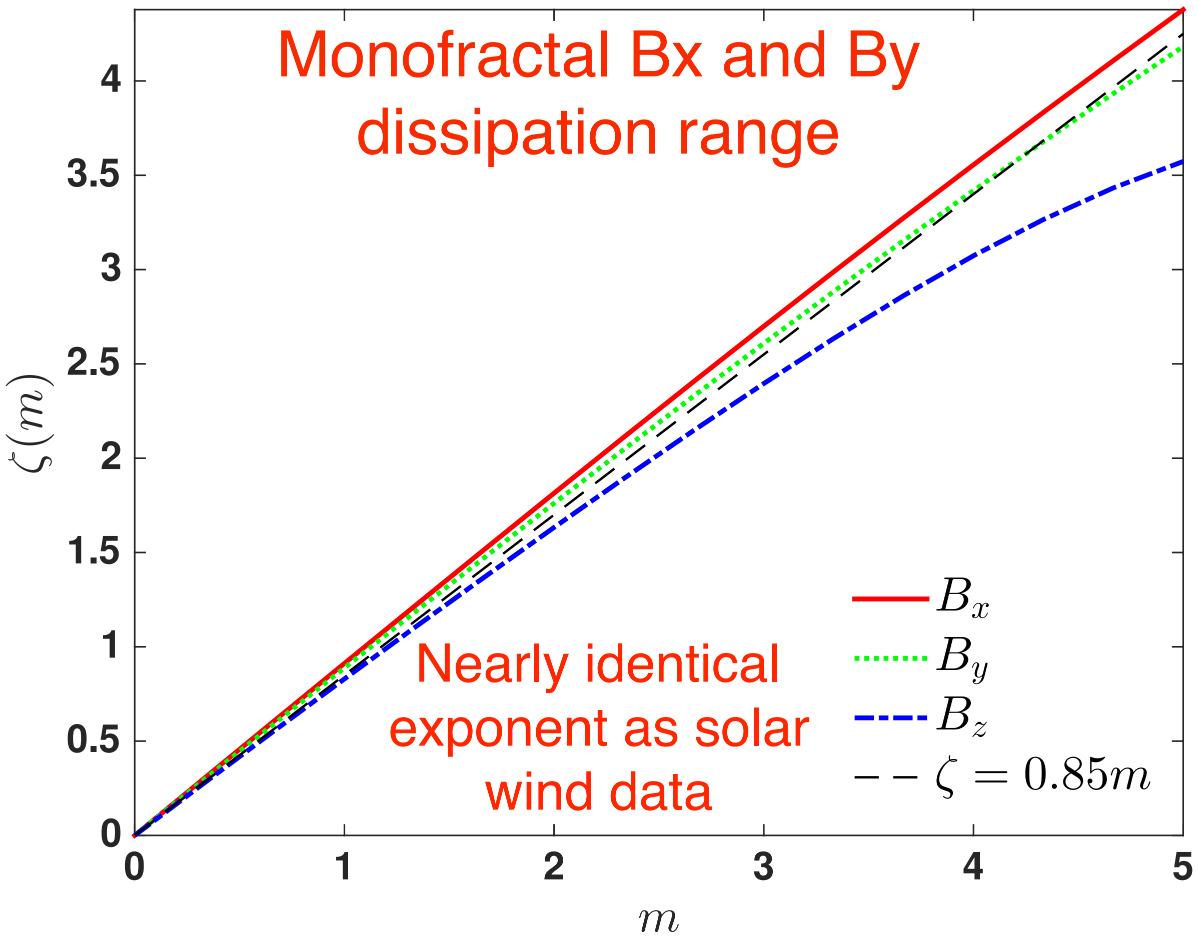

Monofractal Bx and By dissipation range

Nearly identical exponent as solar wind data

Field-Particle Correlations

Vlasov-Poisson [Howes et al submitted]

$$\frac{\partial f_s}{\partial t} + v\frac{\partial f_s}{\partial x} - \frac{q_s}{m_s}\frac{\partial \phi}{\partial x}\frac{\partial f_s}{\partial v} = 0$$

$$f_s(x,v,t) = f_{s0}(v) + \delta f_s(x,v,t)$$

$$\frac{\partial \delta f_s}{\partial t} = -v\frac{\partial \delta f_s}{\partial x} + \frac{q_s}{m_s}\frac{\partial \phi}{\partial x}\frac{\partial f_{s0}}{\partial v} + \frac{q_s}{m_s}\frac{\partial \phi}{\partial x}\frac{\partial \delta f_s}{\partial v}$$

$$\frac{\partial W_s}{\partial t} = \int dx \int dv \frac{1}{2} m_s v^2 \left[-v\frac{\partial \delta f_s}{\partial x} + \frac{q_s}{m_s}\frac{\partial \phi}{\partial x}\frac{\partial f_{s0}}{\partial v} + \frac{q_s}{m_s}\frac{\partial \phi}{\partial x}\frac{\partial \delta f_s}{\partial v} \right]$$

Vlasov-Poisson [Howes et al submitted]

$$\frac{\partial f_s}{\partial t} + v\frac{\partial f_s}{\partial x} - \frac{q_s}{m_s}\frac{\partial \phi}{\partial x}\frac{\partial f_s}{\partial v} = 0$$

$$f_s(x,v,t) = f_{s0}(v) + \delta f_s(x,v,t)$$

$$\frac{\partial \delta f_s}{\partial t} = -v\frac{\partial \delta f_s}{\partial x} + \frac{q_s}{m_s}\frac{\partial \phi}{\partial x}\frac{\partial f_{s0}}{\partial v} + \frac{q_s}{m_s}\frac{\partial \phi}{\partial x}\frac{\partial \delta f_s}{\partial v}$$

$$\frac{\partial W_s}{\partial t} = \int dx \int dv \frac{1}{2} m_s v^2 \left[-v\xcancel{\frac{\partial \delta f_s}{\partial x}} + \frac{q_s}{m_s}\xcancel{\frac{\partial \phi}{\partial x}\frac{\partial f_{s0}}{\partial v}} + \frac{q_s}{m_s}\frac{\partial \phi}{\partial x}\frac{\partial \delta f_s}{\partial v}\right]$$

$$\frac{\partial W_s}{\partial t} = -\int dx \int dv\ q_s \frac{v^2}{2}\frac{\partial \delta f_s(x,v,t)}{\partial v} E(x,t) = \int dx \int dv\ q_s v \delta f_s(x,v,t) E(x,t)$$

Vlasov-Poisson [Howes et al submitted]

$$\frac{\partial f}{\partial t} + v\frac{\partial f}{\partial x} + \frac{q}{m}E\frac{\partial f}{\partial v} = 0$$

$$\frac{\partial w}{\partial t} = \int dx \int dv \frac{1}{2}mv^2 \left[\cancel{-v\frac{\partial f}{\partial x}} - \frac{q}{m}E\frac{\partial f}{\partial v}\right]$$

$$\frac{\partial w}{\partial t} = -\int dx \int dv \frac{1}{2}mv^2 \frac{q}{m}E\frac{\partial f}{\partial v} = \int dx \int dv qvEf = \int j_s E$$

$$\frac{\partial W_s}{\partial t} = -\int dx \int dv\ q_s \frac{v^2}{2}\frac{\partial \delta f_s(x,v,t)}{\partial v}E(x,t) = \int dx \int dv\ q_s v \delta f_s(x,v,t)E(x,t)$$

$$\frac{\partial W_s}{\partial t} = -\int dx \frac{\partial \phi}{\partial x}\int dv\ q_s v \delta f_s = \int dx\ j_s E$$

Vlasov-Poisson

$$\frac{\partial W_s}{\partial t} = -\int dx \int dv\; q_s \frac{v^2}{2} \frac{\partial \delta f_s(x,v,t)}{\partial v} E(x,t) = \int dx \int dv\; q_s v \delta f_s(x,v,t) E(x,t)$$

$$C_1(v,t,\tau) = C_\tau \left(-q_s \frac{v^2}{2} \frac{\partial \delta f_s(x_0,v,t)}{\partial v}, E(x_0,t) \right)$$

$$C_2(v,t,\tau) = C_\tau \left(q_s v \delta f_s(x_0,v,t), E(x_0,t) \right)$$

$$C_1(v,t_i,\tau) = \frac{1}{N} \sum_{j=i}^{i+N} q_s \frac{v^2}{2} \frac{\partial \delta f_{sj}(v)}{\partial v} E_j$$

$$t_j \equiv t(j\Delta t) \qquad\qquad \tau = N\Delta t,$$

Components of the distribution function

$$\frac{\partial \delta f_{sB}}{\partial t} = -v\frac{\partial \delta f_s}{\partial x}$$

$$\frac{\partial \delta f_{sWl}}{\partial t} = \frac{q_s}{m_s}\frac{\partial \phi}{\partial x}\frac{\partial f_{s0}}{\partial v}$$

$$\frac{\partial \delta f_{sWn}}{\partial t} = \frac{q_s}{m_s}\frac{\partial \phi}{\partial x}\frac{\partial \delta f_s}{\partial v}$$

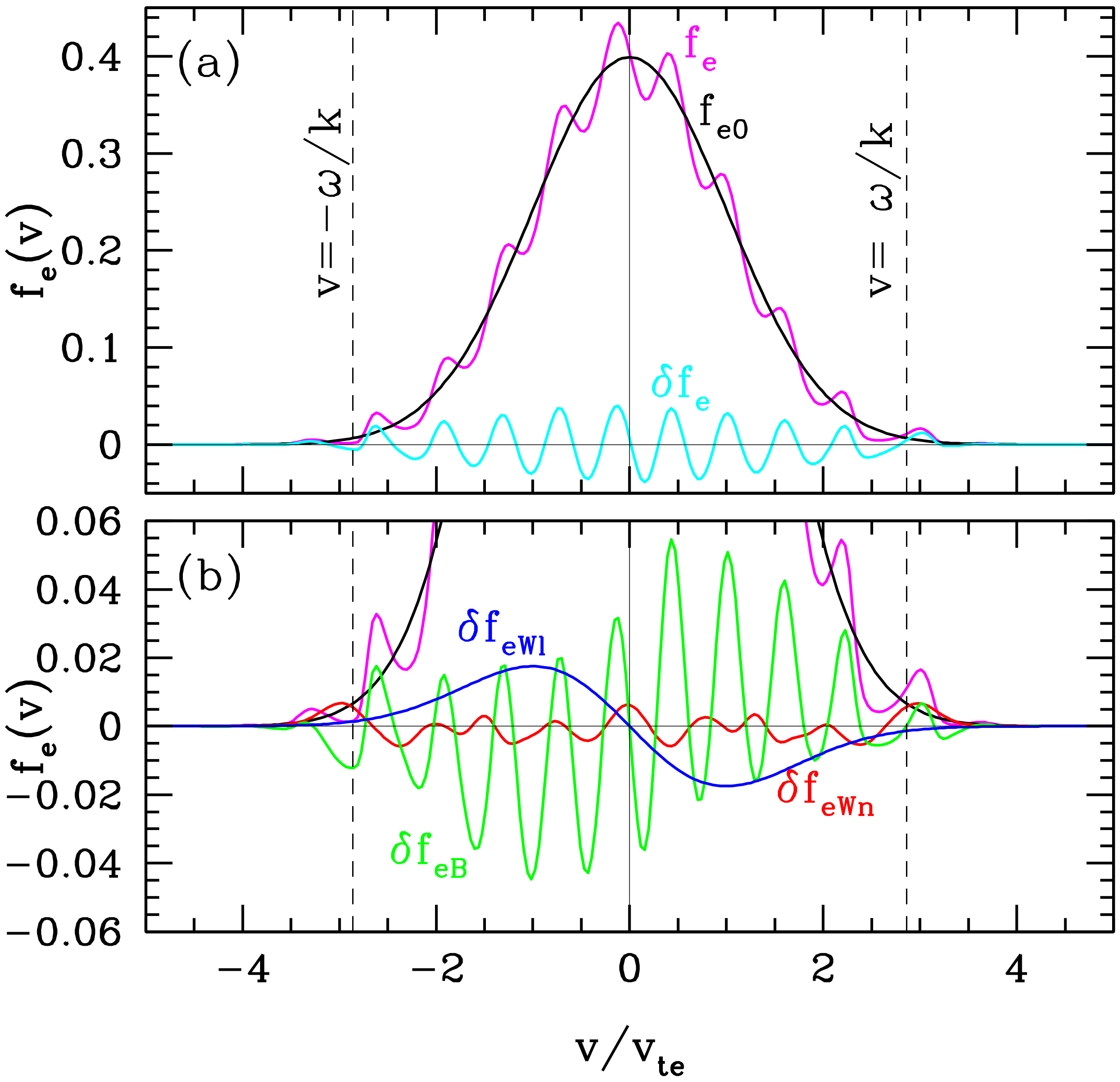

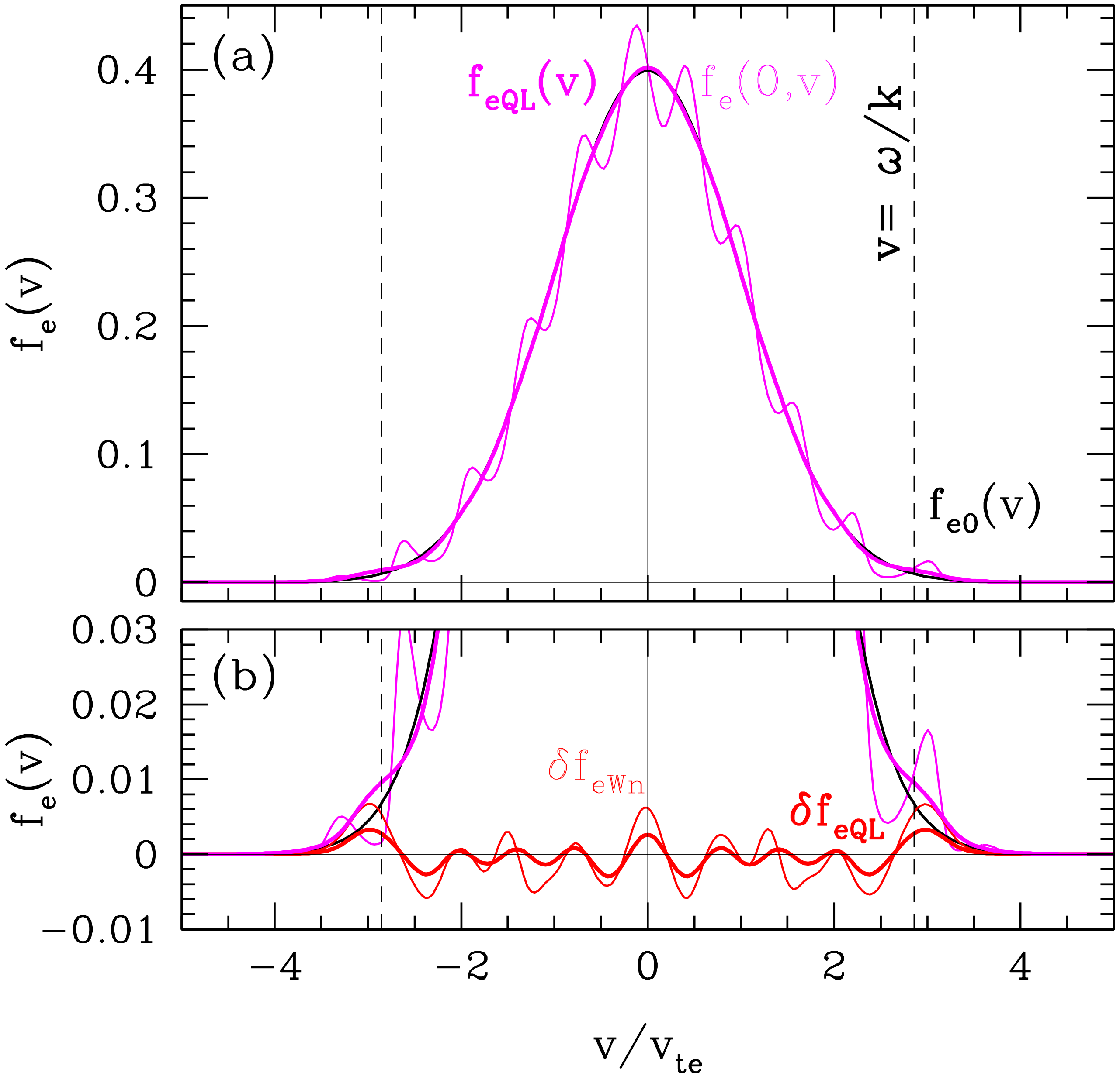

FIGURE 4. (a) Total electron distribution function evaluated at position $x=0$, $f_e(0,v,t)$ (thin magenta), the spatially averaged, quasilinear distribution function $f_{eQL}(v,t)$ (thick magenta), and the equilibirum electron distribution function f_{e0} (black). (b) The nonlinear wave-particle interaction component of the perturbed electron distribution function at position $x=0$, $\delta f_{eWn}(0,v,t)$ (thin red), the quasilinear perturbed distribution function $\delta f_{eQL}(v,t)$ (thick red). The quasilinear flattening of the distribution function at the resonant velocities $v=\pm\omega/k$ (dashed black) is apparent in the total quasilinear distribution function $f_{eQL}(v,t)$ (thick magenta), but this signature is obscured in the total electron distribution function evaluated at position $x=0$, $f_e(0,v,t)$ (thin magenta).

Correlation with zero lag

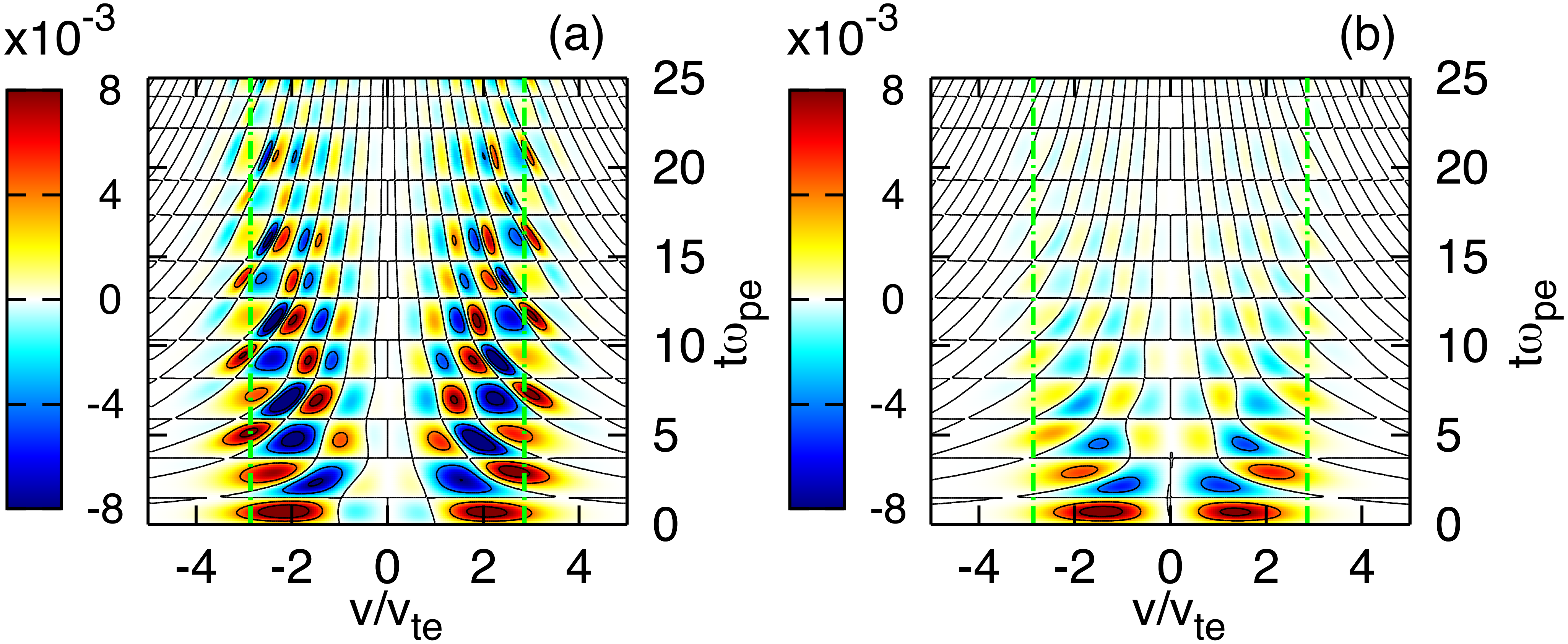

FIGURE 11. For Case I, plots of (a) the $C_1(v,t,\tau)$ correlation quantity, $(q_s v^2/2)(\partial \delta f_s(0,v,t)/\partial v)E(0,t)$, and (b) the $C_2(v,t,\tau)$ correlation quantity, $q_s v \delta f_s(0,v,t)E(0,t)$, at $x = 0$ as a function of velocity v/v_{te} and time $\omega_{pe}t$. The dot–dashed vertical green lines denote the resonant velocities $v = \pm\omega/k$.

$$C_1(v,t_i,\tau) = \frac{1}{N}\sum_{j=i}^{i+N} q_s \frac{v^2}{2}\frac{\partial \delta f_{sj}(v)}{\partial v} E_j$$

Choosing a correlation time

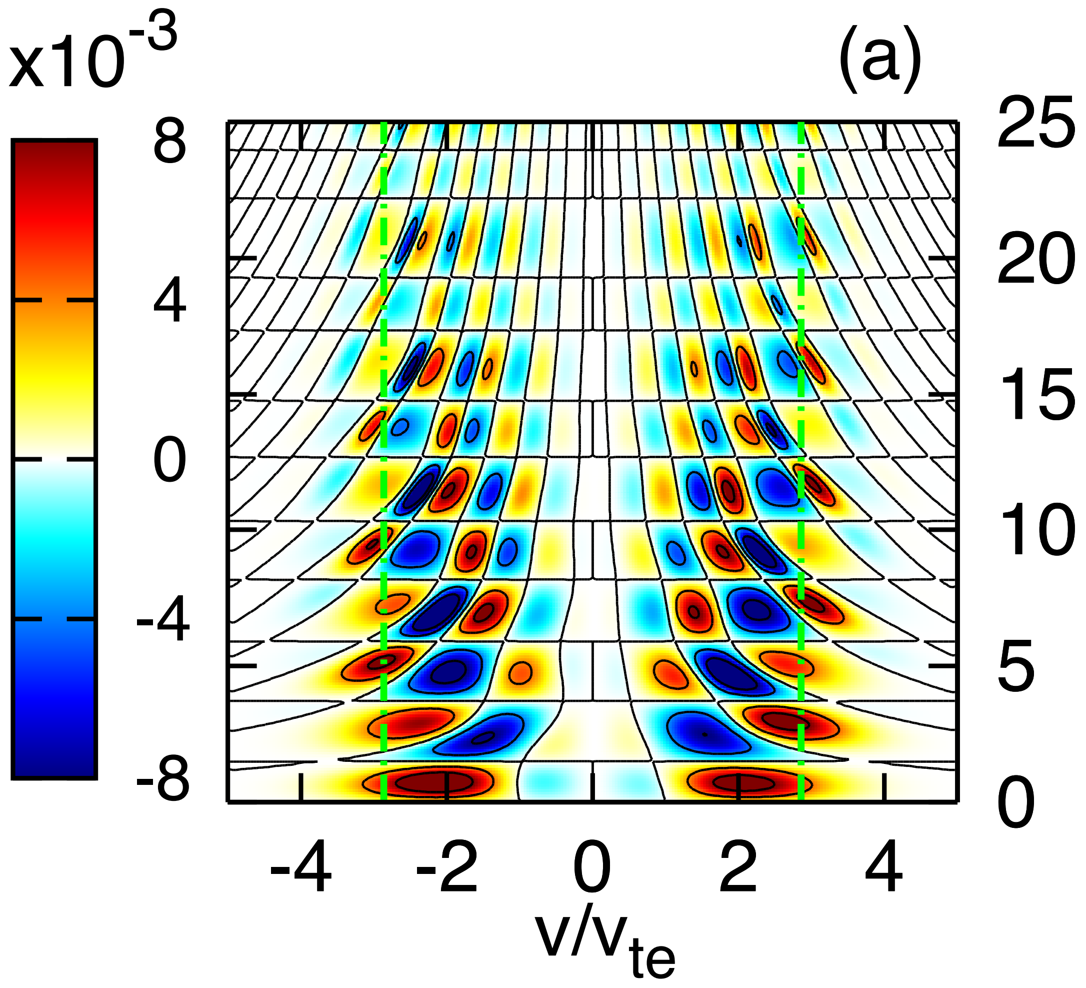

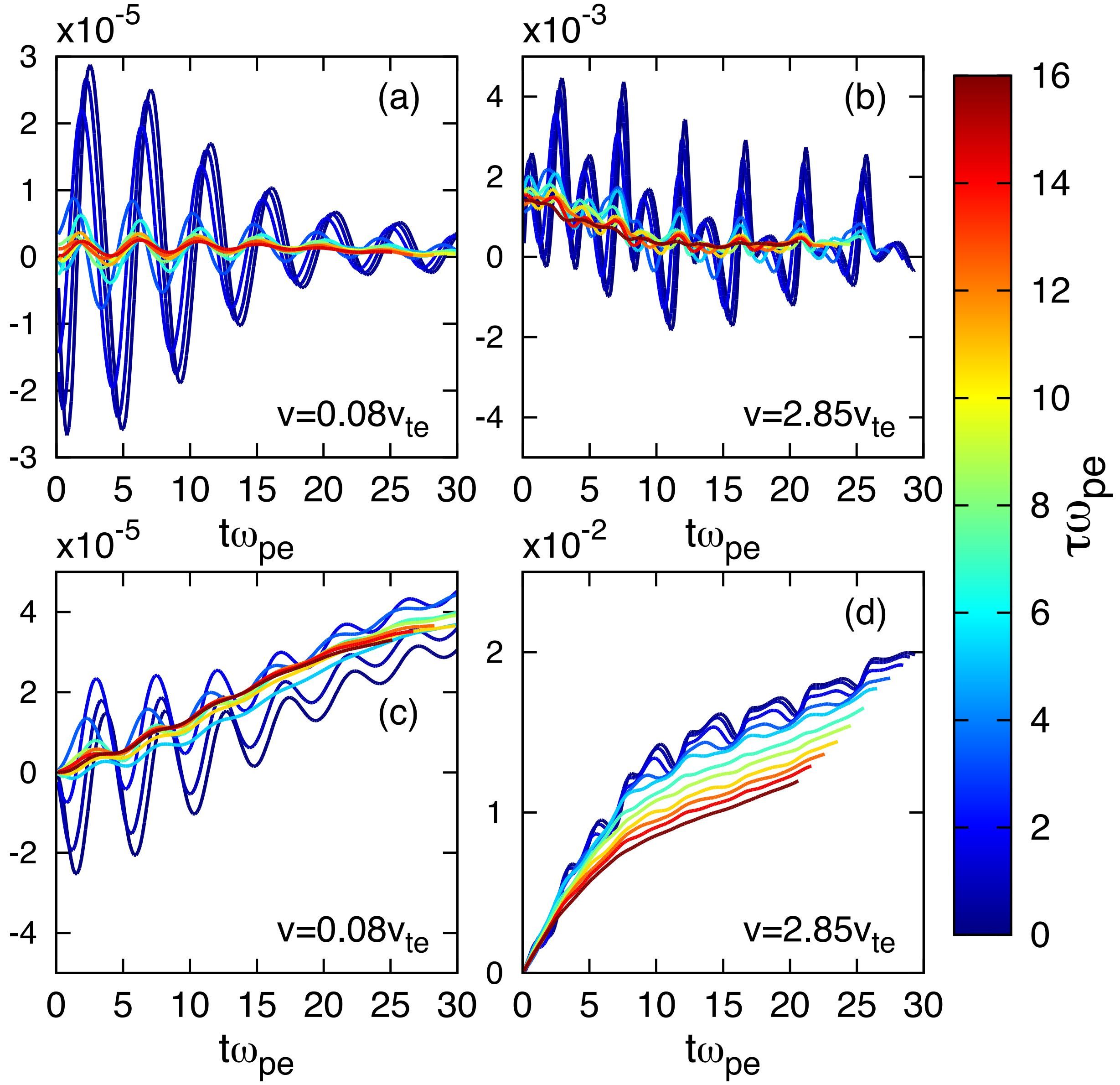

FIGURE 12. The correlation $C_1(v_0, t, \tau)$ from (3.20) over a range of correlation times $0 \leqslant \omega_{pe}\tau \leqslant 16$ at two velocity values, (a) off-resonance at $v_0 = 0.08v_{te}$ and (b) on resonance at $v_0 = 2.85v_{te}$. Also, the change in the electron phase-space energy density $\Delta w_e(x_0, v, t)$ as a function of time $\omega_{pe}t$ at the same two velocity values, (c) off-resonance at $v_0 = 0.08v_{te}$ and (d) on resonance at $v_0 = 2.85v_{te}$. Units of the energy transfer rate (a,b) and change in phase-space energy density (c,d) are arbitrary, but consistent from one panel to another.

$$\Delta w_e(x_0, v, t) = \int_0^t C_1(v, t', \tau)\, dt'$$

Correlation finite time

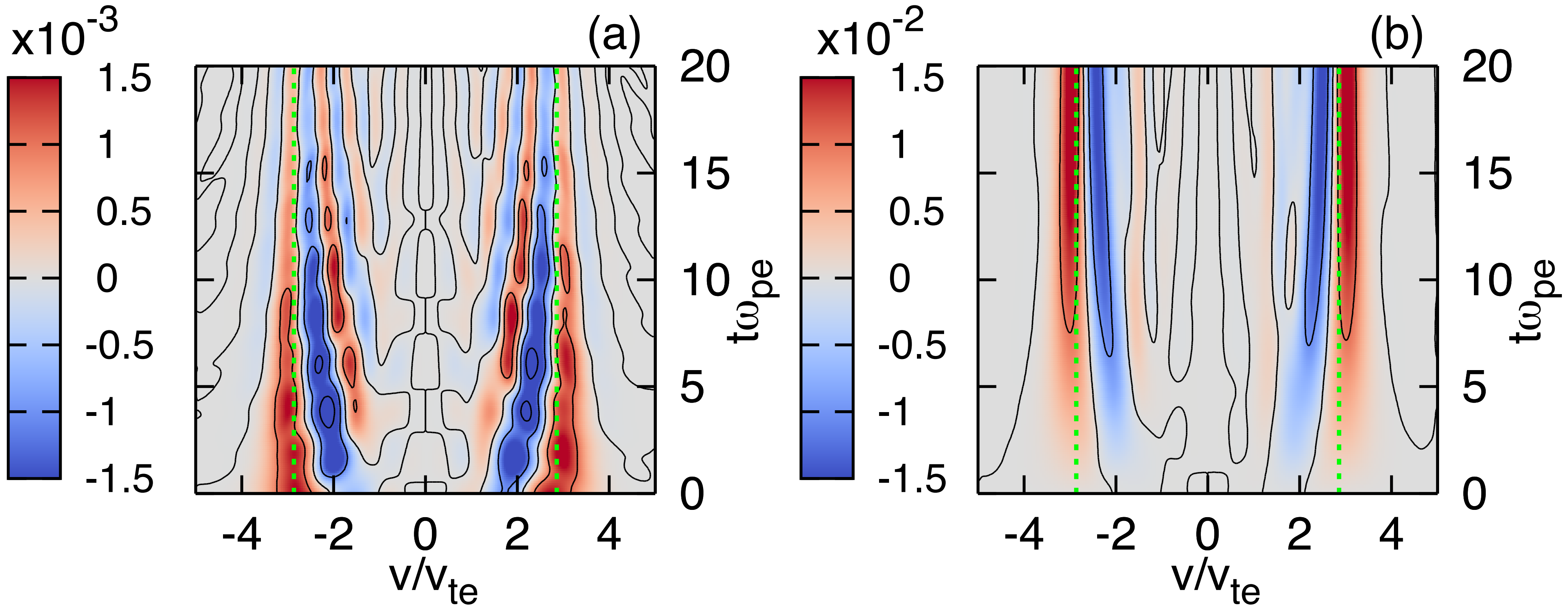

FIGURE 13. (a) The field-particle correlation $C_1(v,t,\tau) = C_\tau(q_s v^2/2 \partial\delta f_s/\partial v, E)$ at $x = 0$ using a correlation time $\omega_{pe}\tau = 6.28$. (b) The time-integrated correlation $\int_0^t C_1(v,t',\tau)dt'$, showing a clear resonant signature of the secular energy transfer about the resonant velocities $v = \pm\omega/k$ (dashed green).

$$\Delta w_e(x_0, v, t) = \int_0^t C_1(v, t', \tau) dt'$$

Alfvénic turbulence

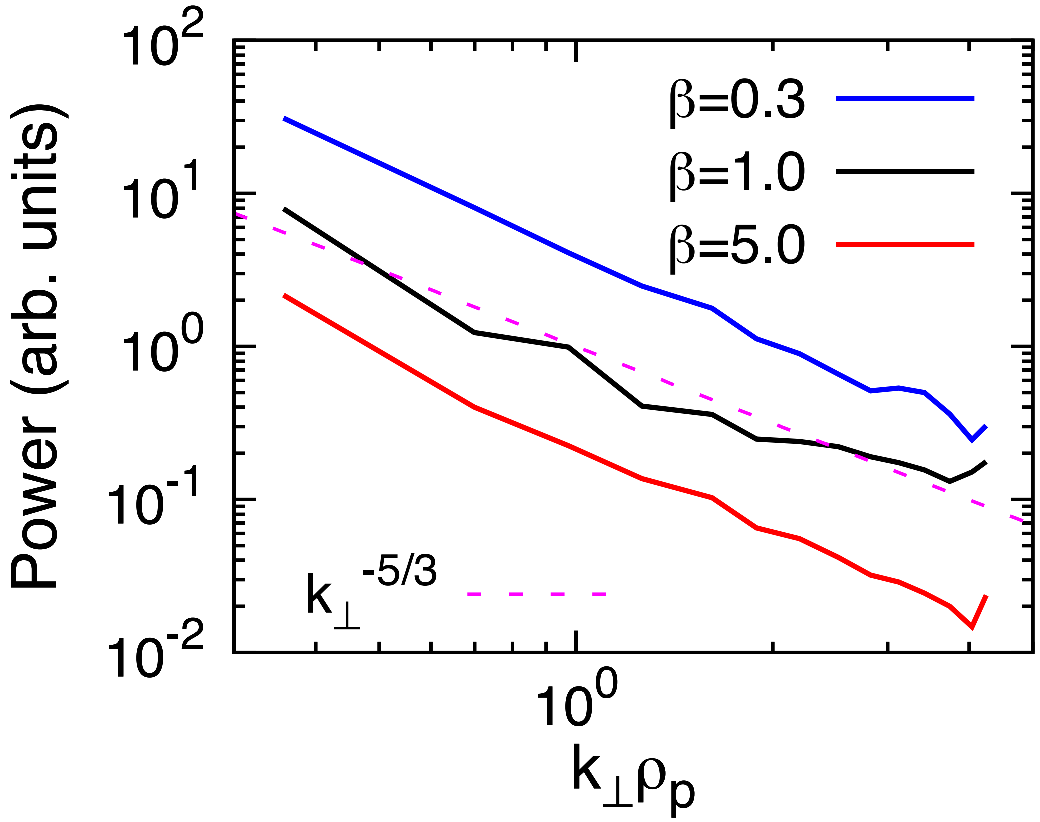

We perform three initial simulations, with the following parameters:

- $k_\perp \rho_p \in [0.3, 3.3]$
- $\beta_p = 0.3, 1.0, 5.0$
- $T_e = T_i$
- $\nu_s \approx 0.1 \gamma_s(k_{\perp,0})$

(Klein et al. 2016, in prep for submission to JPP)

Landau and transit time damping

Coherent damping occurs for particles satisfying the resonance

$$\omega - k_\parallel v_\parallel = 0.$$

The $n = 0$ resonance corresponds to two physical mechanisms, Landau Damping, and Transit Time Damping (Landau 1946, Barnes 1966)

$$-q_s \frac{v_\parallel^2}{2} \frac{\partial \delta f_s}{\partial v_\parallel} E_\parallel; \quad \frac{m_s v_\perp^2}{2|B|} \frac{v_\parallel^2}{2} \frac{\partial \delta f_s}{\partial v_\parallel} \frac{\partial \delta B_\parallel}{\partial z}$$

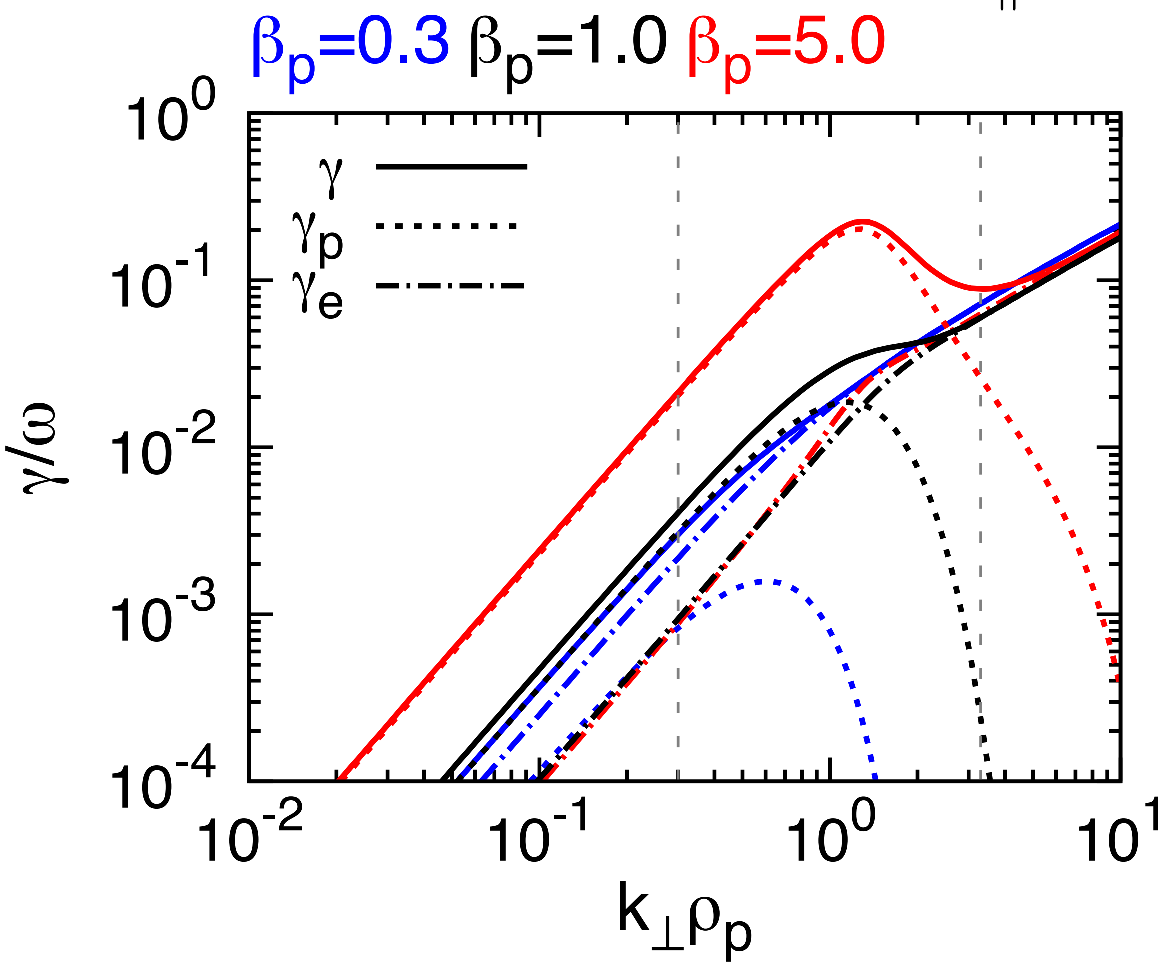

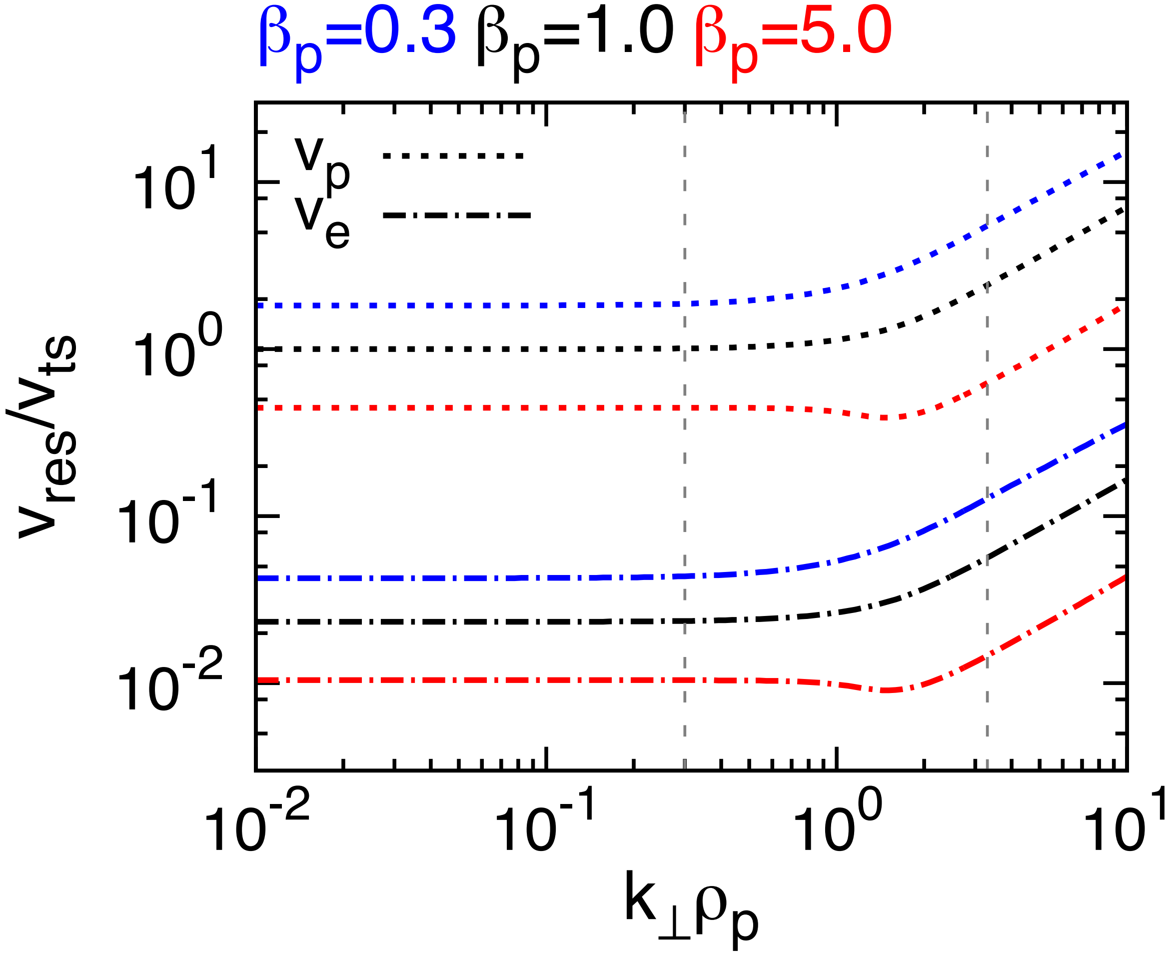

Correlation tests of Landau damping

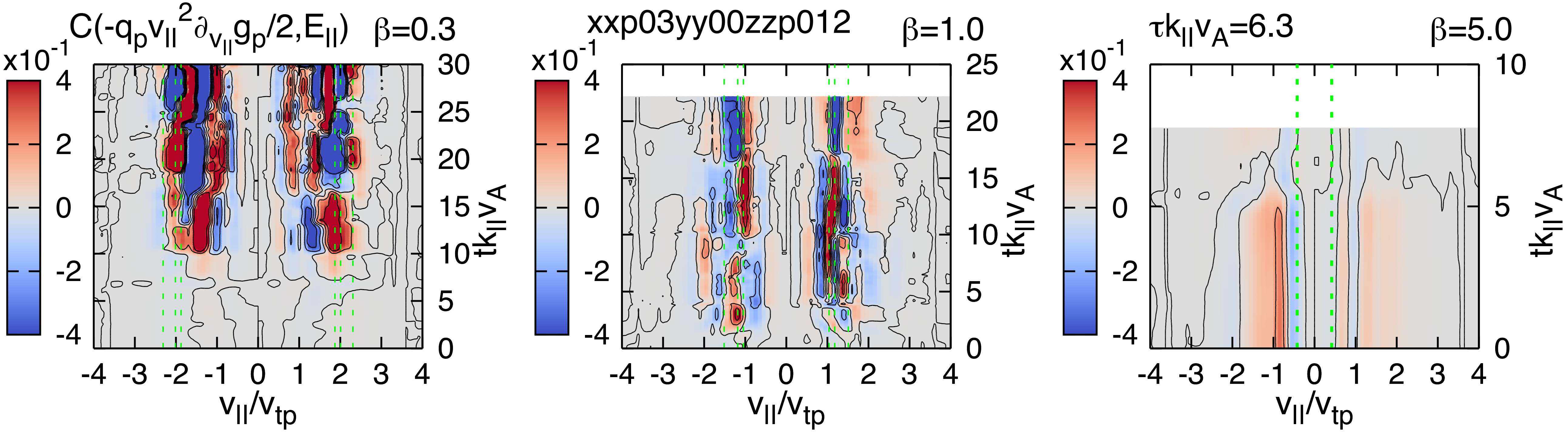

- C_1 peaks near the appropriate resonant velocities.
- Landau Damping weakens for larger β_p.

Transit time damping

$$C_2(v_\parallel, t_i, \tau) \equiv \frac{1}{N}\sum_{j=i}^{i+N} \frac{v_\parallel^2}{2}\frac{\partial}{\partial v_\parallel}\left[\int dv_\perp v_\perp \frac{m_s v_\perp^2}{2|B|} g_{sj}(v_\parallel)\right]\delta B_{\parallel,j}$$

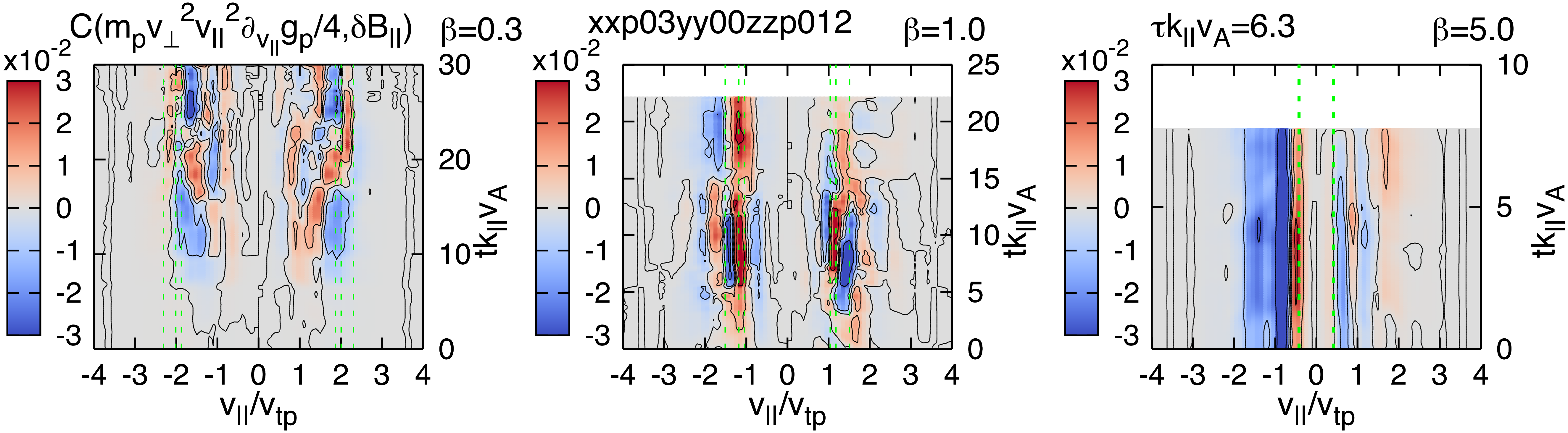

Comparison and ID

As the velocity derivative $\partial_{v_\parallel} g_s$ may be difficult to construct accurately for spacecraft data, we consider the related correlation:

$$C_3(v_\parallel, v_\perp, t_i, \tau) \equiv \frac{1}{N} \sum_{j=i}^{i+N} -q_s v_\parallel g_{sj}(v_\parallel, v_\perp) E_{\parallel,j}$$

$$C_4(v_\parallel, v_\perp, t_i, \tau) \equiv \frac{1}{N} \sum_{j=i}^{i+N} m_s v_\parallel v_\perp^2 g_{sj}(v_\parallel, v_\perp) \delta B_{\parallel,j}$$

Comparison and ID

As the velocity derivative $\partial_{v_\parallel} g_s$ may be difficult to construct accurately for spacecraft data, we consider the related correlation:

$$C_3(v_\parallel, v_\perp, t_i, \tau) \equiv \frac{1}{N} \sum_{j=i}^{i+N} -q_s v_\parallel g_{sj}(v_\parallel, v_\perp) E_{\parallel,j}$$

$$C_4(v_\parallel, v_\perp, t_i, \tau) \equiv \frac{1}{N} \sum_{j=i}^{i+N} m_s v_\parallel v_\perp^2 g_{sj}(v_\parallel, v_\perp) \delta B_{\parallel,j}$$

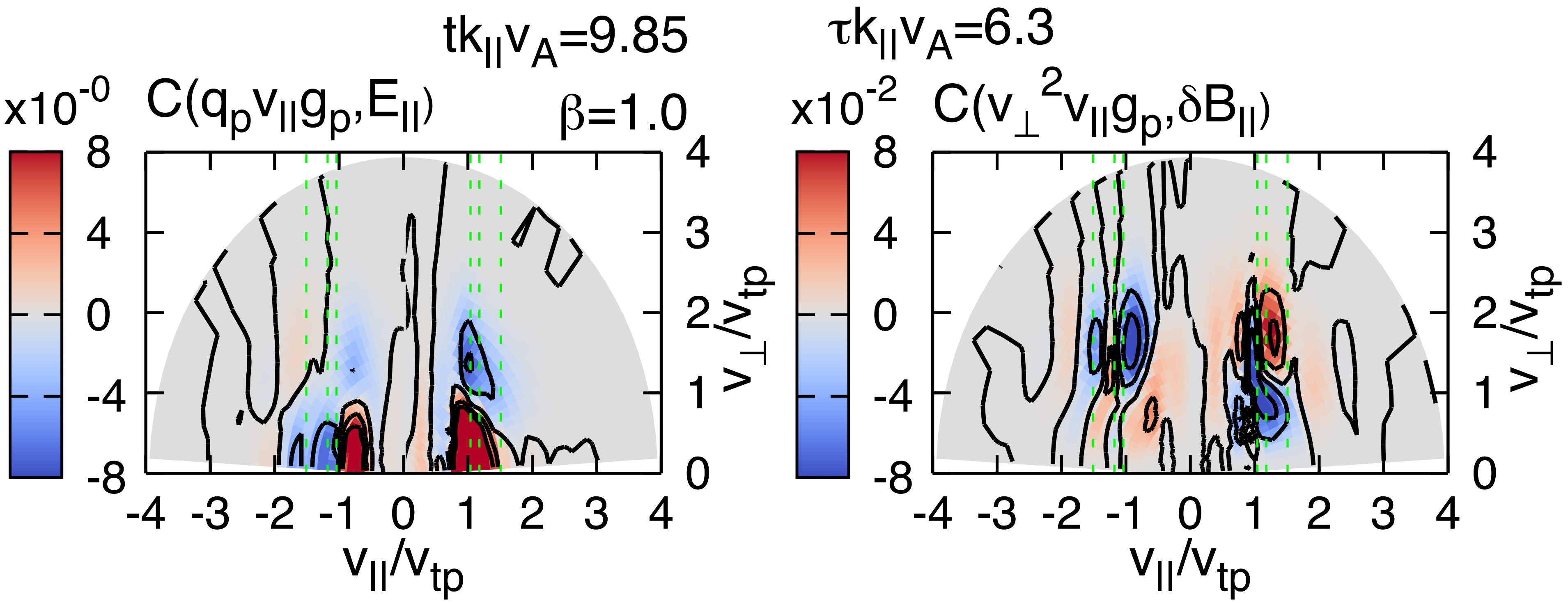

Eulerian Vlasov-Maxwell

The Gkeyll (and Hyde) Framework

“It is one thing to mortify curiosity, another to conquer it.”

- The Gkeyll framework is flexible suite of solvers for plasma physics being developed at the Princeton Plasma Physics Lab and UMD

- Solvers include a finite volume method for equations written in conservative form and a discontinuous Galerkin finite element method for systems of equations which can be written in terms of a Poisson bracket

- Multiple publications already:

    - L. Wang, A. H. Hakim, A. Bhattacharjee, and K. Germaschewski. Comparison of multi-fluid moment models with particle-in-cell simulations of collisionless magnetic reconnection. *Phys. Plasmas*, 22 (1): 012108, (2015).

    - E. L. Shi, A. H. Hakim, and G. W. Hammett. A gyrokinetic one-dimensional scrape-off layer model of an edge-localized mode heat pulse. *Phys. Plasmas*, 22 (2): 022504, (2015).

    - J. Ng, Y. M. Huang, A. H. Hakim, A. Bhattacharjee, A. Stanier, W. Daughton, L. Wang, and K. Germaschewski. The island coalescence problem: Scaling of reconnection in extended fluid models including higher-order moments. *Phys. Plasmas*, 22, 112104, (2015).

The Vlasov-Maxwell system

$$\frac{\partial f}{\partial t} + \nabla_{\mathbf{z}} \cdot (\boldsymbol{\alpha} f) = C[f],$$
$$\frac{\partial \mathbf{B}}{\partial t} + \nabla \times \mathbf{E} = 0$$
$$\epsilon_0 \mu_0 \frac{\partial \mathbf{E}}{\partial t} - \nabla \times \mathbf{B} = -\mu_0 \mathbf{J}$$

- $\nabla_{\mathbf{z}} = (\nabla_{\mathbf{x}}, \nabla_{\mathbf{v}})$ and $\boldsymbol{\alpha} = (\mathbf{v}, \frac{q_s}{m_s}(\mathbf{E} + \mathbf{v} \times \mathbf{B}))$
- Standard approach to solving the Vlasov-Maxwell system numerically is the particle-in-cell (PIC) algorithm, which approximates the plasma as a collection of "macroparticles"
- Each macroparticle's position and velocity are solved for via

$$\dot{\mathbf{x}} = \mathbf{v}$$
$$\dot{\mathbf{v}} = \frac{q_s}{m_s}(\mathbf{E} + \mathbf{v} \times \mathbf{B}))$$

Direct discretization

- What if we solved for the distribution function, as well as the fields, on a grid? A completely Eulerian (or continuum) algorithm?
- **Advantages**
  - Resulting distribution function would be noise-free, allowing for diagnosis of many dissipation mechanisms much more easily
  - The fields would also be noise-free
  - Numerically, the algorithm requires no dynamic load-balancing at extreme scale computing, don't have to worry about tracking particles
- **Disadvantages**
  - All of velocity space must be solved at each configuration space point
  - All of the same time step constraints as explicit PIC (speed of light and plasma frequency)
  - One additional constraint when compared to the Boris push. Requires careful treatment of magnetic field because Larmor radii are not automatically closed
  - Production simulation distribution functions are enormous data structures. Either must sacrifice write frequency or only write out distribution function in small subdomain for analysis

Discontinuous Galerkin method

In the discontinuous Galerkin (DG) finite element method framework, one selects a discontinuous approximation space (usually piecewise polynomials). Unlike FV schemes which only evolve cell averages, in DG we also evolve higher moments.

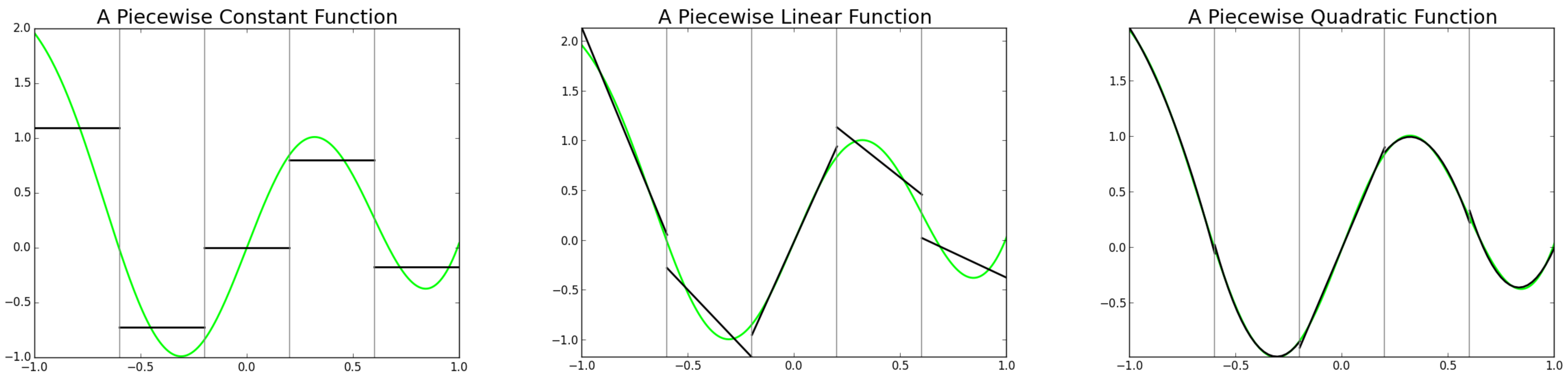

Figure: The projection of $x^4 + \sin(5x)$ onto piecewise constant (left), linear (middle) and quadratic (right) spaces.

Why DG?

- Why use this particular numerical method?
- **Advantages**
    - Flexible accuracy. Can pick an appropriately high order polynomial representation to get most “bang for your buck”
    - Dominant computation is matrix-vector multiplication. Easily vectorized, and matrices can be cached if polynomial order is picked appropriately for dimension of problem
    - High arithmetic intensity. Number of computations per byte of data communicated is large and without load balancing
    - Highly parallelizable. Only requires one layer of ghost cells

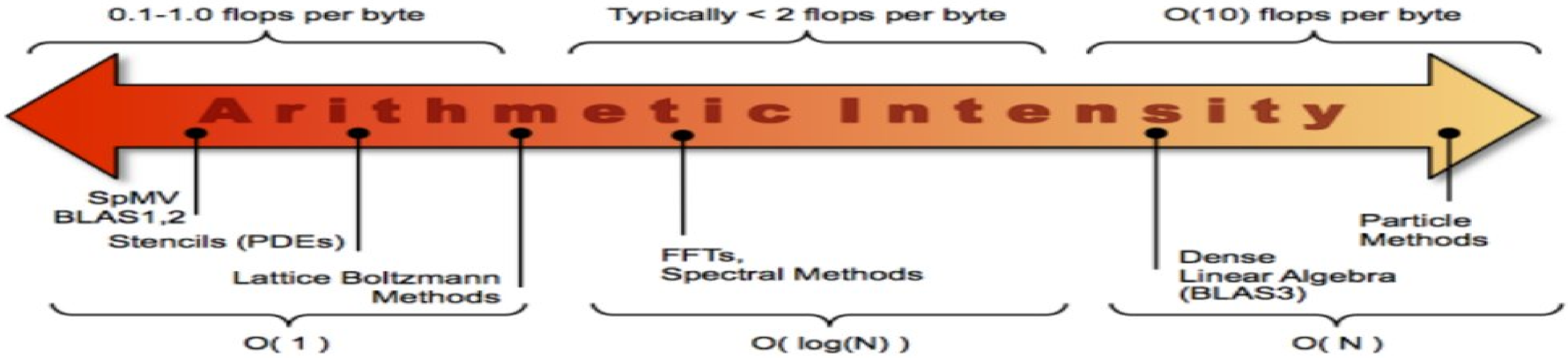

Source: http://crd.lbl.gov/departments/computer-science/PAR/research/roofline/

Where is Gkeyll now?

- Currently in the benchmarking, debugging, and optimization phase
- Addition of a collision operator, Lenard Bernstein
- Other improvements: sparse grids, reduced basis sets, sub-cycling, semi-implicit, etc

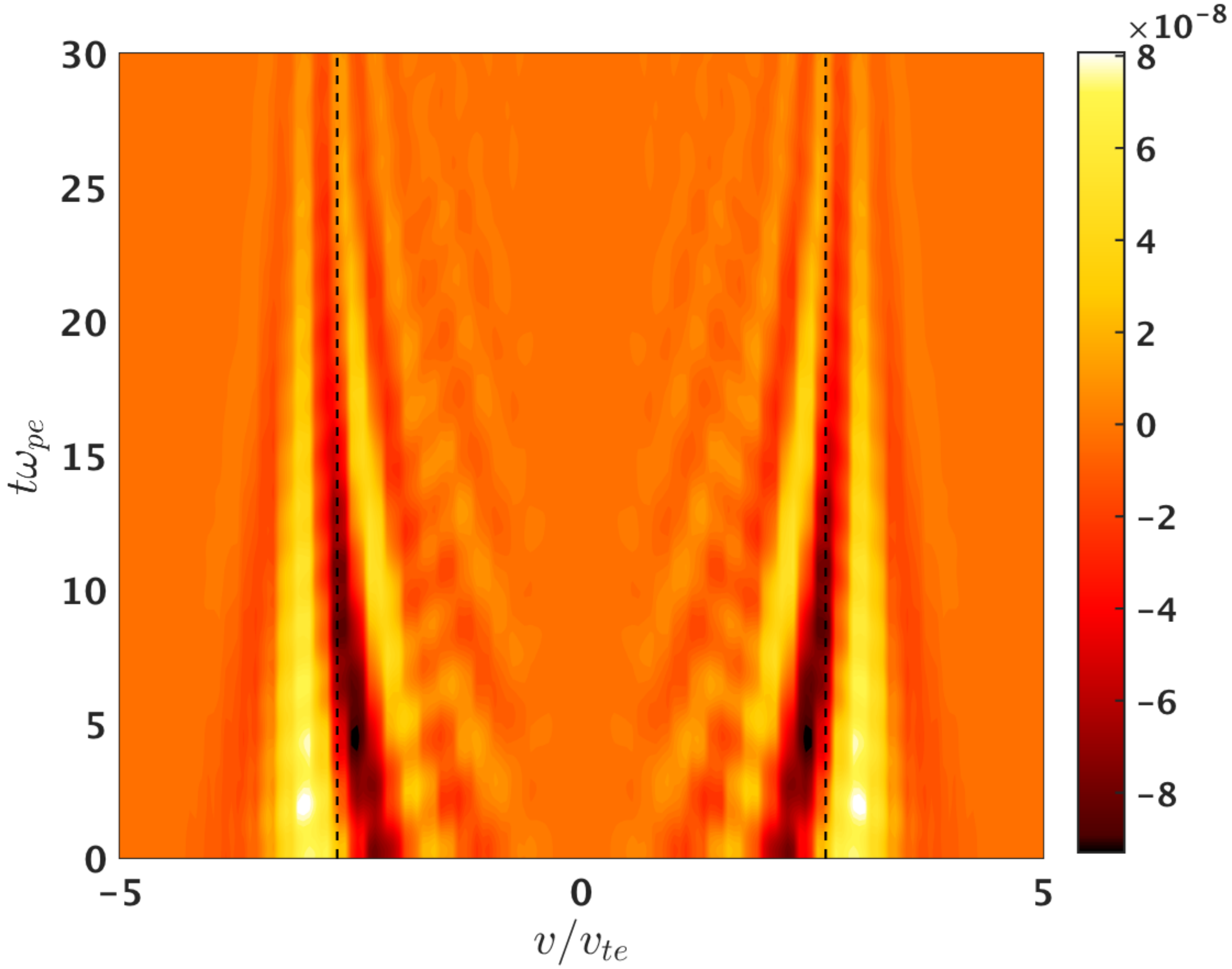

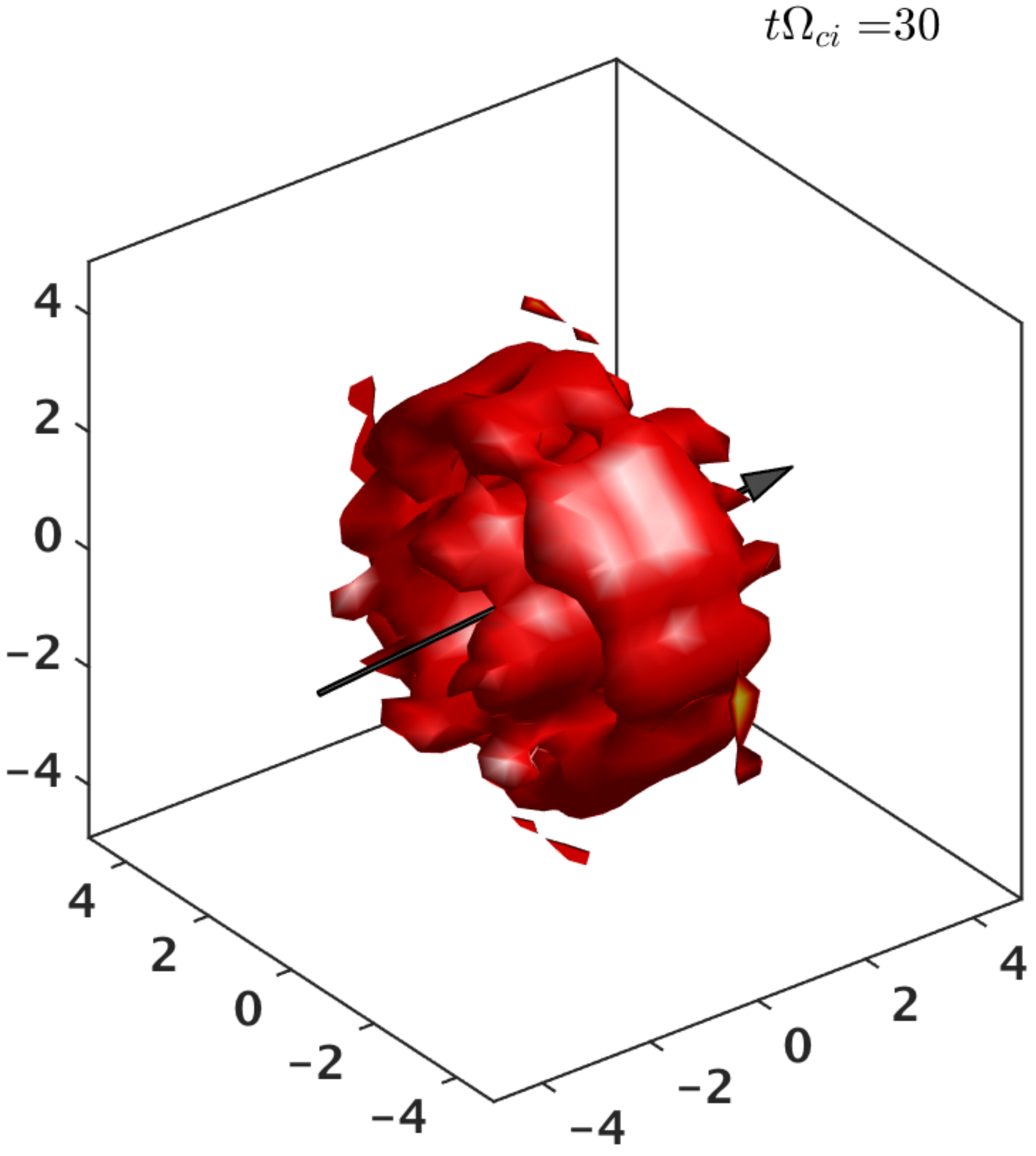

Summary

- Dissipation is consistent with (inhomogeneous) Landau damping

- Intermittent structures form naturally and are similar to those observed in the solar wind

- Field-particle correlations support the Landau damping picture and are applicable to 1D in situ spacecraft data

- Gyrokinetics is a powerful tool for studying solar wind turbulence, but we are developing a full Eulerian Vlasov-Maxwell simulation code to move beyond gyrokinetics.

Supplemental slides

Consequences of the GK ordering

- Cyclotron, plasma wave, and the fast magnetosonic branch are ordered out of system
- Subsonic drifts: $v_d \sim \epsilon v_{th}$
- In the absence of collisions, magnetic moment conserved
- Rigorously quasi-neutral, i.e., $\delta n_e = \delta n_e$
- Must choose an ϵ to connect to reality
- Most codes do not evolve the transport time-scale, i.e., the background does not evolve

Cascade model [Howes et al (2008)]

Ideally, one would like a turbulence model wherein the spectral exponents, spectral anisotropy, and ion and electron heating can be simply predicted

$$\frac{\partial b_k^2}{\partial t} = -k_\perp \frac{\partial \epsilon}{\partial k_\perp} + S - 2\gamma b_k^2,$$

where S is a source term and γ is the linear damping rate.

$$\epsilon = C_1^{-2/3} \omega_{nl} b_k^2$$

$$\omega_{nl} = k_\perp b_k \bar{\omega}(k_\perp)$$

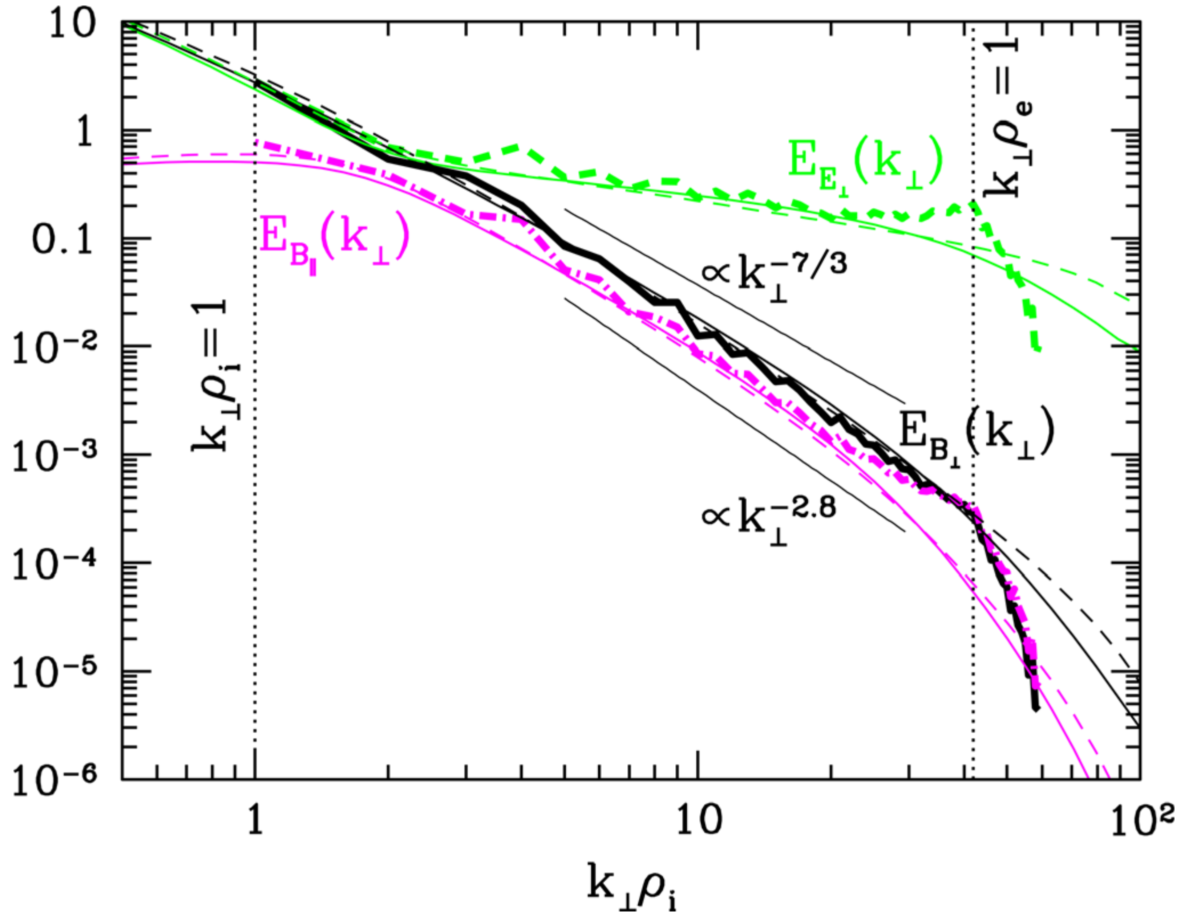

Energy spectra from fully nonlinear AstroGK simulation with $\beta_i = 1$ and $T_i/T_e = 1$ (thick) compared to predictions from the weakened cascade model (thin solid) and the local cascade model (thin dashed). From Howes et al (2011).

Weakened cascade model [Howes et al (2011)]

$$\frac{\partial b_k^2}{\partial t} = -k_\perp \frac{\partial \epsilon}{\partial k_\perp} + S - 2\gamma b_k^2$$

$$\epsilon = C_1^{-2/3}\omega_{nl} b_k^2$$

$$\omega_{nl}^{loc}(k'_\perp) = \chi(k'_\perp)k'_\perp b_k(k'_\perp)\bar{\omega}(k'_\perp)$$

$$\chi(k'_\perp) = \min(1, \frac{C_2 k'_\perp b_k(k'_\perp)}{k_\parallel(k'_\perp) v_A})$$

$$\frac{d\ln k_\parallel}{d\ln k_\perp} = \left[\frac{2/3+(1/3)(k_\perp\rho_i)^2}{1+(k_\perp\rho_i)^2}\right]\chi^2$$

$$\omega_{nl}(k_\perp) = \int_{k_{\perp 0}}^{k_{\perp max}} d\ln k'_\perp\, \omega_{nl}^{loc}(k'_\perp) \left[\Theta(k_\perp - k'_\perp) + \frac{k_\perp^2}{k'^2_\perp}\Theta(k'_\perp - k_\perp)\right]$$

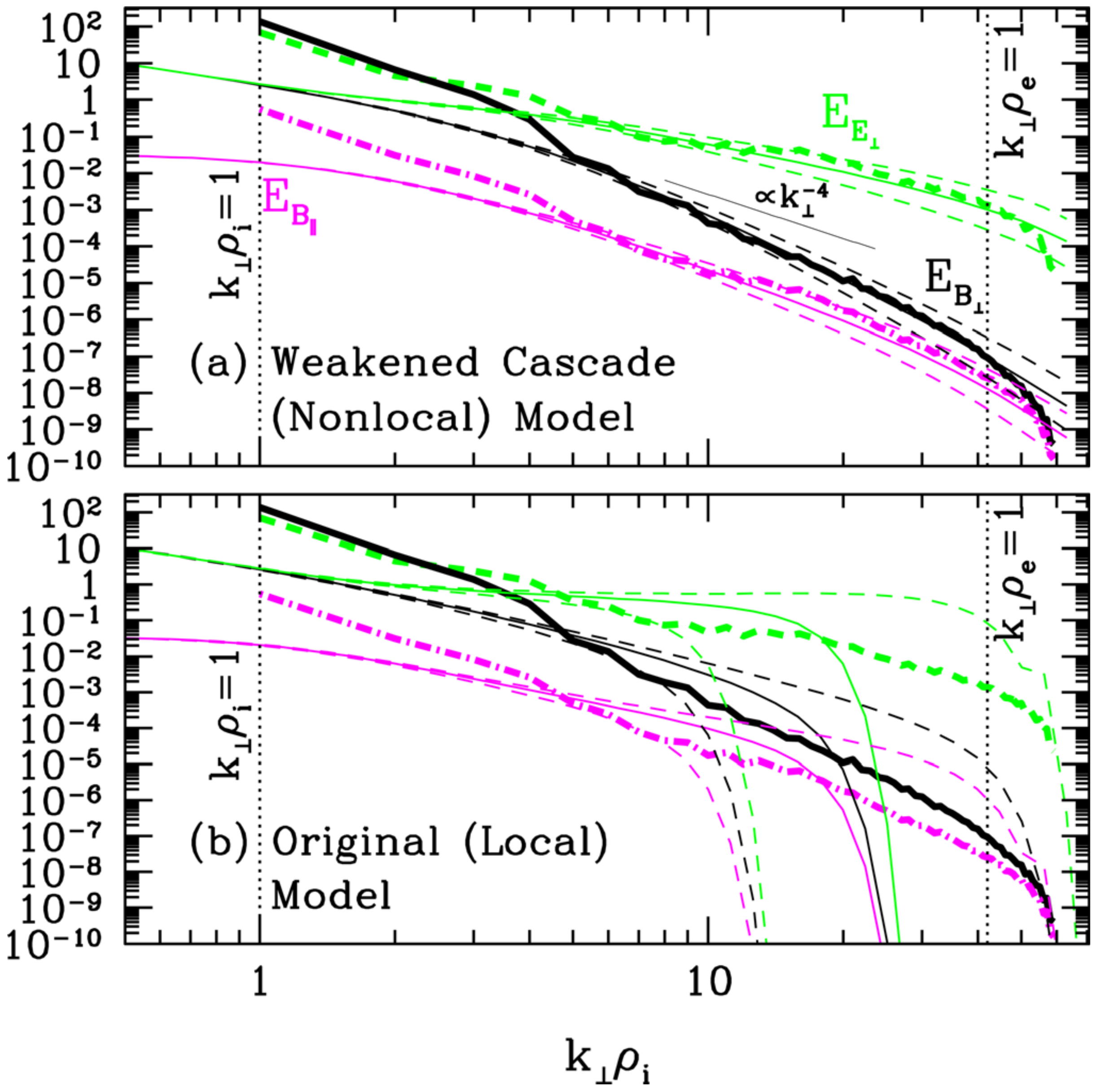

Energy spectra from fully nonlinear AstroGK simulation with $\beta_i = 0.01$ and $T_i / T_e = 1$ (thick) compared to predictions from the weakened cascade model (upper panel, thin) and the local cascade model (lower panel, thin). From Howes et al (2011).

Antenna energy injection

- Using the energy transfer diagnostic, the non-conservative contribution of the antenna source.
- By $k_0\rho_i = 1$, the injected energy has fallen by two orders of magnitude.
- The kinetic range is effectively free of source effects.

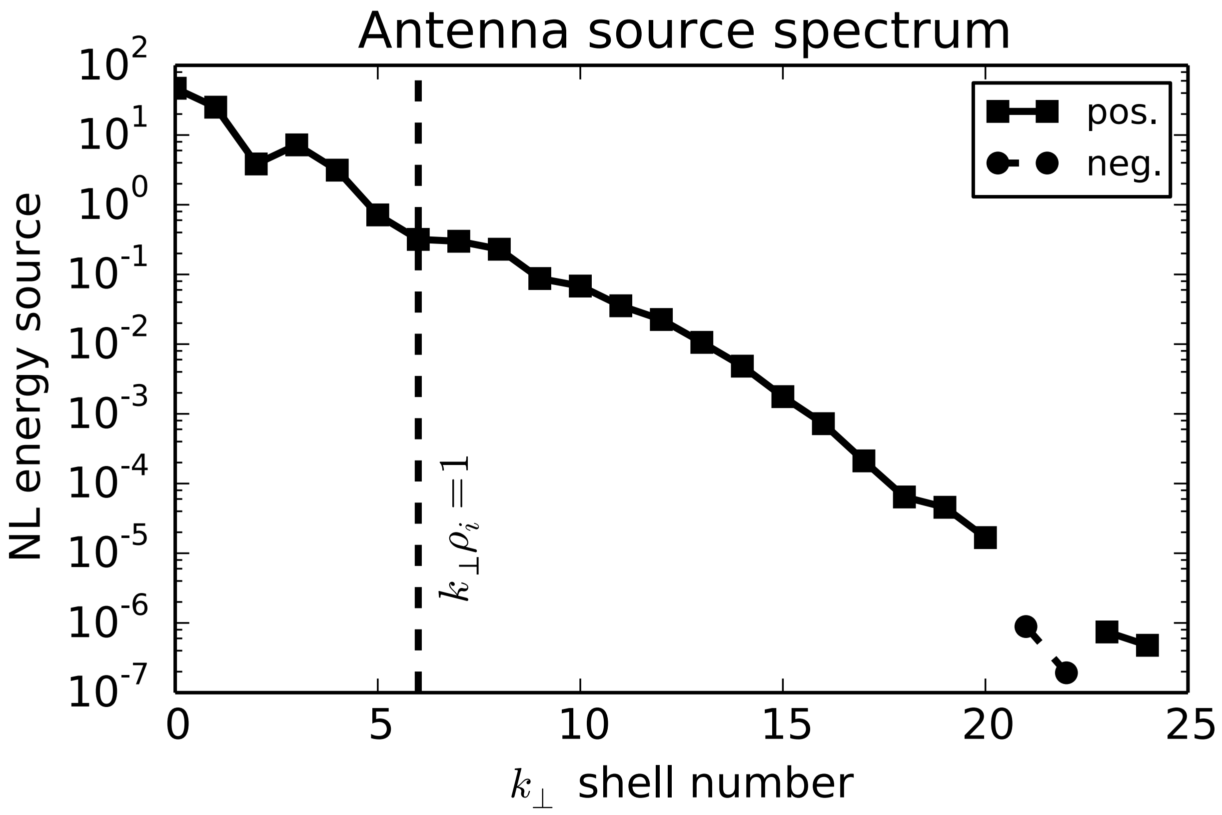

Locality of energy transfer

Local versus non-local energy transfer

Local transfer

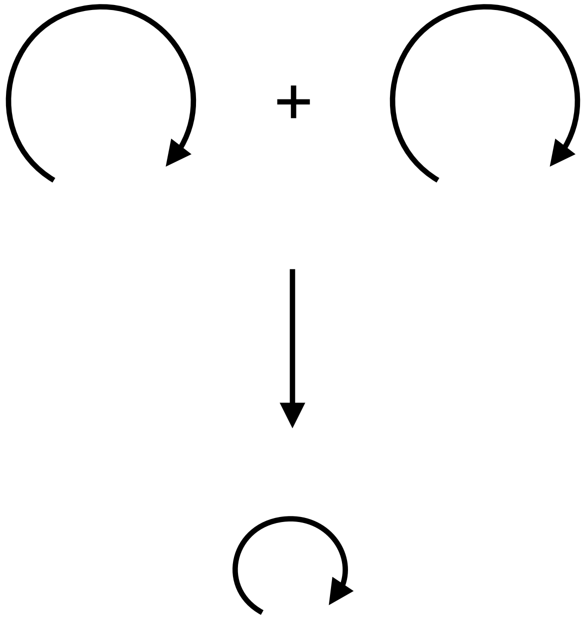

Large scale shearing

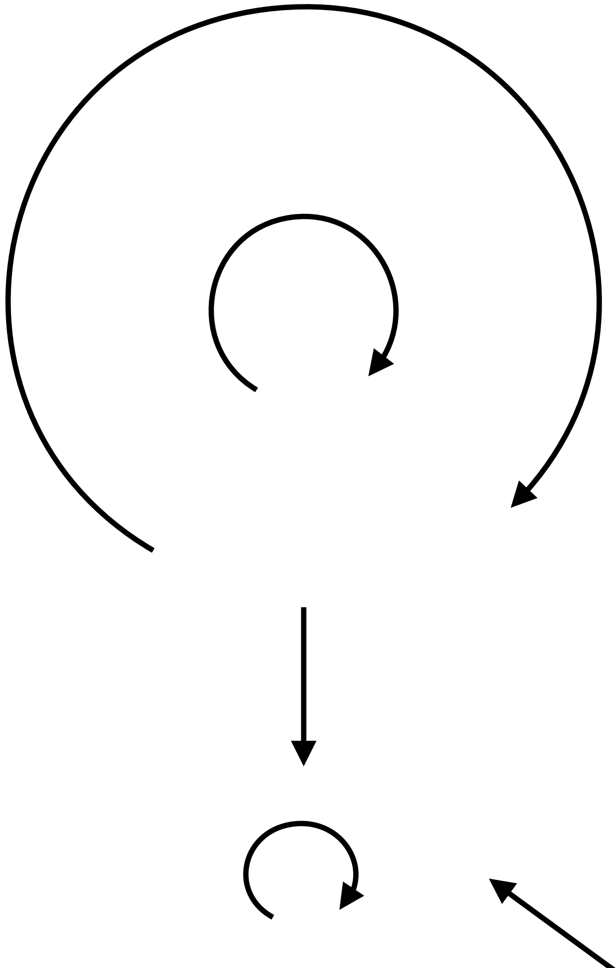

Small scale diffusion

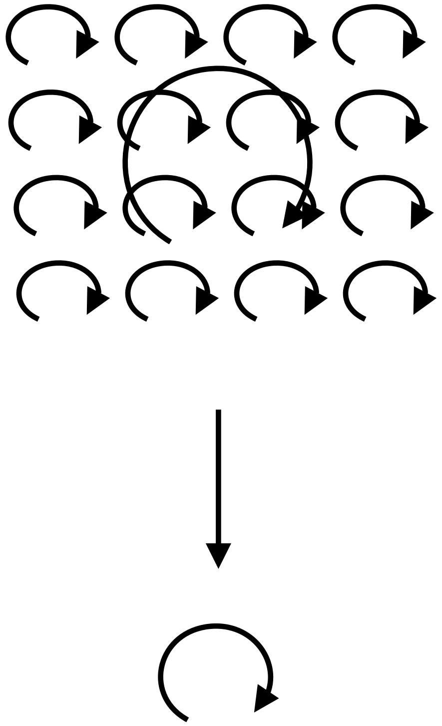

In neutral fluid turbulence, these can be transformed away via random Galilean transformations. In a plasma, Alfvén waves counter-propagating along a large scale B field adds a preferred direction, breaking the symmetry and increasing the importance of non-local energy transfer.

Nonlocal energy transfer

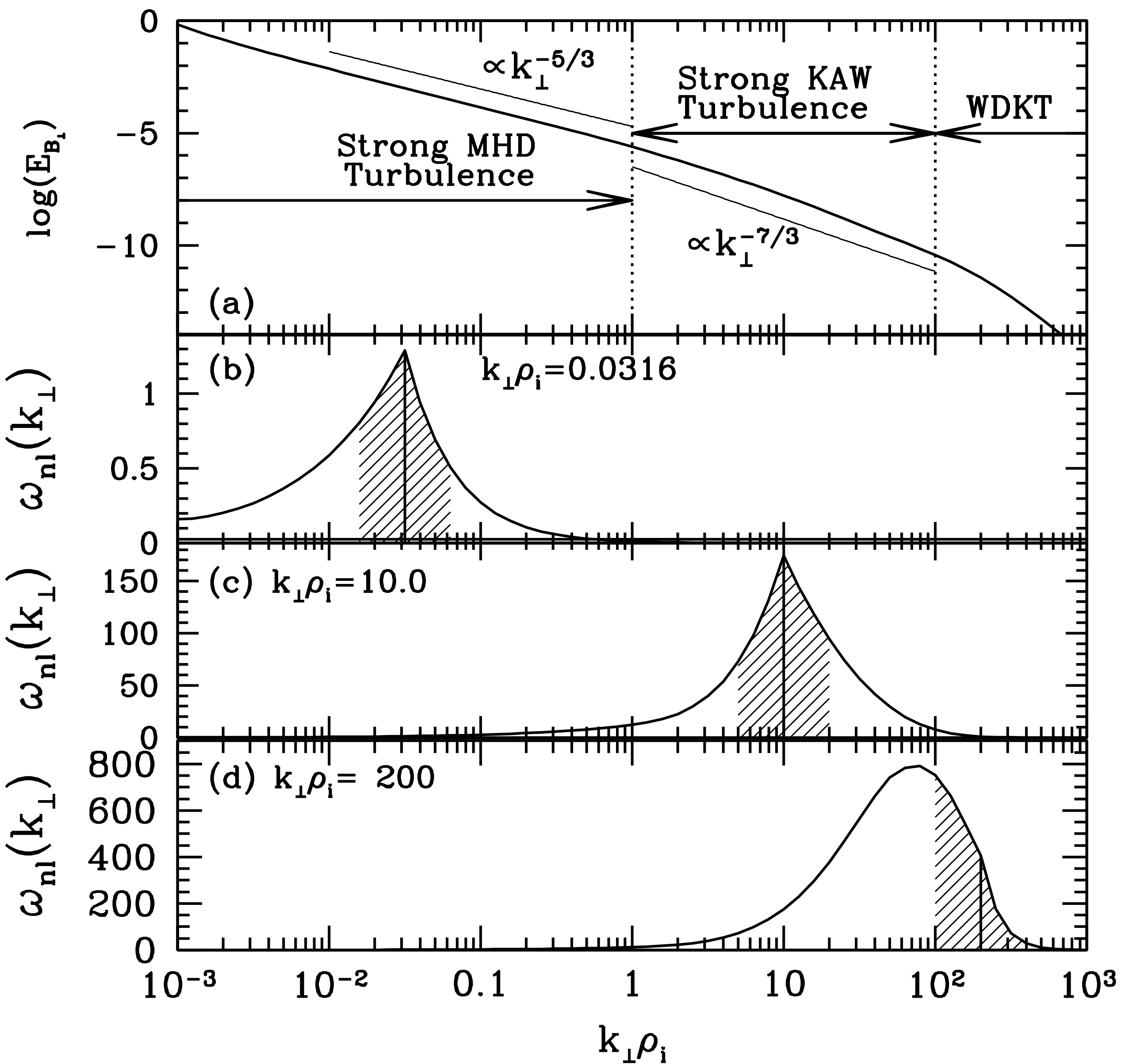

a) The perpendicular magnetic energy from the weakened cascade model with $\beta_i = 1$ and $T_i / T_e = 16$. In the lower three panels are plotted the non-local contribution to the nonlinear frequency at wavenumbers in the inertial, KAW, and weak dissipating KAW turbulence regimes respectively. From Howes et al (2011).

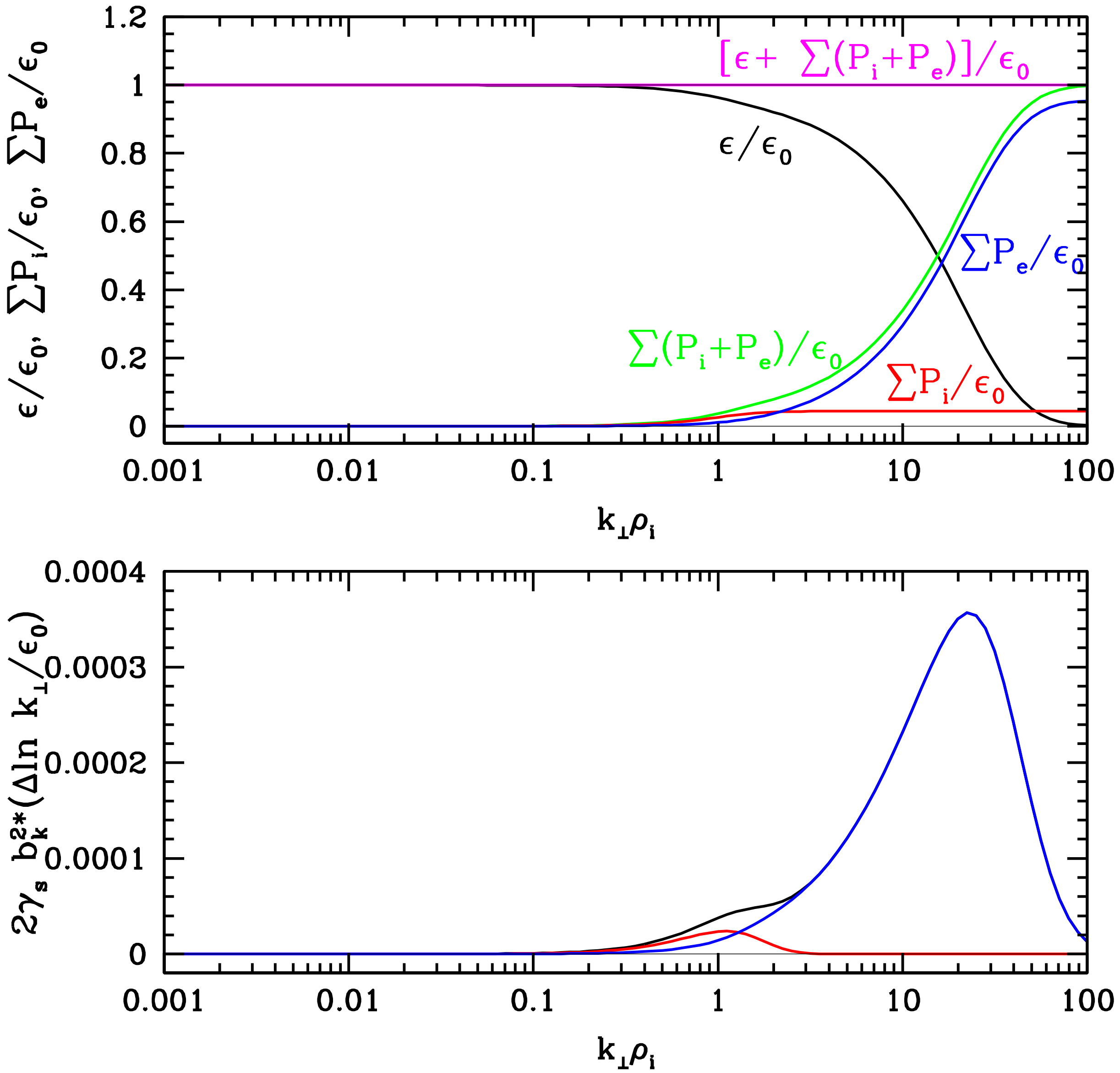

(Top) $\beta_i = 1$ normalized cascade rate (black), cumulative ion (red) and electron (blue) heating rates. (Bottom) The ion (red), electron (blue), and total (black) damping rates at each scale.

Transfer function diagnostics

Non-linear transfer function from modes p and q to k:

$$T_{kpq} = \int \pi B_0 dv_{\|} d\mu \frac{T_{0j}}{2F_{0j}}[q_x p_y - q_y p_x][\bar{\chi}_{1jq} h_{jp} - \bar{\chi}_{1jp} h_{jq}][h_{jk} + q_j v_{thj} \mathcal{C} \bar{A}_{ant,k} F_{0j}/T_{0j}]$$

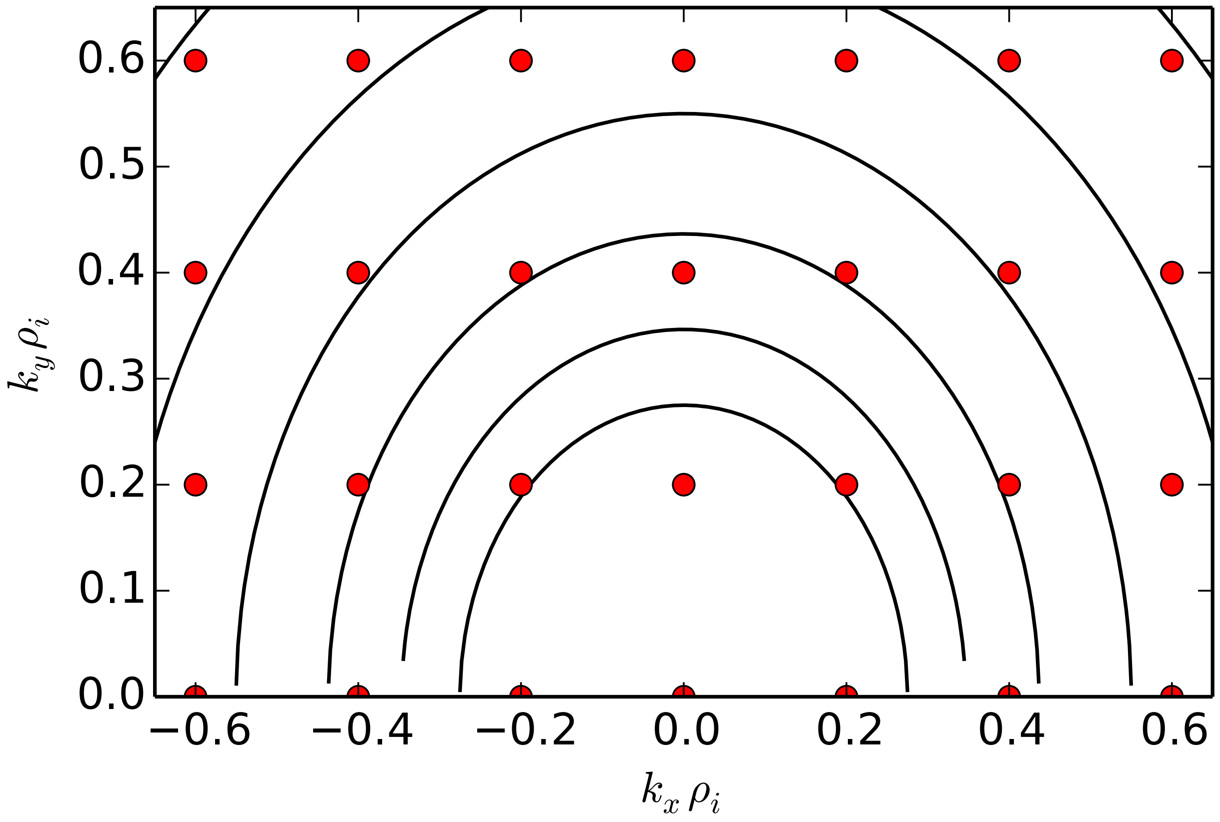

- Instead of transfers in terms of k, p, q, condense data into shells K, P, Q
- Shell setup: $k_n = k_0 \times 2^{n/3}$, where n = 25 and $k_0 \rho_i = 0.275$
- $k_0 \rho_i = 0.275$ chosen to place all driven modes in lowest shell and still resolve $k_0 \rho_i < 1$

Net transfer of energy for electrons

- Examine the net non-linear transfer of energy by summing over all Q mediator shells
- Net energy transfer is local beyond shell 5, $k\rho_i >\sim 1$

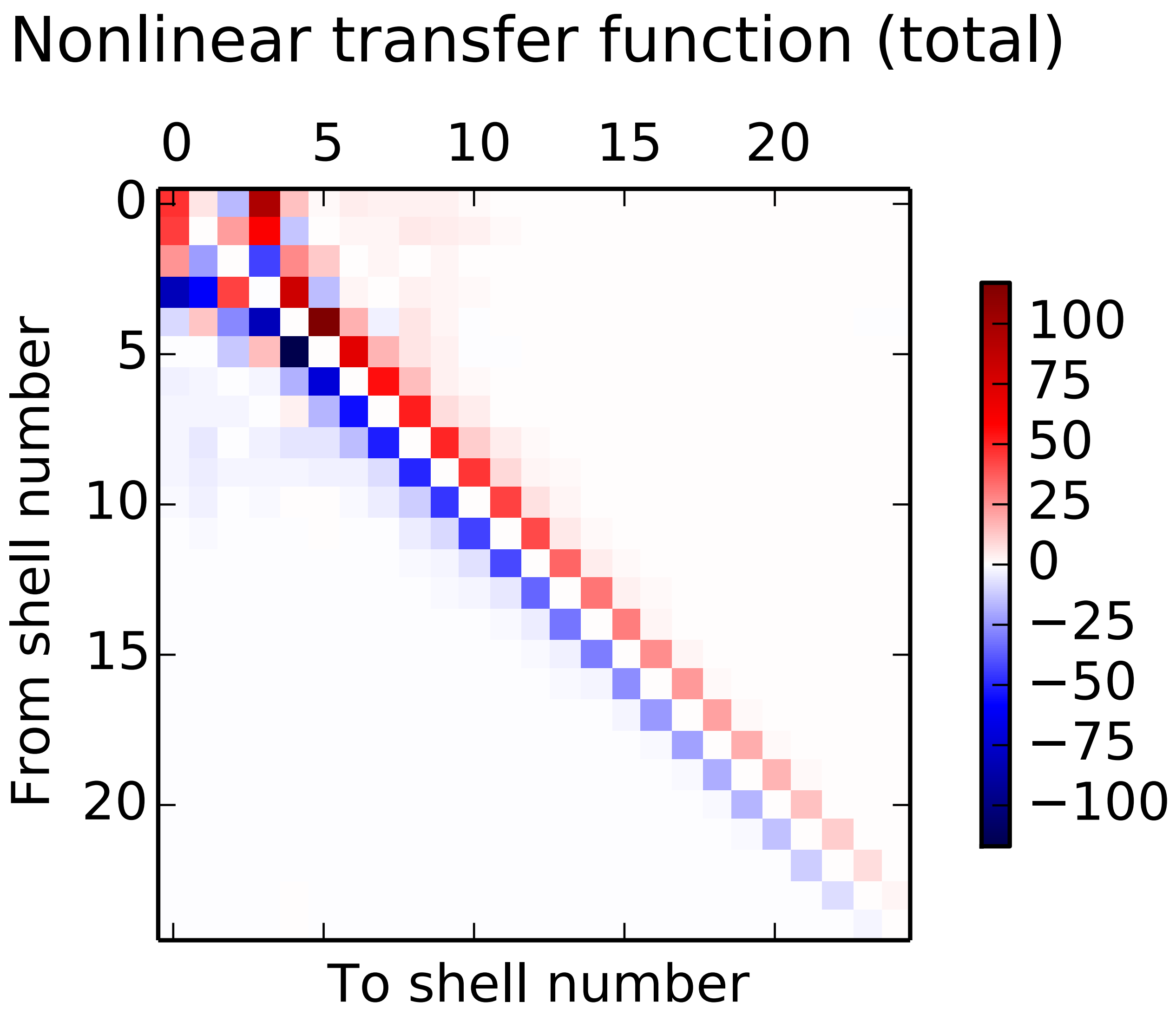

Local versus non-local energy transfer

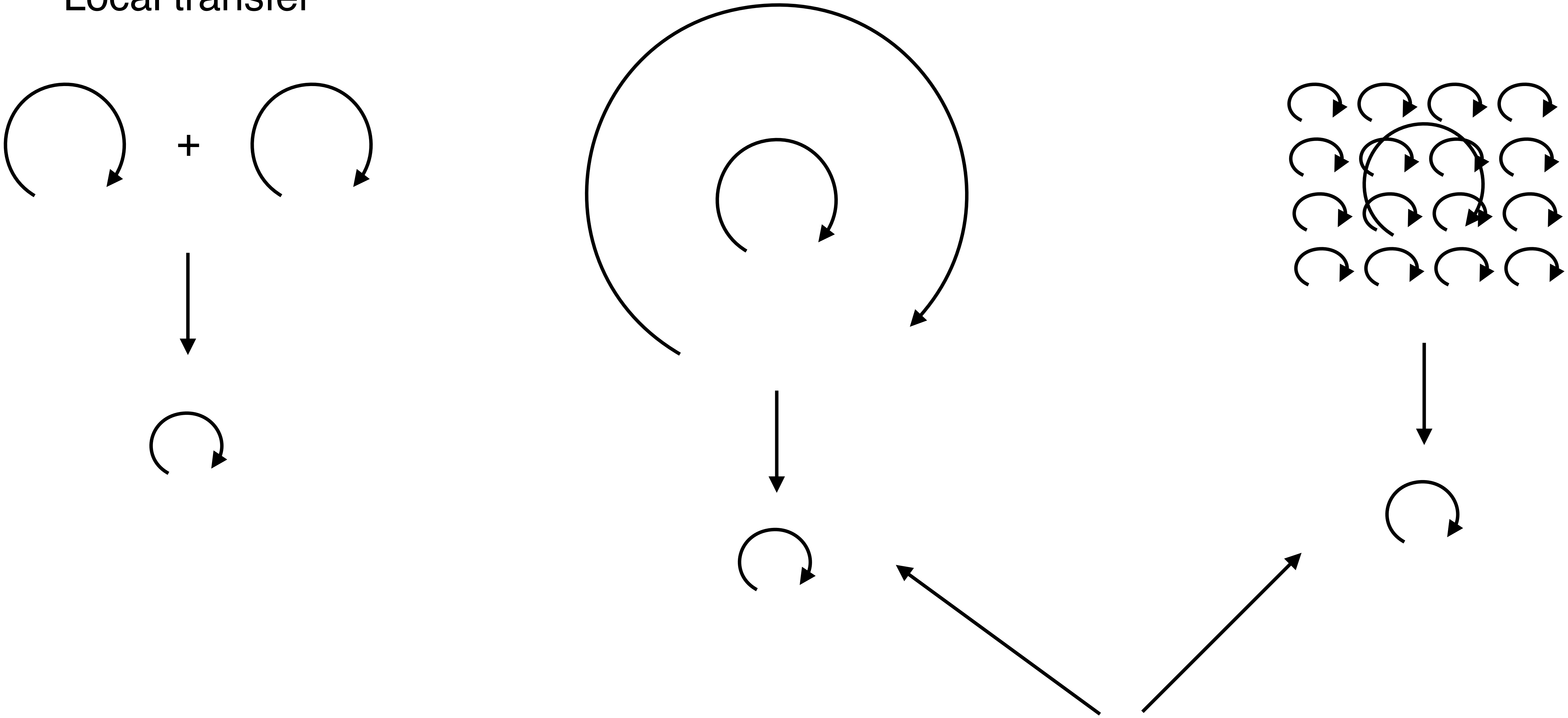

Local transfer

Large scale shearing

Small scale diffusion

In neutral fluid turbulence, these can be transformed away via random Galilean transformations. In a plasma, Alfvén waves counter-propagating along a large scale B field adds a preferred direction, breaking the symmetry and increasing the importance of non-local energy transfer.

Results at MHD scales

Use Kraichnan (1959) locality functions

$$\Pi(k_p|k_c) = \sum_{K=c+1}^{N}\left[\sum_{P=1}^{N}\sum_{Q=1}^{p} + \sum_{P=1}^{p}\sum_{Q=p+1}^{N}\right]\mathcal{T}_{K,P,Q}$$

- Fix a shell, k_c and vary a probe shell k_p
- Consider all transfers for which one leg (p,q) is smaller than k_p
- Start with $k_p = k_c$ and move k_p further away, retaining increasingly non-local contributions
- Neutral fluids find a locality exponent, $\gamma \sim 4/3$, that is universal in the inertial range
- Incompressible MHD simulations find $\gamma \sim 2/3$ for the total flux

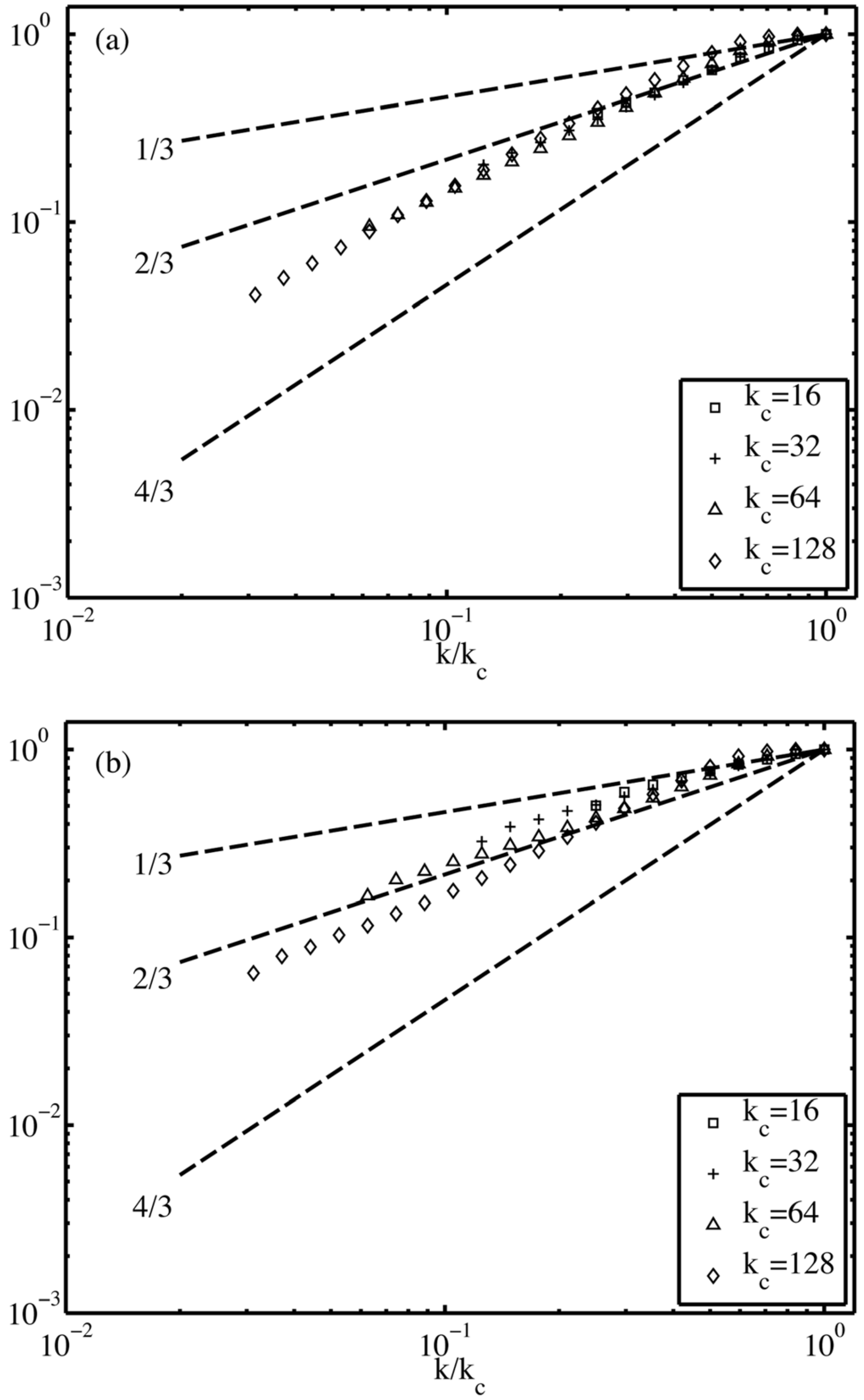

IR locality functions for the total energy flux in two incompressible MHD simulations. From Teaca et al (2011).

Mediators of kinetic scale turbulence

- Mediators are more non-local than neutral fluid or MHD turbulence
- Non-locality increases at small scales, implying non-self-similar behavior
- Behavior at large scale closer to neutral fluid

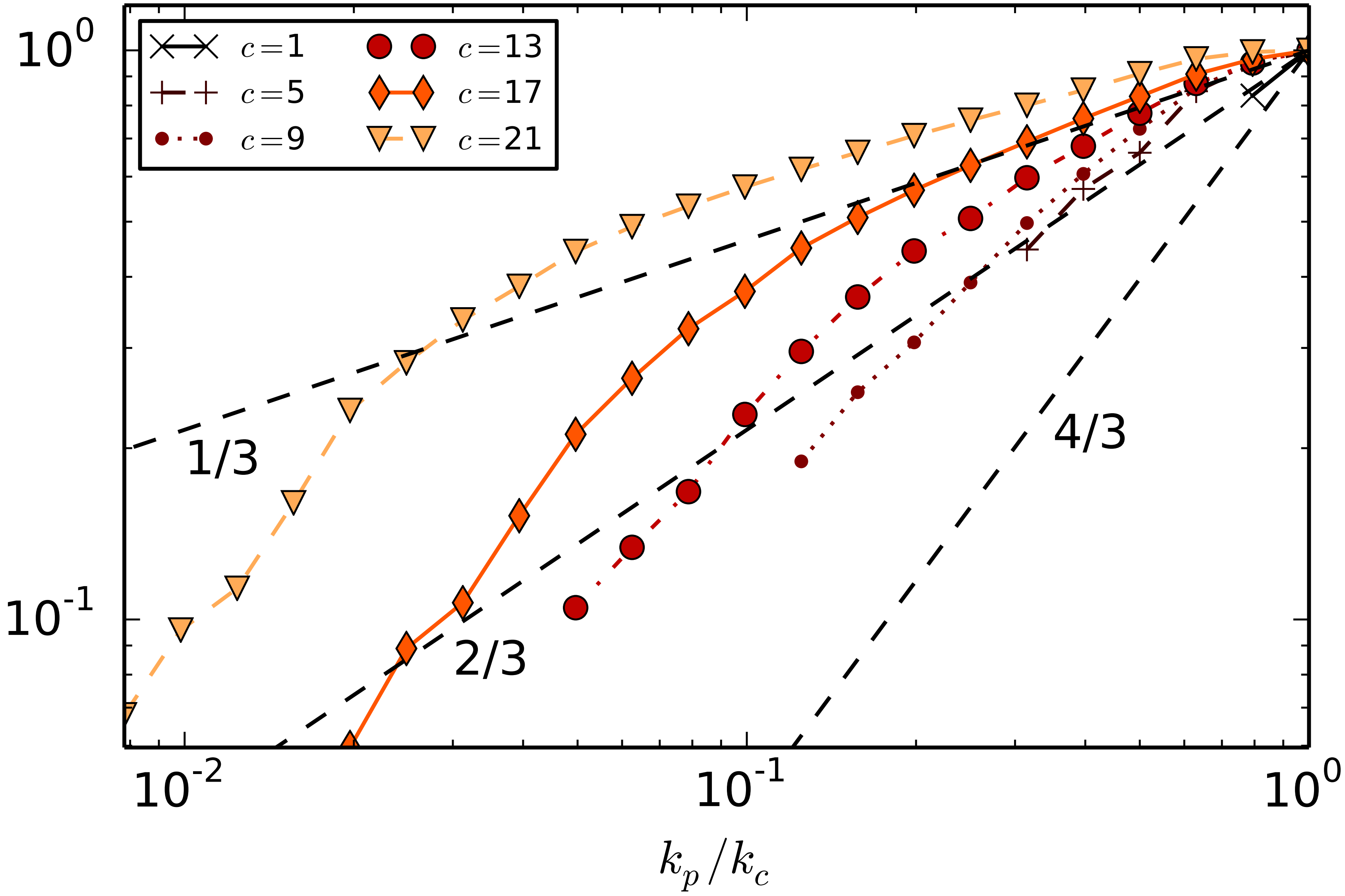

Evolution of the distribution function and E

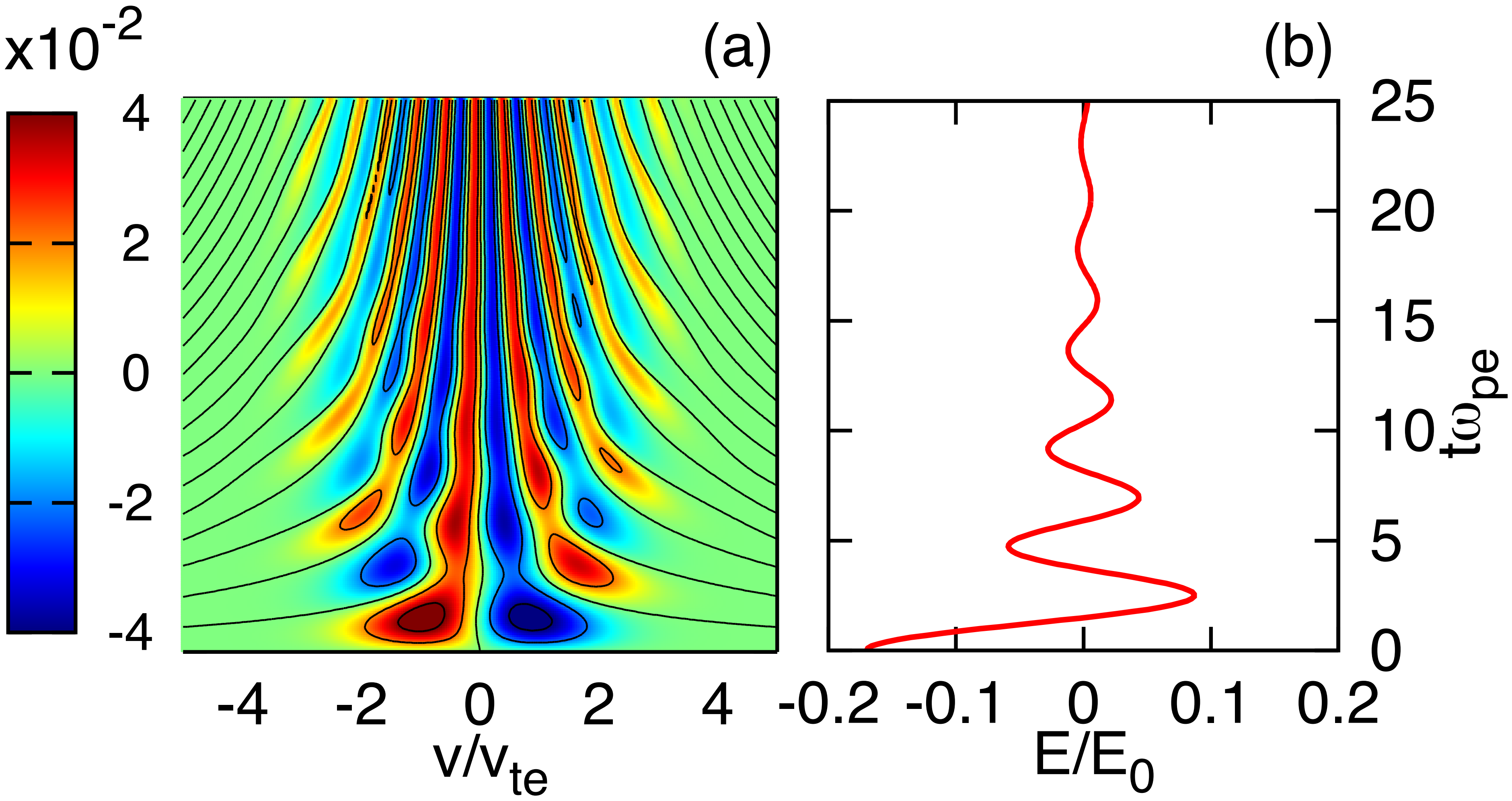

FIGURE 10. For Case I, (a) the total perturbed electron distribution function $\delta f_e(0, v, t)$ (colormap) and (b) electric field $E(0, t)$ measured at $x = 0$ as a function of normalized time $\omega_{pe} t$.

Transform to g

We transform to the complementary perturbed distribution: (Schekochihin et al 2009 ApJS, §5.1)

$$g_s(\mathbf{R}_s, v_\perp, v_\parallel) = h_s(\mathbf{R}_s, v_\perp, v_\parallel) - \frac{q_s F_{0s}}{T_{0s}} \left\langle \phi - \frac{\mathbf{v}_\perp \cdot \mathbf{A}_\perp}{c} \right\rangle_{\mathbf{R}_s}$$

g_s describes perturbations to the Maxwellian velocity distribution in the frame moving with an Alfvén wave.